STS-1
Operational Flight Profile

Volume V

Descent - Cycle 3

Appendix D
GRTLS Six-Degree-of-Freedom
Monte Carlo Dispersion Analysis

Mission Planning and Analysis Division

July 1980

NASA

National Aeronautics and
Space Administration

Lyndon B. Johnson Space Center
Houston Texas

SHUTTLE PROGRAM

STS-1
OPERATIONAL FLIGHT PROFILE

VOLUME V
DESCENT - CYCLE 3

APPENDIX D
GRTLS SIX-DEGREE-OF-FREEDOM
MONTE CARLO DISPERSION ANALYSIS

By Moises N. Montez
Flight Analysis Branch
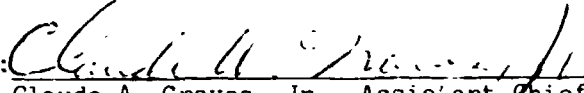
Approved: _____
Claude A. Graves, Jr., Assistant Chief
Flight Analysis Branch
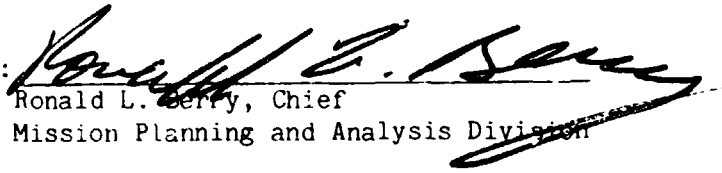
Approved: _____
Ronald L. Berry, Chief
Mission Planning and Analysis Division

Mission Planning and Analysis Division

National Aeronautics and Space Administration

Lyndon B. Johnson Space Center

Houston, Texas

July 1980

CONTENTS

TABLES

FIGURES

ACRONYMS AND SYMBOLS

ADS	air data system
AOA	abort once around
BETA	sideslip angle
C_d	drag coefficient
c.g.	center of gravity
Cn	change of yawing moment coefficient due to beta
CR	change request
DOF	degrees of freedom
EOM	end of mission
ET	external tank
fcs	flight control system
fps^2	feet per second squared
GET	ground elapsed time
GN&C	guidance, navigation, and control
GRTLS	glide return-to-landing site
GSTDN	ground spaceflight tracking data network
H-DOT	altitude rate
Isp	specific impulse
KSC	Kennedy Space Center
L/D	lift-to-drag
MSBLS	microwave scanning beam landing system
MEP	minimum entry point
psf	pounds per square foot
RCS	reaction control system

STS-1   Space Transportation System-1

Tacan   tactical air navigation system

TAEM   terminal area energy management

1.0 SUMMARY

This appendix presents the results of a six-degree-of-freedom (6-DOF) nonlinear Monte Carlo dispersion analyses for the latest glide return-to-landing site (GRTLS) abort trajectory for the Space Transportation System-1 (STS-1), cycle 3 (ref. 1). For this GRTLS, the number two main engine fails at 262.5 seconds ground elapsed time (GET). Fifty randomly selected simulations were analyzed. This analysis compares the flight environment with systems and operational constraints on the flight environment and, in some cases, uses simplified system models as an aid in assessing the GRTLS flight profile. In addition, GRTLS flight envelopes are provided as a data base for use by system specialists in determining the flight readiness for STS-1.

The 6-DOF option of the LAND program was used to generate the 50 random trajectories that were analyzed. The GRTLS simulations are initialized at external tank (ET) separation. The initial covariance matrix (ref. 2) is a 20 by 20 matrix and includes navigation errors and dispersions in position and velocity, time, accelerometer bias, and inertial platform misalinements.

The April atmospheres (ref. 3) are presented in this document. The baselined tactical air navigation (Tacan) selection logic, which selects one out of ten Tacan stations (based on the best Tacan geometry) are also presented. Data from the air data system (ADS), below an Earth-relative velocity of 2500 fps, are used. Baroaltitude was not processed between velocities of 1600 and 900 fps. Runway redesignations or ground state vector updates are not included in this analysis.

In all 50 samples analyzed, speedbrake, rudder, elevon, and body-flap hinge moments are acceptable. All landing simulations begin transition to autoland before an altitude of 9000 feet, and there are no tailscrapes. Navigation-derived dynamic pressure accuracies exceed the flight ontrol system (FCS) constraints above Mach 2.5 and several cases violated the change of yawing moment coefficient because of beta (Cn_β) dynamic and lateral trim constraint line. In addition, normal load factor transients occur at microwave scanning beam landing system (MSBLS) acquisition and at terminal area energy management (TAEM)/autoland interface. The tire specification limit speed of 222 knots was exceeded in one out of fifty landings, and the tire certification limit speed of 208 knots was exceeded in three out of fifty landings.

Navigation-derived dynamic pressure accuracies exceed the FCS constraints above Mach 2.5. Violation of these constraints will affect the FCS moding and gains because dynamic pressure is used to perform these two functions. Several cases violated the Cn_β dynamic and lateral trim contraint line. This constraint line was generated by using the April 1979 aerodynamic data, X c.g. = 66.7 trim flight, 1-inch Y c.g. offset worst-case elliptical variations, two yaw jets used for trim, maximum sideslip angle of 1.5° and bent airframe effects. Violation of the two constraints (dynamic pressure and Cn_β dynamic) did not cause any problems. Several metering methods were used to reduce the normal load transients at MSBLS acquisition but were unsuccessful. Therefore, the pilot should expect these transients if he is in the auto guidance mode at this point. The MSBLS variances have been increased and will reduce the magnitude of these transients The landing statistics indicate that three out of fifty landings

exceeded the tire specification limit speed of 222 knots. Because the landing is expected to be manual (rather than using the autoland guidance for STS-1), the pilot landing techniques are expected to land farther downrange to reduce the landing speed to within landing gear constraints.

2.0 INTRODUCTION

This appendix presents the results of a 6-DOF nonlinear Monte Carlo analyses for the latest GRTLS abort trajectory, STS-1, cycle 3 (ref. 1). The flight environment is compared with systems and operational constraints on the flight environment, and in some cases, simplified system models are used as an aid in assessing the GRTLS flight profile. In addition, GRTLS flight envelopes are provided as a data base for use by system specialists in determining the flight readiness for STS-1.

The 6-DOF Monte Carlo option of the LAND program was used to generate the 50 random trajectories that were analyzed. The GRTLS simulations are initialized at ET separation. The initial covariance matrix (ref. 2) is a 20 by 20 matrix and includes navigation errors and dispersions in position and velocity, time, accelerometer bias, and inertial platform misalinements.

April atmospheres (ref. 3), which are the best atmospheres to use for a March 31 launch, were used. The baselined Tacan selection logic, which selects one out of ten Tacan stations based on the best Tacan geometry, was used in this study. Also, data from the ADS were used below an Earth-relative velocity of 2500 fps. Baroaltitude was not processed between velocities of 1600 and 900 fps. Runway redesignations or ground state vector updates were not included in this analysis.

Statistical summaries for selected parameters and scatter traces for selected parameters are presented in this appendix. The scatter traces include the expected three-sigma dispersions for the parameters that are normally distributed.

This appendix first defines a set of criteria that is used to determine the acceptability of the flight profile. Model updates and additional models are discussed next. A discussion of the atmosphere dispersions, navigation performance, control surface hinge moments, GRTLS guidance performance, and landing performance follows, respectively. The results, in the form of scatter traces, are then compared to system and operational constraints. These flight envelopes and results from simplified system models can be used by system specialists to determine areas that need more detailed analysis before the STS-1 flight readiness review.

3.0 SUCCESS CRITERIA

The following criteria are used in determining successful results:

a. Control surface hinge-moment constraints (ref. 4); defined in table I

b. Normal load factor less than 2.5g's (ref. 5)

2

c. Dynamic pressure less than the 400 psf (ref. 5)

d. Maximum descent rate of 400 fps in the transonic region to conform to compartment venting contraints (ref. 5)

e. TAEM/autoland interface box; satisfied before an altitude of 5000 feet (ref. 6); defined in table II

f. Pitch attitude with respect to the horizontal less than 15.0° at landing (ref. 7)

g. Descent rates at landing less than 9.5 fps (ref. 7)

h. Landing speeds less than the tire limit speed of 222 knots (ref. 8)

i. Lateral position within 60 feet of the runway centerline (ref. 8)

j. Lateral velocity less than 50 fps (ref. 8)

4.0 ADDITIONAL MODELS AND MODEL UPDATES

This section presents the models added to the LAND program to simulate GRTLS and updates to existing models. A GRTLS guidance simulation (ref. 6) was added and modified to include change requests (CR's) 19078A, 19199, 19209, and 19370. Also added was a GRTLS FCS simulation (ref. 9) and CR's to functionally simulate the auto/FCS model in the October 16, 1979 IBM software delivery. The entry navigation software was modified to functionally simulate the navigation model documented in reference 10. The supporting base data for the navigation model is presented in reference 11.

Aerodynamic data were updated to the April 1979 (ref. 12). In addition, a dispersion model was added to simulate bent airframe effects. No aeroelastic effects or reaction control system (RCS) interaction effects were included.

5.0 DISCUSSION

This section presents a discussion of the simulations results for the latest GRTLS abort trajectory. For this GRTLS, the number two main engine fails at 262.5 seconds GET.

5.1 ATMOSPHERIC DISPERSIONS

Figure 1 presents the atmospheric dispersions for the month of April, with respect to the 1962 Standard Atmosphere (ref. 13) and the wind magnitudes and headings for altitudes greater than 800 feet. Figure 2 presents the lower altitude winds. The lower altitude winds (ref. 14) are generated by sampling peak wind statistics at the surface, which describe the wind magnitude distributions between 6:00 and 8:00 a.m. at KSC during April. Wind heading statistics at the

surface are sampled and a wind turning function is used to relate the two-
kilometer rawinsonde data point to the surface wind he ng. The statistical at-
mospheres and winds aloft were generated by using the vertical atmosphere genera-
tion option (ref. 3). The atmospheres are a function of altitude and month and
are consistent with the Space Shuttle Orbiter environment specifications (ref.
15). Turbulence (ref. 14) is superimposed on the steady state winds. This tur-
bulence model statistically varies the gust intensity and scale length and as-
sumes that the Orbiter is always in some kind of turbulence.

Figure 1(a) presents the density dispersions. In the altitude interval between
80 000 and 200 000 feet, the mean density deviation for April is more dense than
the 1962 Standard Atmosphere. This results in a small mean deviation in the al-
titude error when the drag altitude is incorporated in the navigation data pro-
cessing. Pressure dispersions of the atmosphere (fig. 1(c)) affect the baro-
baroaltitude measurements. Dispersed static pressures are input in the ADS simu-
lation which, in turn, derives a pressure altitude. The ADS uses a curve fit
based on a 1962 Standard Atmosphere to derive pressure altitude. This pressure
altitude is corrected based on a nonstandard monthly mean model and a baroset,
which calibrates the barometer to measured pressure at the landing site before
landing to minimize the effects of the nonstandard atmospheres. Since only sea-
sonal nonstandard corrections are available, this analysis used the April correc-
tions above an altitude of 12 000 feet mean-sea-level altitude. Below 12 000
feet, the baroset was used. At approximately 26 000 feet (jet stream), wind mag-
nitudes (fig. 1(d)) approach the design values. The mean wind headings (fig.
1(e)) is toward the east. The discontinuities in the plot of wind heading re-
flect the crossing of the 180° wind heading rather than wind heading change.

5.2 NAVIGATION PERFORMANCE

The navigation measurement incorporation schedule for the latest GRTLS profile
is presented in table III. First, drag altitude is initially processed when the
drag acceleration is greater than 11 fps^2 (a 186 600-feet altitude) and termin-
ated at an altitude of 85 200 feet or when the barometric altitude is valid,
whichever occurs first. Tacan data are initially processed at an altitude of ap-
proximately 227 000 feet and are terminated when the MSBLS data are valid or at
landing, whichever occurs first. Table IV presents the Tacan stations used in
this analysis. Only two of the ten Tacan stations were selected by the Tacan se-
lection logic (Savannah and Mobile).

Figure 3 presents the navigation-derived and/or ADS-derived parameter perfor-
mance. Figure 3(a) shows that in the three-sigma case, the FCS accuracy require-
ments (ref. 16) for dynamic pressure will be violated for Mach numbers greater
than 2.5. The mean bias seen in figure 3(a) is due to the inaccuracies in the
drag coefficient (C_d) curve fit used to derive dynamic pressure. This curve fit
will be updated in the near future. The large initial errors are due to RCS
firings. Below Mach 2.5, when the ADS dynamic pressure is used, the errors in
the three-sigma case, slightly exceed the requirements (ref. 17) during the Mach
jump region (Mach 0.9 to 1.6). In this region, dynamic pressure is sensitive to
navigation error since the navigated altitude is used to derive the free stream
static pressure which, in turn, is used in deriving dynamic pressure. Dynamic

pressure is used in moding the FCS and in computing gains. These error magnitudes did not cause any problems in any of the simulations.

Figure 3(b) presents angle-of-attack accuracy. The angle-of-attack error, above Mach 2.5, is the difference between the navigation-derived angle of attack and the actual angle of attack. Below Mach 2.5, the angle-of-attack error is the difference between the ADS angle of attack and the actual angle of attack. The biggest contributor to errors in the navigation-derived angle of attack are winds because the navigation routine derives angle of attack from the navigation Earth-relative velocity, which does not include the effects of winds. Angle-of-attack errors are cleaned up by the ADS below Mach 2.50. Figure 3(c) presents the Mach number errors. The baroaltitude performance is shown in figure 3(d). This figure shows that the ADS altitude accuracy requirement is satisfied.

The navigated state vector performance is shown in figure 4. Figure 4(g) shows the Tacan station locations relative to the groundtrack. Altitude errors and altitude rate errors are the navigated data minus actual data for these two parameters, respectively. All other state vector errors are equal to the actual quantity minus navigation quantity. The errors are computed in a radial, downrange, and crossrange (UVW) coordinate system determined by the actual state. Altitude and attitude rate errors are plotted in figure 4 in place of the radial position error and the radial rate error. The accuracy requirements (ref. 18) used in figure 4 are used by open-loop navigation analysts as an indicator of performance. While meeting these constraints ensures satisfactory performance, violation of these constraints does not necessarily mean unacceptable performance. Integrated guidance, navigation, and control (GN&C) performance analysis, such as this Monte Carlo analysis, provides a more direct method of assessing the navigation performance.

Table V presents a statistical summary of the state vector navigation errors, and table VI presents the initial state vector dispersions. All the samples were taken at a constant altitude. The errors are expressed in a UVW coordinate system defined at each sample; U is radial, V is downrange, and W is crossrange.

5.3 CONTROL SURFACE DEFLECTIONS AND HINGE MOMENTS

Table I contains the elevon, body flap, and speedbrake hinge-moment capability (ref. 4). The stall limits in the table were used as part of the success criteria. Figure 5 presents the control surface deflections and hinge moments. Also plotted on the elevon hinge-moment plots are the stall limits. The maximum allowable control surface rates in the LAND program are functions of the hinge moments. The elevon hinge moments are conservative because the total variation in the hinge-moment coefficient is assumed to be the same for the inboard and outboard elevon. The data book specifies that the variation must be divided by the square root of two. The hinge moments for the right inboard elevon, right outboard elevon, left inboard elevon, left outboard elevon, body flap, speedbrake, and rudder are all acceptable.

5.4 GUIDANCE PERFORMANCE

Figures 6 and 7 present the guidance performance parameters. Actual data, instead of navigation data, are plotted unless otherwise stated. These figures are divided into the GRTLS guidance performance parameters (fig. 6) and the autoland guidance performance parameters (fig. 7).

5.4.1 GRTLS

Figure 6 presents the GRTLS guidance performance parameters. Actual energy as a function of predicted navigated range during the TAEM phase are illustrated in figure 6(a). The S-turn boundary, S-turn terminate boundary, minimum entry point boundary, and the maximum lift-to-drag (L/D) line are also included. The results in figure 6(a) show that there are no minimum entry points (MEP's); all simulations had one S-turn in the angle-of-attack transition phase except four cases, which had no S-turns. Figure 6(b) presents actual altitude as a function of predicted navigated range-to-go to the runway threshold. Figure 6(c) contains the dynamic pressure dispersions. Also plotted in this figure are the structural design limit line, the flight control design limit line, the minimum dynamic pressure limit in the GRTLS guidance, the venting constraint line, and the sonic boom 2-psf over-pressure guideline. Most cases cut across the sonic boom 2-psf over-pressure line. The sonic boom boundary is a function of angle of attack and dynamic pressure. Analysis with similar dynamic pressure dispersions have shown maximum over-pressures of approximately 2.2 psf for the nominal entry. Figure 6(d) presents the angle-of-attack dispersions. Several limit lines are also plotted on these figures. These are the FCS design limits, rolloff, nose slice, buffet onset line, Cn_β dynamic and lateral trim line, and the venting constraint line. Several cases violated the Cn_β dynamic and lateral trim constraint line. This constraint line was generated using the April 1979 aerodynamic data, X c.g. = 66.7, trim flight, 1-inch Y c.g. offset, worst-case elliptical variations, two yaw jets used for trim, maximum sideslip angle of 1.5°, and bent airframe effects. These boundaries are also functions of dynamic pressure, so the dispersions are compared to the constraints in the dynamic pressure/ angle-of-attack plane (figs. 6(e) to 6(k)). In this plane, the 1.5° degree sideslip angle constraint is violated at Mach = 2. No problems were encountered encountered because of the violations in the velocity/angle-of-attack plane and the dynamic pressure/angle-of-attack plane.

Figures 6(l) and (m) present the sideslip angle and the bank-angle histories, respectively. All the simulations bank over to 45° (S-turn) except four. In these four cases, a bank maneuver is executed to line the vehicle with the heading alinement cylinder and then most of the flight is close to wings level. The point at which the heading alinement phase begins is clearly seen on these figures at a velocity of approximately 600 fps. Figure 6(n) presents pitch angle as a function of velocity. This figure shows that there were no tailscrapes and that adequate margins exist. Figure 6(o) presents normal load factors as a function of velocity. Normal load factors, as seen in these figures, are approximately 2.0g's three-sigma at velocities of 3200 fps and 2500 fps. At 3200 fps, the load factor transients are due to a change from an angle-of-attack control to an NZ control, altitude errors, altitude-rate errors, energy errors, and bank reversals. At 2500 fps, the transients result from the difference in the

navigation-derived dynamic pressure and the air data dynamic pressure. This dif-
ference divided by 0.96 seconds results in dynamic pressure rates, which cause
the guidance to fly the dynamic pressure limits. Also, when MSBLS cleans up the
state vector, the guidance drives the Orbiter back to the reference profile and
some of these maneuvers lead to large normal load factors. Figure 6(p) presents
the radial rate dispersions. Figures 6(q) through 6 (bb) present aerodynamic
and acceleration parameters that will be used for postflight analysis.

5.4.2 Autoland

For the approach and landing phase, most of the parameters are plotted with
predicted range (as in the independent parameters) because the actual range is
not available. The MSBLS measurements are very accurate and make the navigated
range a close approximation of the actual range. Figure 7 presents the autoland
guidance performance parameters. Figures 7(a) and (b), groundtrack and altitude
range, indicate that all the simulations were delivered to the vicinity of the
runway threshold satisfactorily. Figure 10(c) shows that none of the cases
landed short of the runway. The 0.5° elevation line in figure 10(c) represents
the elevation angle below which no elevation data will be available from the
MSBLS. Figure 7(d) contains the dispersions in the altitude and altitude-rate
plane. The radial-rate error, navigated minus actual, is shown in figure 7(e).
The bias that builds up below an altitude of 225 feet is the result of using the
MSBLS elevation data between 1.3° and 0.5° elevation angle. In this region, the
model used (and is considered realistic) exhibits a mean bias in the elevation
measurement. Figure 7(f) presents dynamic pressure versus navigated range.
Also plotted in figure 7(f) are the FCS design limit line and the certification
criteria line. The dynamic pressure dispersions in this figure are acceptable.
Figure 7(g) presents the angle-of-attack dispersions and show adequate margins
with respect to the FCS design limit. Sideslip angle, bank angle, and pitch
angle are presented in figures 7(h), (i), and (j), respectively. Figure 7(j) in-
dicates that there are no tailscrape cases. Normal load factors (fig. 7(k))
are less than the STS-1 guideline of 2.5g's. Figure 7(e) presents the altitude
rate, and figures 7(m), (n), and (o) present the altitude rates above the body
axis.

The elevator deflection (fig. 7(p)) exhibits an increase when the body flap is
retracted (fig. 7(r)) to the trail position at autoland guidance initiation. A
decrease in the elevator setting occurs when the speedbrake is retracted (fig.
7(s)) prior to the preflare maneuver. This decrease, in four cases (fig. 7(p)),
was delayed until a range of approximately 9000 feet was reached because the
speedbrake for these cases was not retracted until an altitude of 1000 feet
(fig. 7(s)) was reached. Figure 10 (q) presents the aileron histories and fig-
ure 7(t) presents the rudder deflections. The maximum allowable surface rates
in the LAND program are functions of the hinge moments and are presented in fig-
ures 7(u) through (y). Hinge moments are presented in figures 7(z) through
(ff). The elevon hinge moments are conservative because the total variation in
the hinge-moment coefficient is assumed to be the same for the inboard and
outboard elevon. The data book specifies that the variation must be divided by
the square root of two. Stall limits (ref. 4) are also plotted on the hinge-
moment traces. All hinge moments are acceptable.

Table VII contains the landing statistics. This table gives the mean maximum value and minimum value (instead of means and sigmas) because the distribution of some of the listed parameters cannot be reasonably approximated by a normal distribution (fig. 8). Figure 9 presents the cumulative distribution of the surface winds for Kennedy Space Center (KSC). These winds are valid for runway 15 at KSC for the month of April between 6 a.m. and 8 a.m. local time. Three out of fifty landings had crosswinds at landing that were greater than or equal to 10 knots. The landing statistics indicate that one out of fifty landings exceeded the tire specification limit speed of 222 knots, and three out of fifty landings exceeded the tire certification limit speed of 208 knots. Because the landing is expected to be manual, rather than using the autoland guidance for STS-1, the pilot landing techniques are expected to increase the landing point dispersion to reduce the landing speed within landing gear constraints. Table VII also contains an estimate of the energy margin at landing.

6.0 CONCLUSIONS

In all fifty samples analyzed, speedbrake, rudder elevon, and body-flap hinge moments are acceptable. All landing simulations are transitioned to autoland before an altitude of 9000 feet. Also, there are no MEP's or tailscrapes. Navigation-derived pressure accuracies exceed the FCS constraints above Mach 2.5, and several cases violated the $C_{n\beta}$ dynamic and lateral trim constraint line. Normal load factor transients occur at MSBLS acquisition and at TAEM/autoland interface. One out of fifty landings exceeded the tire specification limit speed of 222 knots. The tire certification limit speed of 208 knots was exceeded three times. Crosswind magnitudes at landing exceeded the constraint of 10 knots in three cases.

Violation of navigation-derived dynamic pressure above Mach 2.5 will affect the FCS moding and gains to some degree because dynamic pressure is used to perform the moding and gain scaling. Several cases violated the $C_{n\beta}$ dynamic and lateral trim constraint line. This constraint line was generated with April 1979 aerodynamic data, X c.g. = 66.7 percent, trim flight 1-inch Y c.g. offset, worst-case elliptical variations, 2 yaw jets used for trim, maximum sideslip fo 1.5° and bent airframe effects. Violation of the navigation-derived dynamic pressure error constraint, the $C_{n\beta}$ dynamic and lateral trim constraint, and the rolloff, nose slice, and buffet onset constraint did not cause any problems. Several metering methods were used to reduce the normal load transients at MSBLS acquisition but were unsuccessful. Therefore, the pilot should expect these transients when using the auto guidance mode. The MSBLS variances have been increased and will reduce the magnitude of these transients. The landing statistics indicate that one out of fifty landings exceeded the time specification limit speed of 222 knots, and three out of fifty landings exceeded the tire certification limit speed of 208 knots. Since the landing is expected to be manual, rather than using the autoland guidance for STS-1, the pilot landing techniques are expected to increase the landing point dispersion to reduce the landing speed within landing gear constraints.

7.0 <u>REFERENCES</u>

1. Flight Planning Branch: STS-1 Operational Flight Profile, Vol. VI, Abort Analysi - Cycle 3. Rev. 1, JSC IN 78-FM-51, June 1980.

2. Flight Planning Branch: STS-1 Operational Flight Profile, Vol. VI, Abort Analysis - Cycle 2. JSC IN 78-FM-51, May 1979.

3. Justus, C. G.; Woodrum, A. W.; Roper, R. G.; and Smith, O. E.: Four D Global Reference Atmosphere. NASA TM X-64872, Sept. 1974.

4. Bartor, Richard L.: Hinge Moment Constraints for Monte Carlo Program. JSC Mei rrandum EX43/7903-21, March 30, 1979.

5. Mission Planning and Analysis Division: STS-1 Operational Flight Profile, Groundrules and Constraints - Cycle 3. JSC 14483, Vol. I, Rev. 2, Sept. 1979.

6. Space Shuttle Orbital Flight Test Level C Functional Subsystem Software Requirements Document - Guidance, Navigation, and Control (Part A) Guidance, Entry through Landing. SD-76-SH-0001C, Dec. 15, 1978.

7. Shuttle Operational Data Book, Shuttle Systems Performance and Constraints. Systems Requirements and GFE Branch, Integration Division, Program Office. JSC-08934, Vol. I, Rev. A, Amendment 74, Oct. 1976.

8. Orbiter Vehicle End Item Specification for the Space Shuttle System Part 1, Performance and P sign Requirements. Rockwell International MJ070-0001-1B, Jan. 15, 1976.

9. Space Shuttle Orbital Flight Test Level C Functional Subsystem Software Requirement Document - Guidance, Navigation, and Control Part C - Flight Control - Ascent (GRTLS) Vol. III. SD-76-SH-0008B, Sept. 1978.

10. Space Shuttle Orbital Flight Test Level C Functional Subsystem Software Requirements Document, Guidance, Navigation, and Control (Part B) Navigation - GRTLS, SD-76-SH-0005C, Dec. 1978.

11. Shifrin, Dav l: STS-1 Cycle 2 (Version 2.4) Navigation Software I-Load Data Base 1.4TM-01234-100, Oct. 24, 1979.

12. Aerodynamic Design Data Book - Vol. I, Orbiter Vehicle, Rev. K. Rockwell International SD72-SH-0060-L, Oct. 1978 (with April 1979 update).

13. U. S. Standard Atmosphere. NASA, USAF, USWB. 1962.

14. Fichtl, G. H.. Stochastic Wind and Turbulence Models for Application to Monte Carlo Simulation of Return Trajectories of the Space Shuttle Orbiter from 30 km to the Surface at KSC. MSFC Memorandum S and E-AFRUYA-44-73, July 10, 1973.

15. Smith, O. E.: A Global Reference Atmosphere for Space Shuttle Engineering Analysis. MSFC Memorandum ES42-7-75, March 19, 1976.

16. Orbital Flight Test Program Phase II (Entry) Systems Design Review. Rockwell International SV75-BB, Sept. 1975.

17. Air Data Substantiation Report. STS Aero Sciences, Rockwell International SD-75-SH-0038, Rev. B, Dec. 1978.

18. Hutchinson, N. B.: Guidance, Navigation, Control Panel Meeting Number 22, CF-NBH-77-323, May 25, 1977.

TABLE I.- CONTROL SURFACE ACTUATOR HINGE-MOMENT CONSTRAINTS

Control surface	Stall hinge moment x 10^6; in.-lb, HM_{STALL}	Reference dimension; ft^2-in.(Sc)	Maximum rate; deg/sec	Surface weight; lb, W	Moment arm; in., ℓ	Comment
Inboard elevon	±0.955	19 047	43	1220	37.3	MOOG actuator at 2900 psi near $\delta_e = 0$
Outboard elevon	±.460 +	19 047	43	728	26.8	
Body flap	±1.400	10 935	1.5	1325	24.3	For two hydraulic systems operation
Speedbrake	± 2.400	7 331	16.0	Not applicable	Not applicable	For two hydraulic systems operation
Rudder	±.750	7 331	23.0	Not applicable	Not applicable	For two hydraulic systems operation

TABLE II.- AUTOLAND CAPTURE ZONE

Altitude, ft	Altitude[a] error, ft	Crossrange error, ft	Flightpath angle error, deg	Dynamic pressure error, psf
>10 000	1000	1000	4	24
10 000	1000	1000	4	24
[b]5 000	50	100	.5	24

[a]All errors are with respect to the reference values.
[b]Linear ramp as a function of altitude between 10 000 and 5000 feet.

TABLE III. - MEASUREMENT INCORPORATION SCHEDULE

Measurement	Nominal measurement[a]
	Incorporation altitude, ft
	GRTLS
First Tacan station acquistion	226 950 Savannah (SAV)
Drag altitude	186 800
Second Tacan station acquisition	105 574 Mobile (MBL)
Barometric altimeter	83 400
MSBLS	18 500
Radar altimeter[b]	100

[a]Altitude with respect to runway.
[b]Radar altimeter data sent directly to the autoland guidance.

TABLE IV.- TACAN STATION LOCATIONS, STS-1 GRTLS

Location	Channel	ID	Latitude	Longitude	Altitude
Savannah	74	SAV	32.160604N	81.112526W	-205.
Brunswick	35	SSI	31.050635N	81.445873W	-203.
Jacksonville	92	JAX	30.450374N	81.564211W	-188.
Ormand Beach	73	OMN	29.303463N	81.112811W	-169.
Orlando	59	ORL	28.542876N	81.334986W	-98.
Vero Branch	120	VRB	27.678570N	80.489574W	-189.
Palm Beach	102	PBI	26.687492N	80.156121W	-192.
Patrick	96	COF	28.237802N	80.611743W	-198.
Mobile[a]	11	MBL	28.644081N	80.696375W	-200.
Mobile	11	MBL	28.64408N	80.696375W	2127

[a]U.S. Air Force mobile Tacan station.

TABLE V.- STATE NAVIGATION ERRORS (NAV-ACTUAL) (THREE-SIGMA), GRTLS

Parameter, unit	ET separation	H = 200 000 ft	H = 140 000 ft	H = 80 000 ft	H = 20 000 ft	Landing
U, ft[a]	2391	2166	2245	2782	987	8
V, ft[a]	4387	3560	3279	1634	1086	42
W, ft[a]	4423	2305	1602	2090	998	15
UDOT, fps	7	6	6	8	7	.8
VDOT, fps	10	9	9	8	10	2
WDOT, fps	14	13	12	16	9	.9
H, ft		2169	2247	2781	986	8
HDOT, fps		6	6	8	7	.8
GAMMA, deg		.051	.058	.233	.834	.831

[a]U = radial, V = downrange, and W = crossrange.

TABLE VI.- STATE DEVIATIONS (ACTUAL REFERENCE) (THREE-SIGMA), GRTLS

Parameter, unit	ET separation entry
U, ft	2 859
V, ft	98 441
W, ft	29 293
UDOT, fps	89
VDOT, fps	299
WDOT, fps	56

TABLE VII.- LANDING STATISTICS

Parameter	Nominal	Mean	Maximum	Minimum
Altitude rate, fps	1.98	2.22	5.4	0.8
Pitch angle, deg	9.17	9.25	11.37	7.75
Groundspeed, knots	189	183	232[a]	- --
Equivalent airspeed, knots	188	182	220	
True airspeed, knots	189	183	223	162
Range from threshold, ft	2435	2100	4328	600
Lateral position, ft	0	0	15	-9
Lateral rate, fps	0	0	2.2	-1.9
Energy margin, sec	4.21	3.75	6.8	1.4

[a]Exceeds tire specification limit of 222 knots.
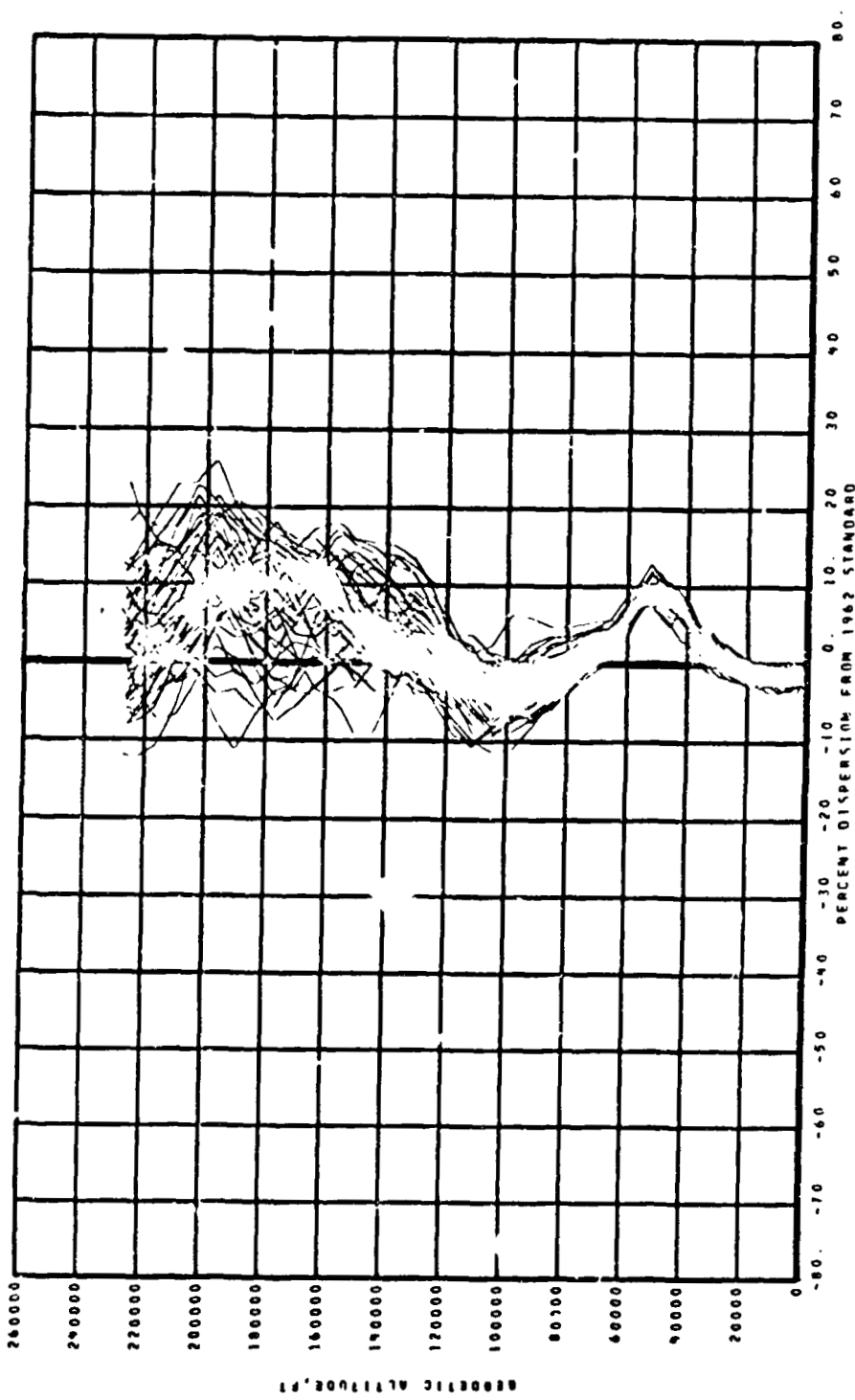
(a) Density.

Figure 1.- Atmospheric dispersions - April - GRTLS.

18
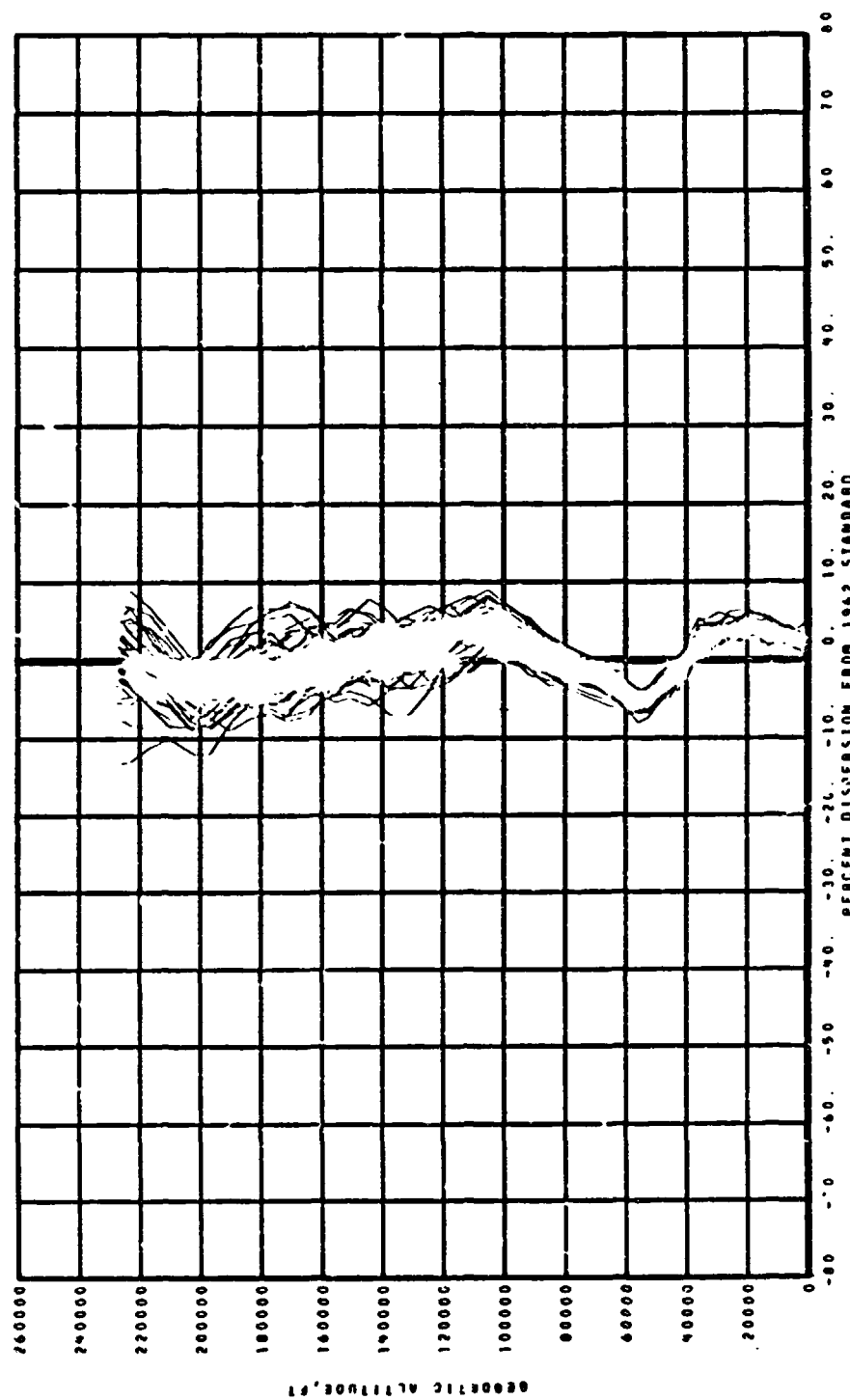
(b) Temperature.

Figure 1.- Continued.
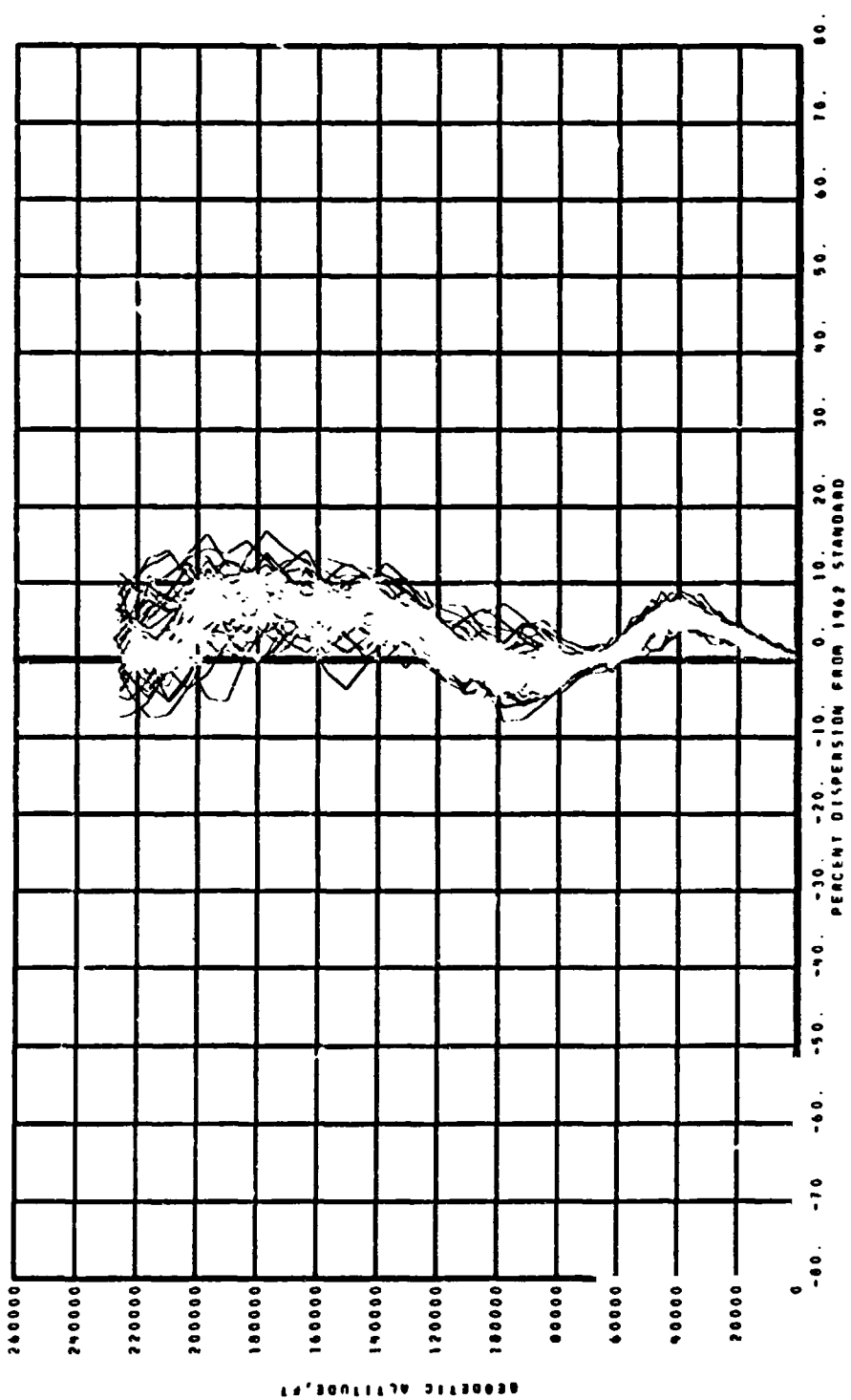
(c) Pressure.

Figure 1.- Continued.
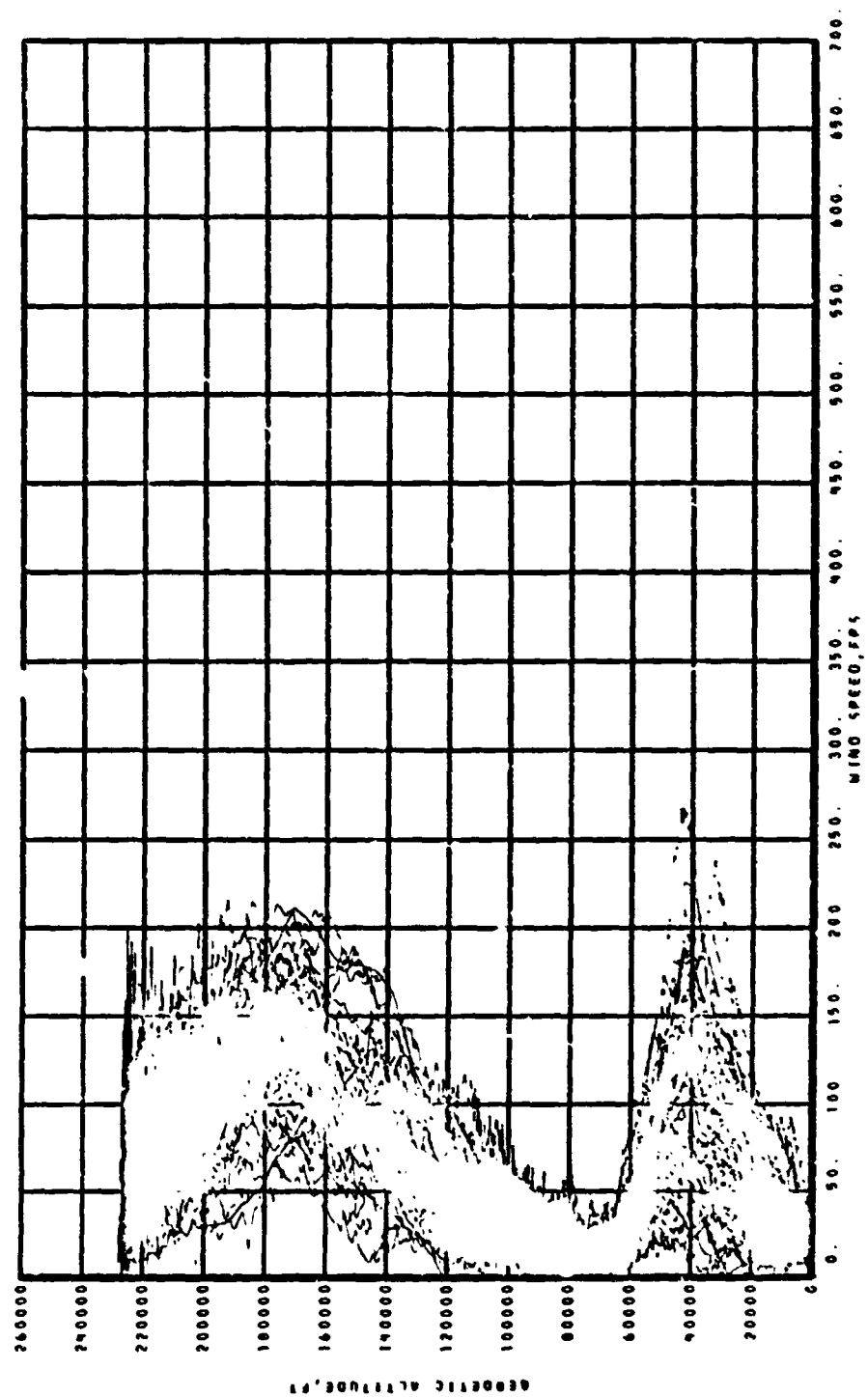
(d) Wind magnitude.

Figure 1.- Continued.

21
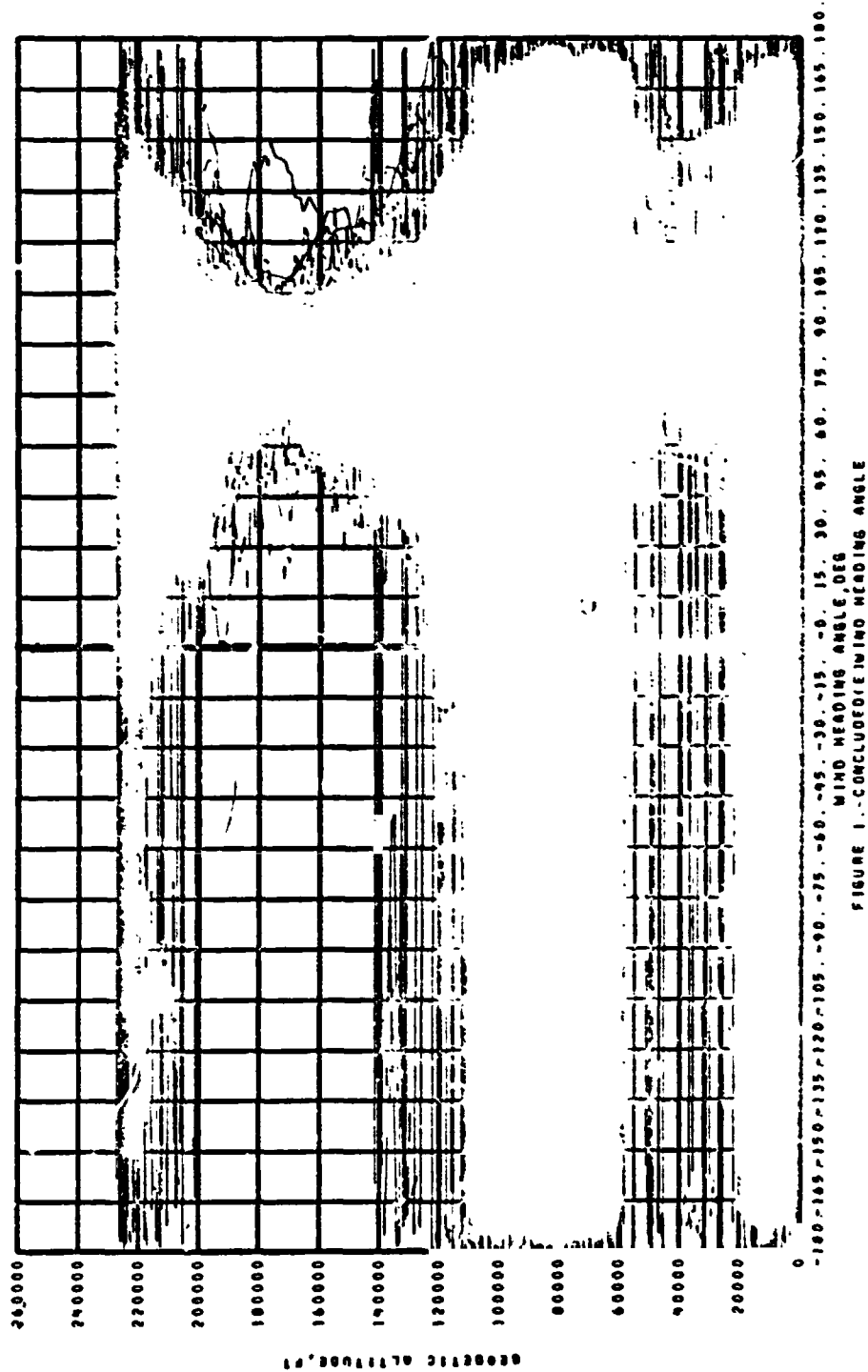
(e) Wind heading angle.

Figure 1.- Concluded.

Tailwinds | Headwinds
Magnitude, fps
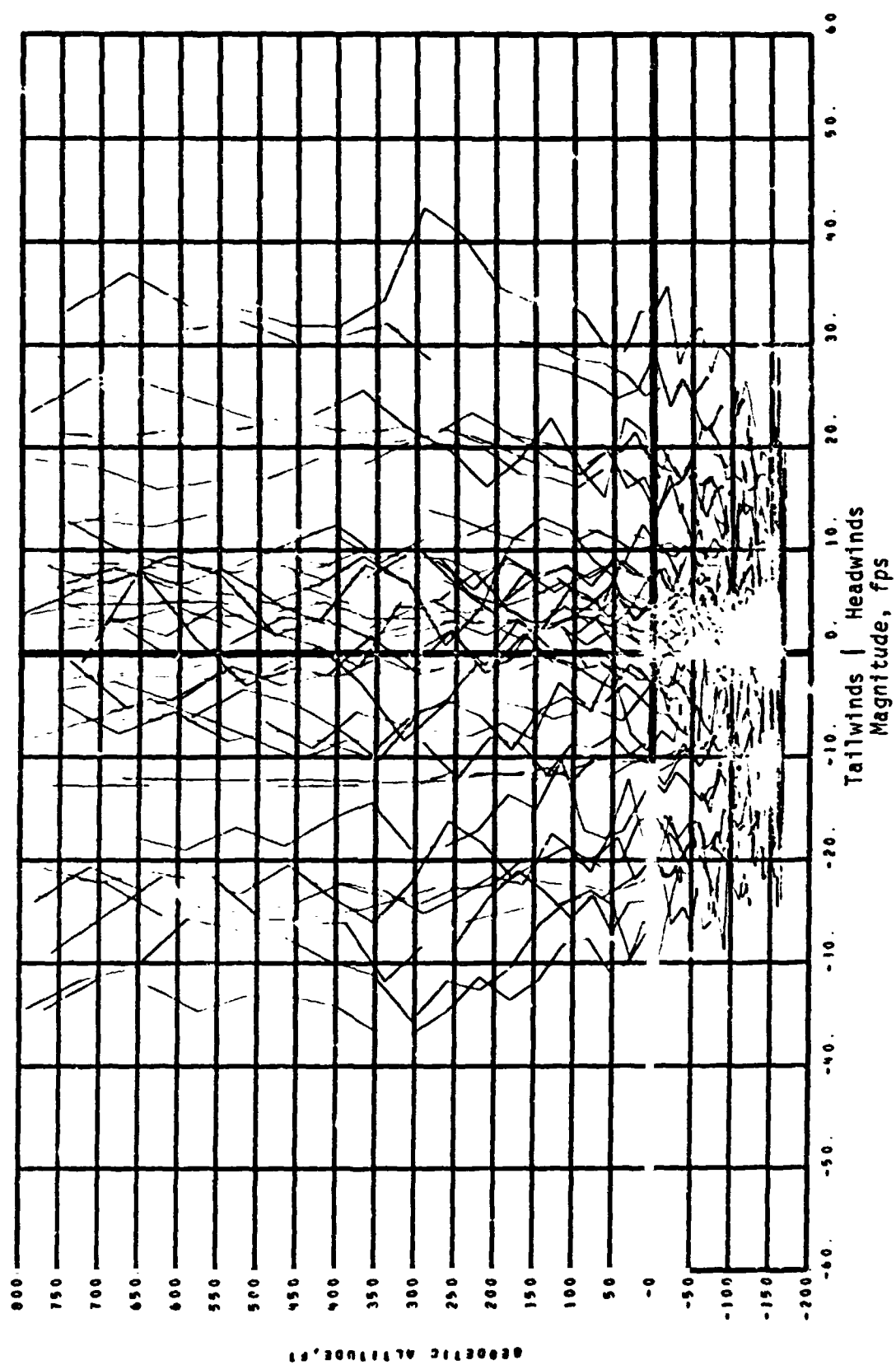
(a) Head or tailwinds.

Figure 2.- Surface winds - GRTLS.

23
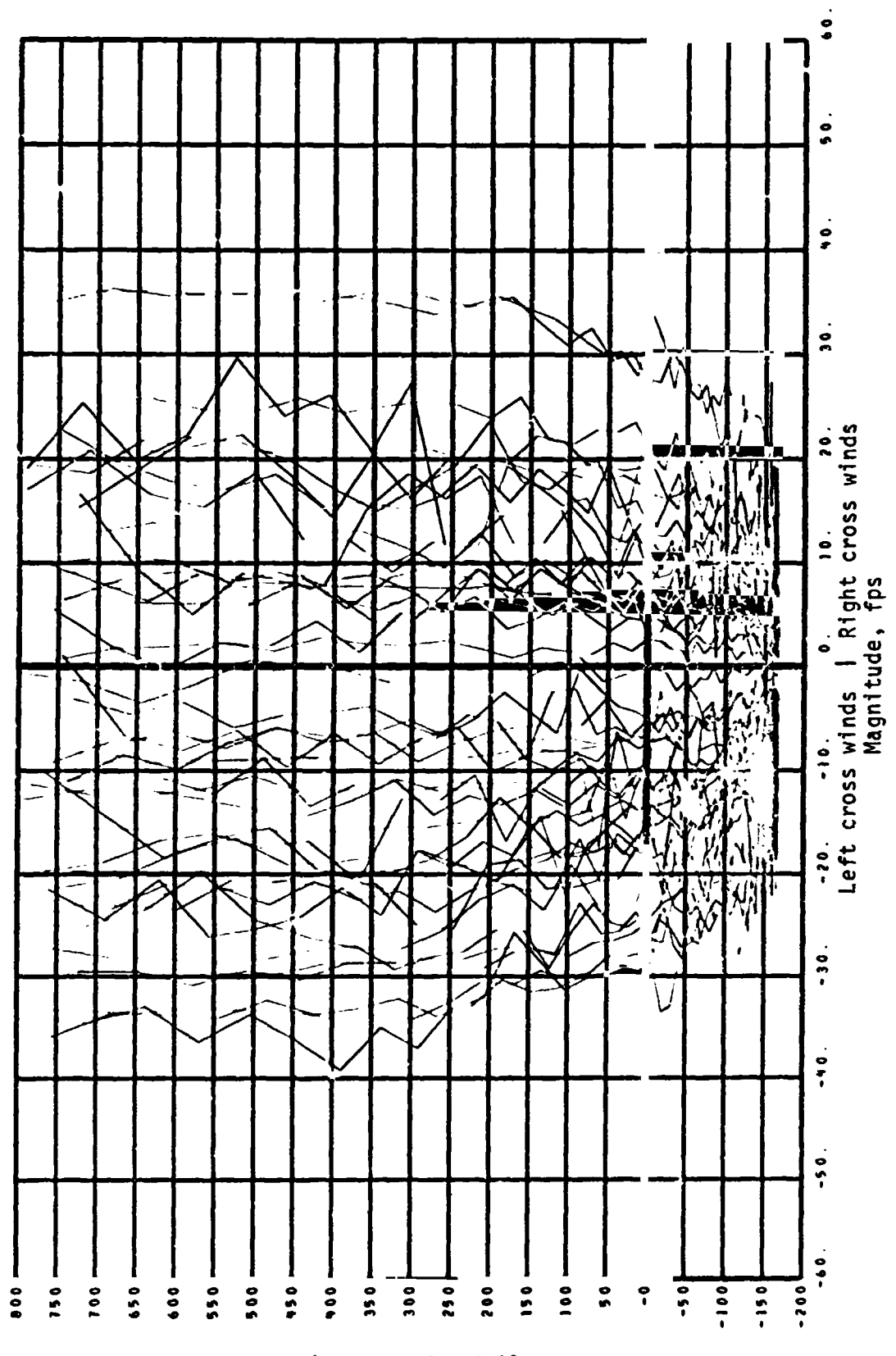
(b) Crosswind magnitude.

Figure 2.- Concluded.

24
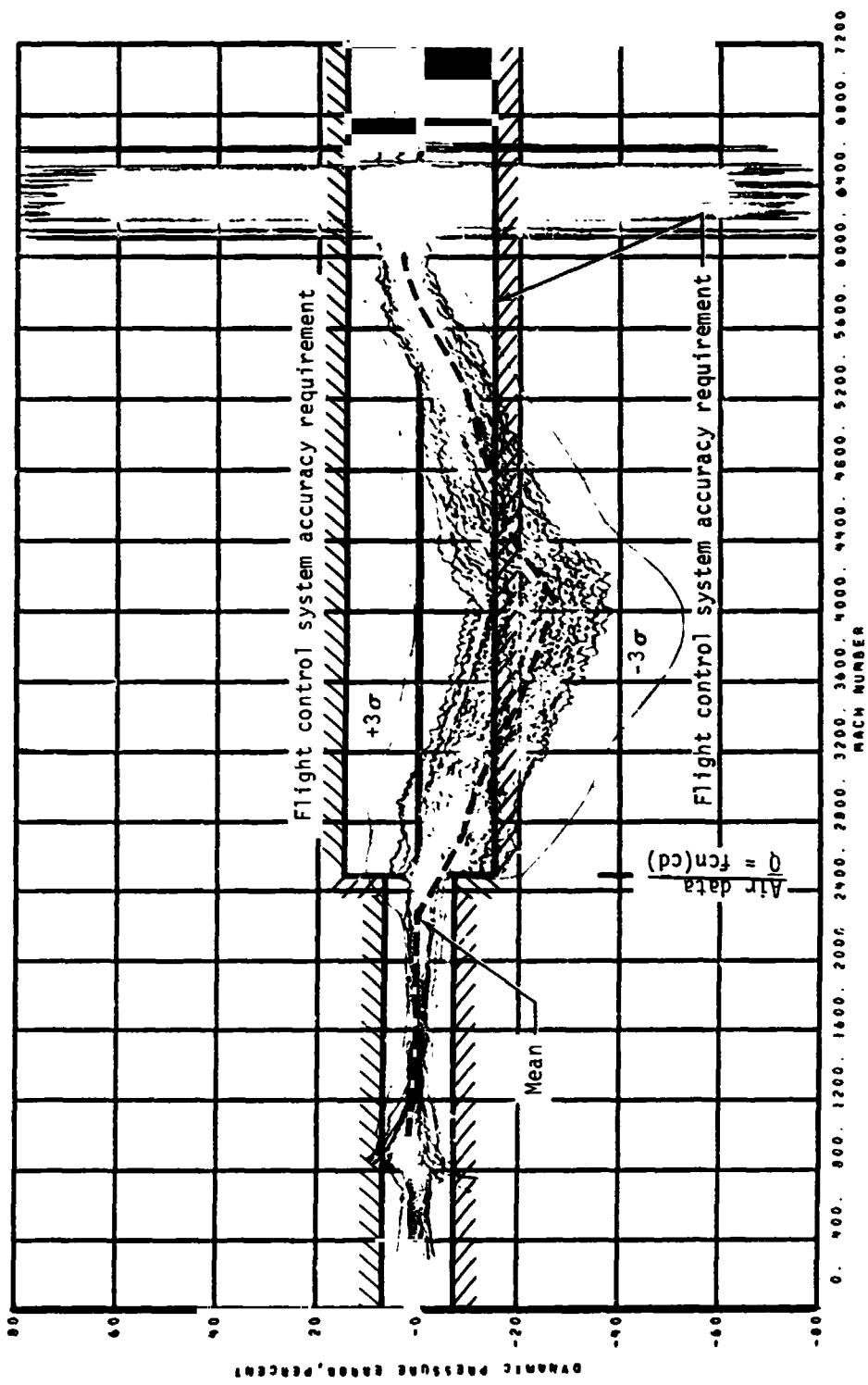
(a) Percent dynamic pressure error.

Figure 3.- Nav and/or air data parameter performance - GRTLS.

25
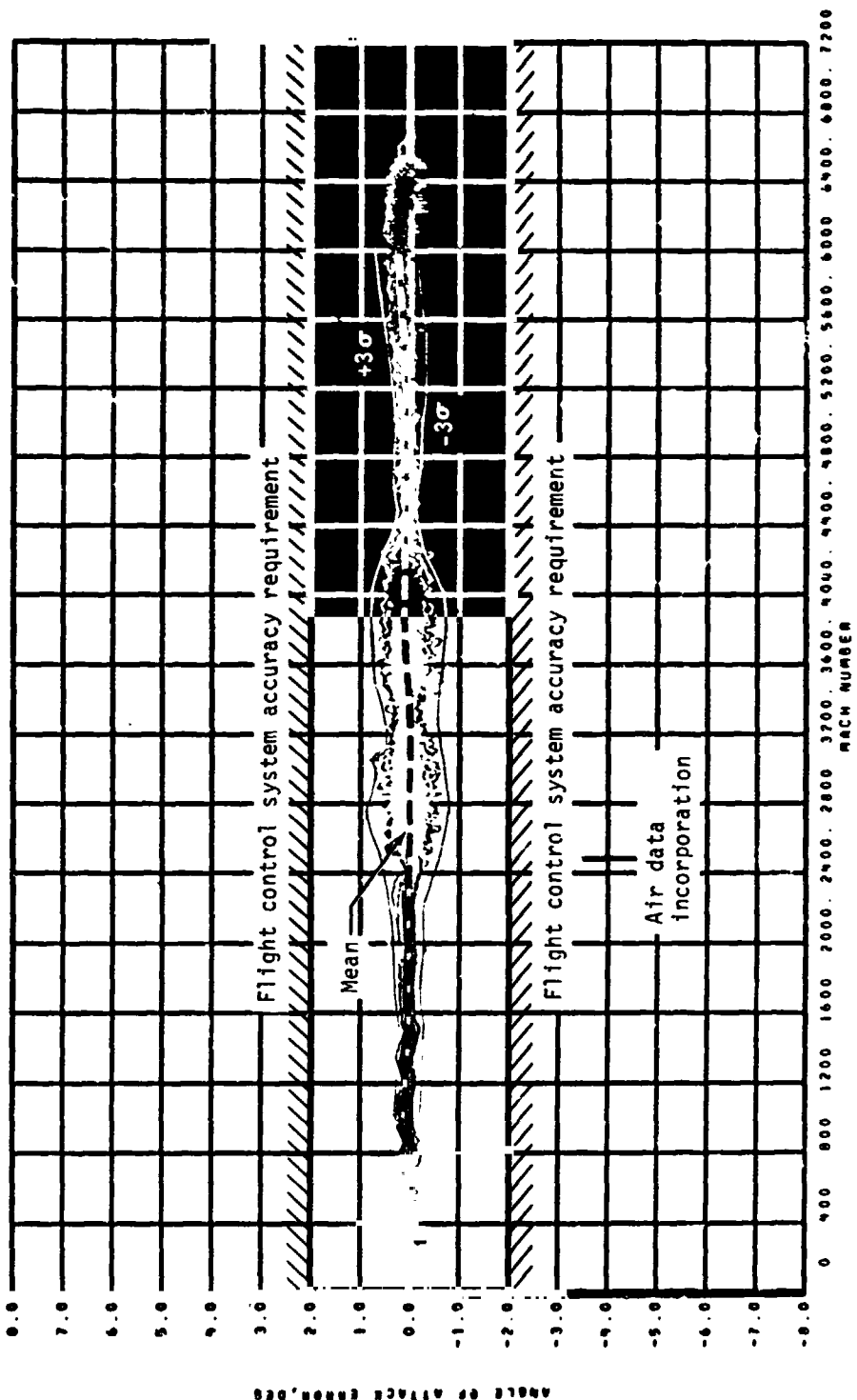
(b) Angle-of-attack error.

Figure 3.- Continued.
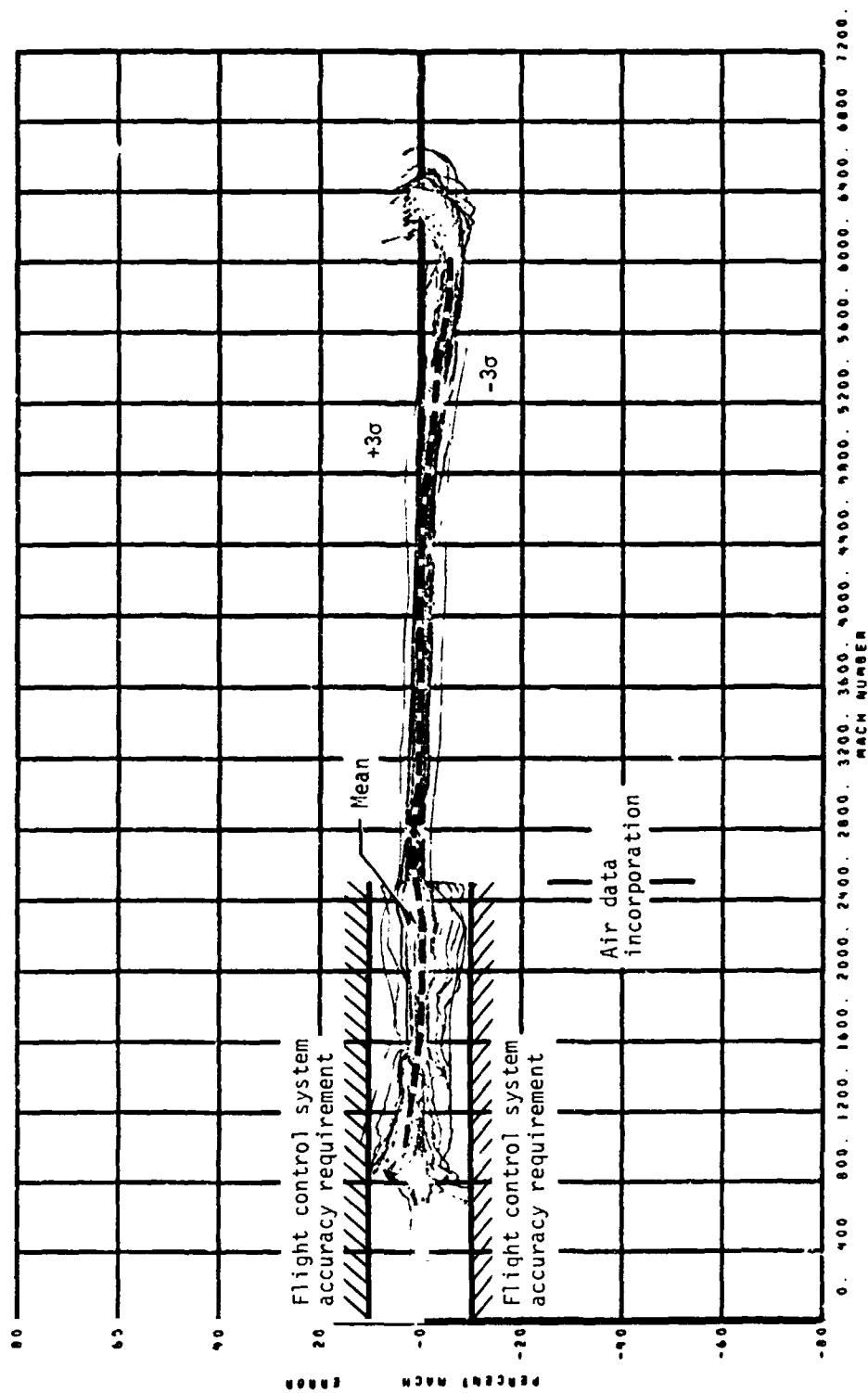
(c) Percent Mach number error.

Figure 3.- Continued.

27
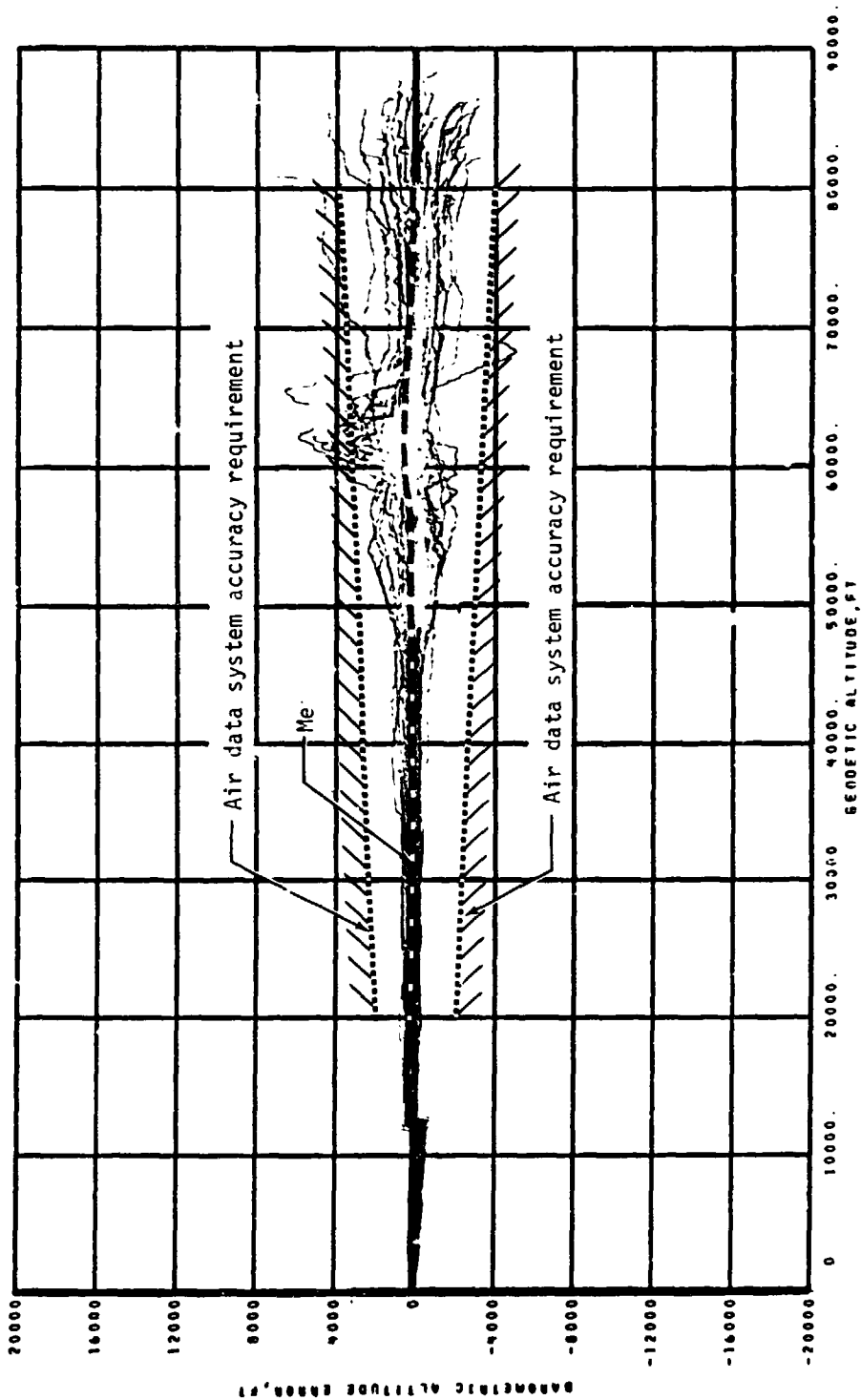
(d) Barometric altitude error.

Figure 3.- Concluded.

28
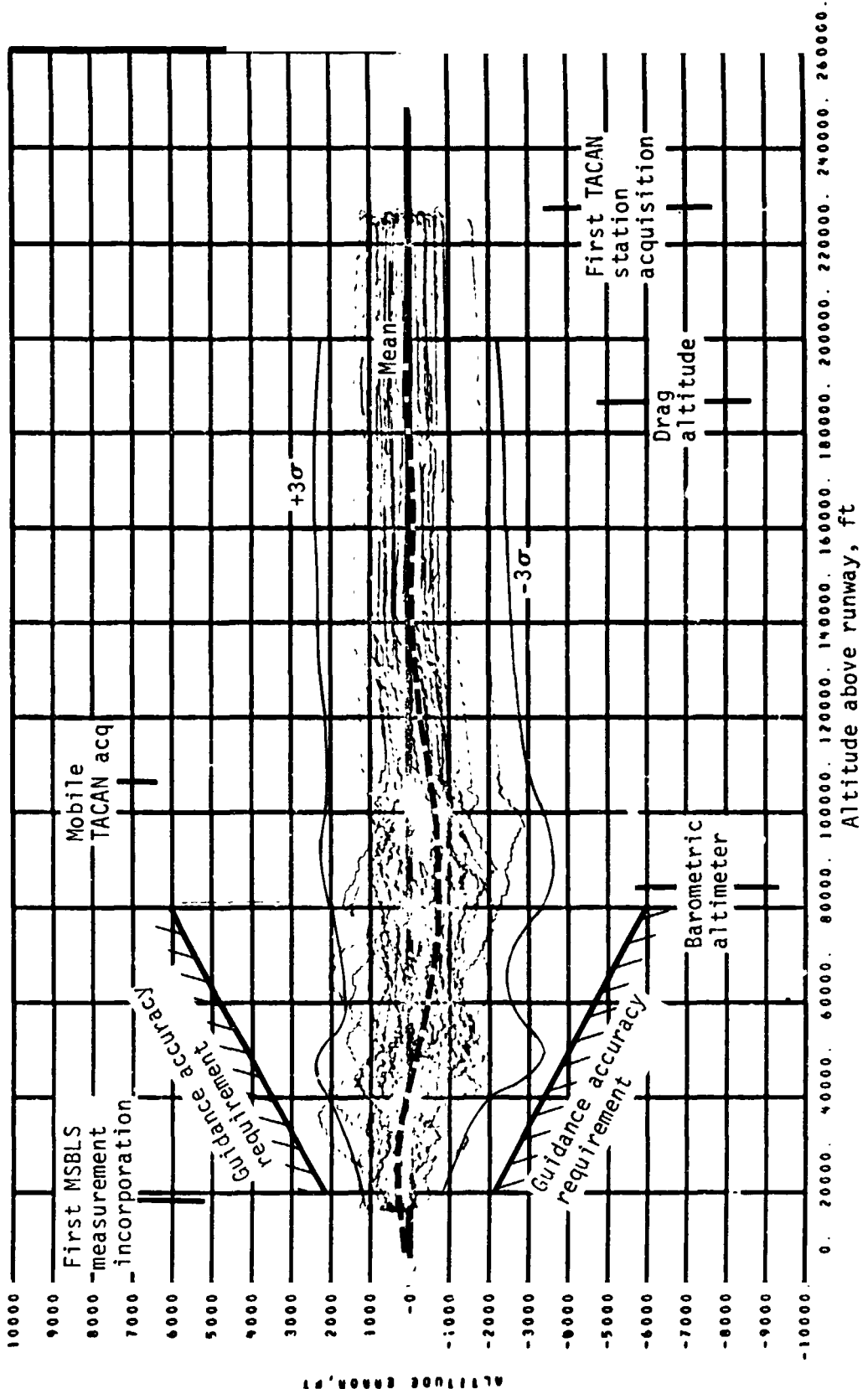
(a) Altitude error.

Figure 4.- Navigated state vector performance - GRTLS.

29
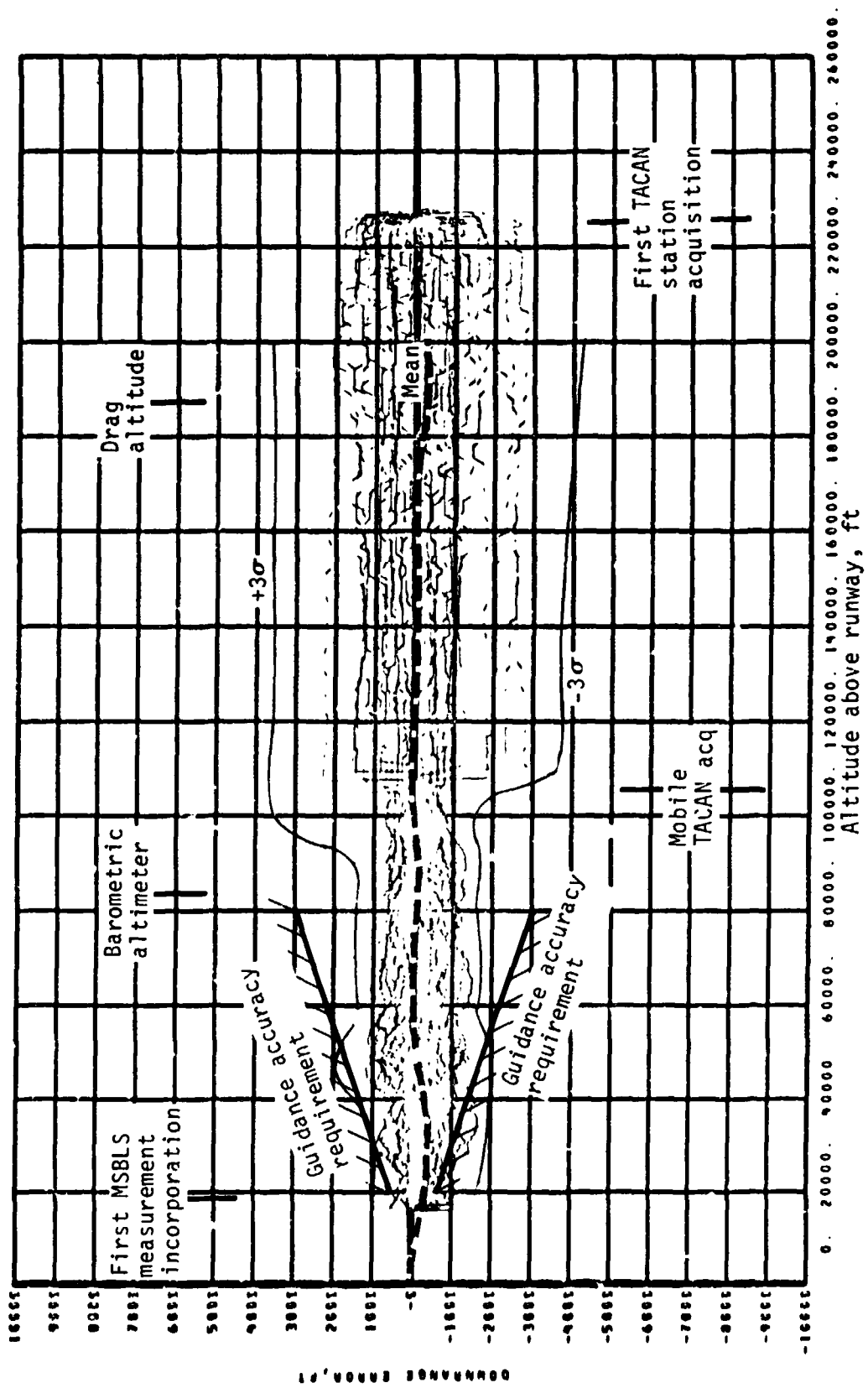
(b) Downrange error.

Figure 4.- Continued.

30
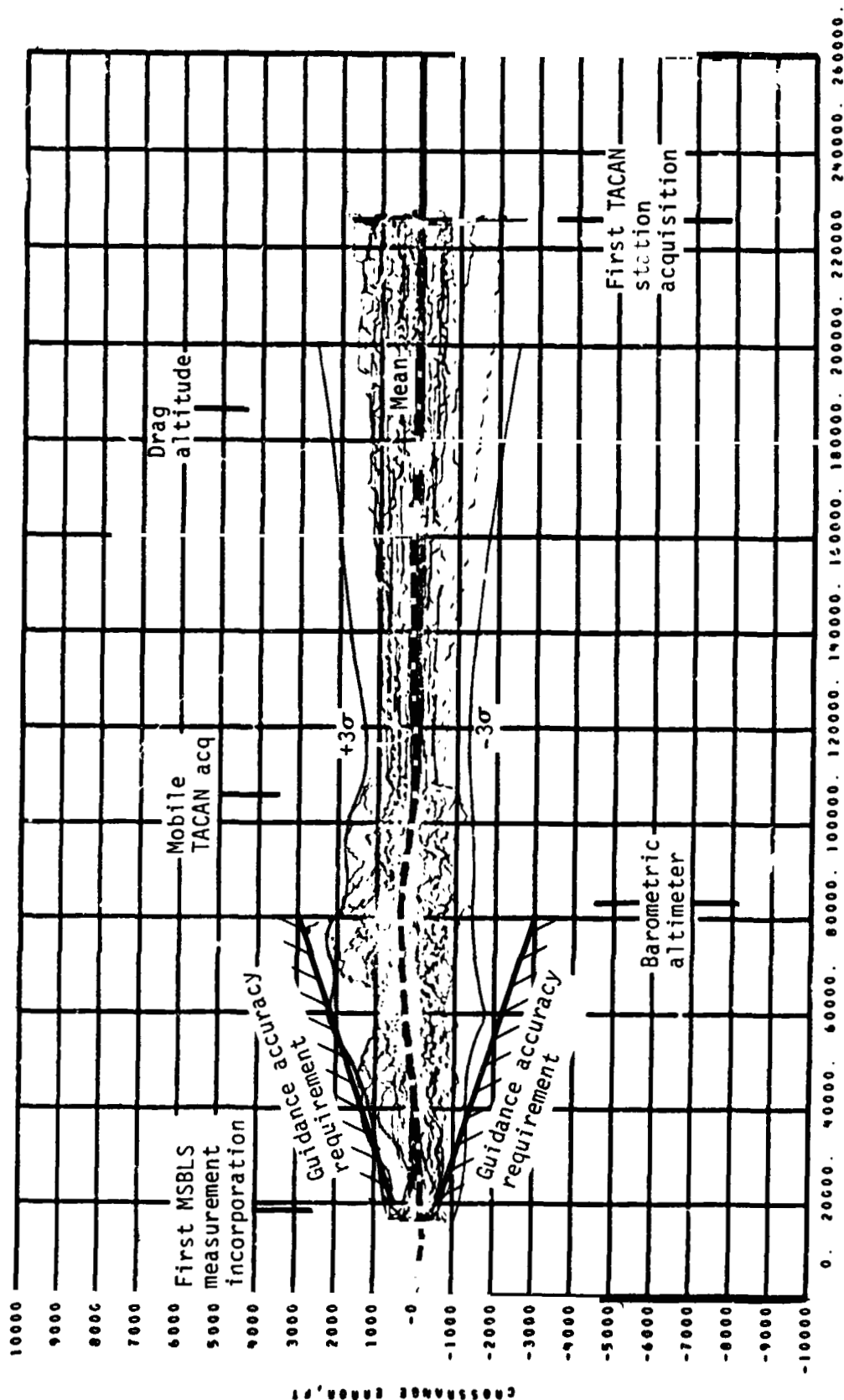
(c) Crossrange error.

Figure 4.- Continued

31
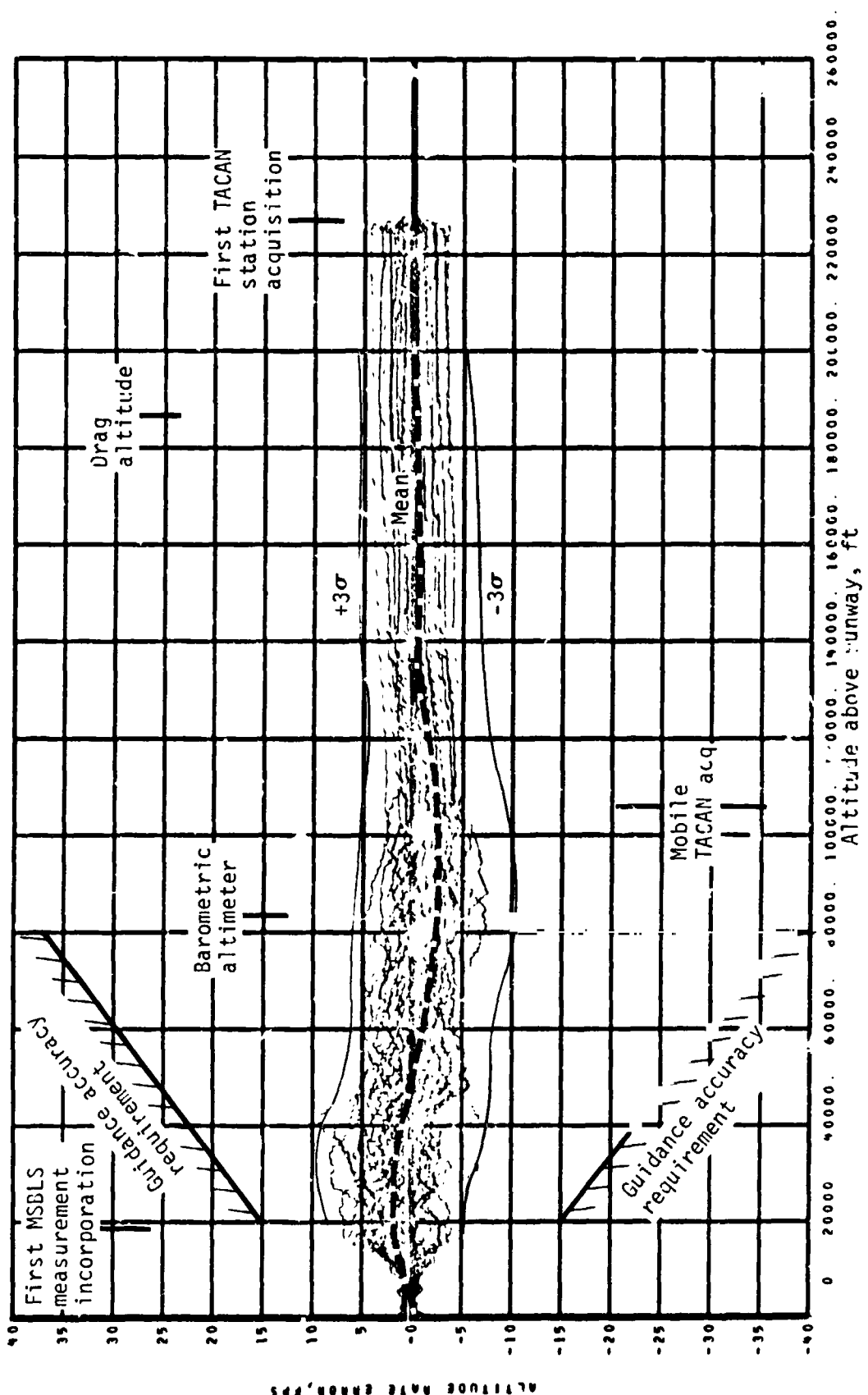
(d) Altitude rate error.

Figure 4.- Continued.

32
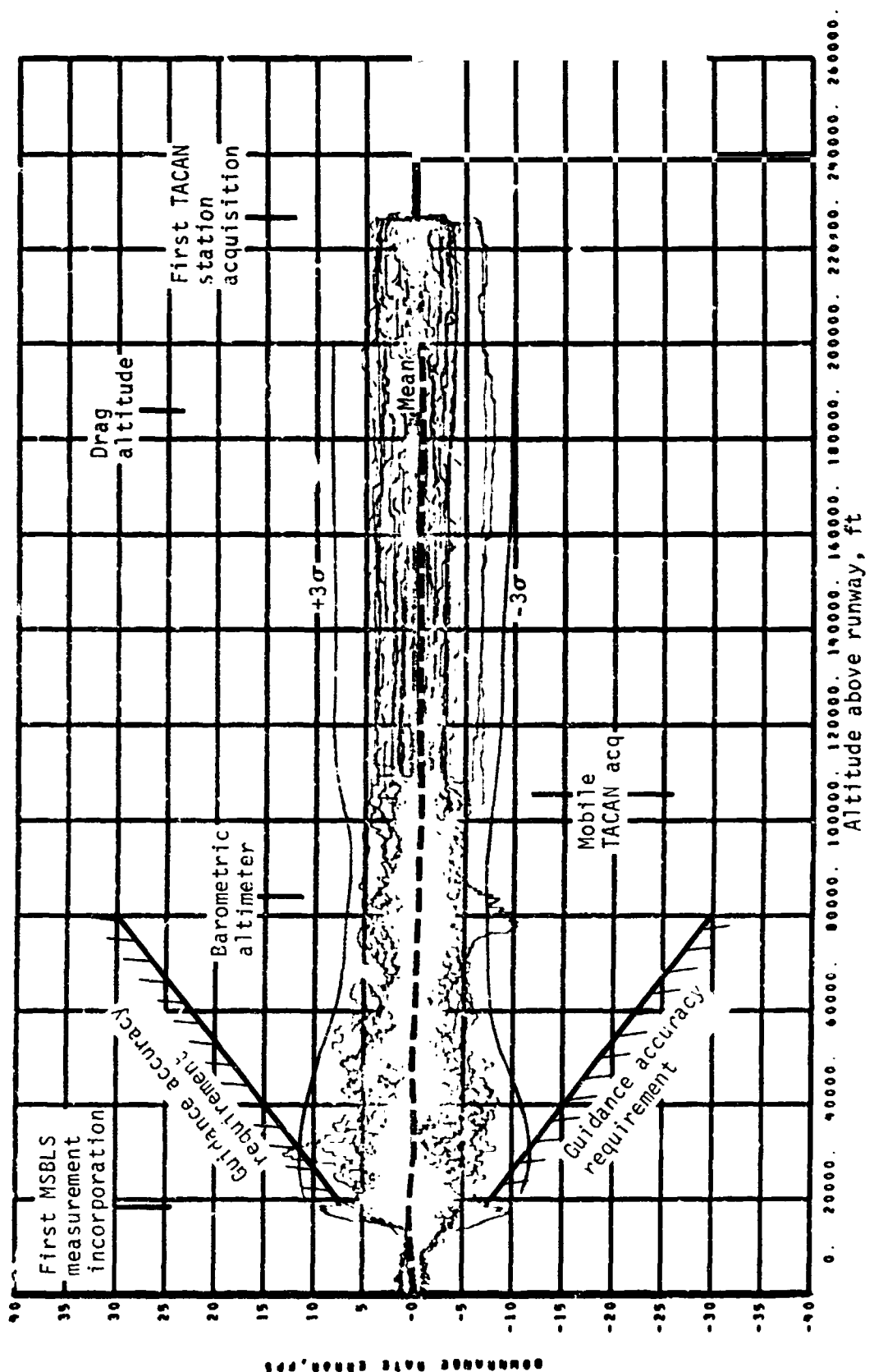
(e) Downrange rate error.

Figure 4.- Continued.

33
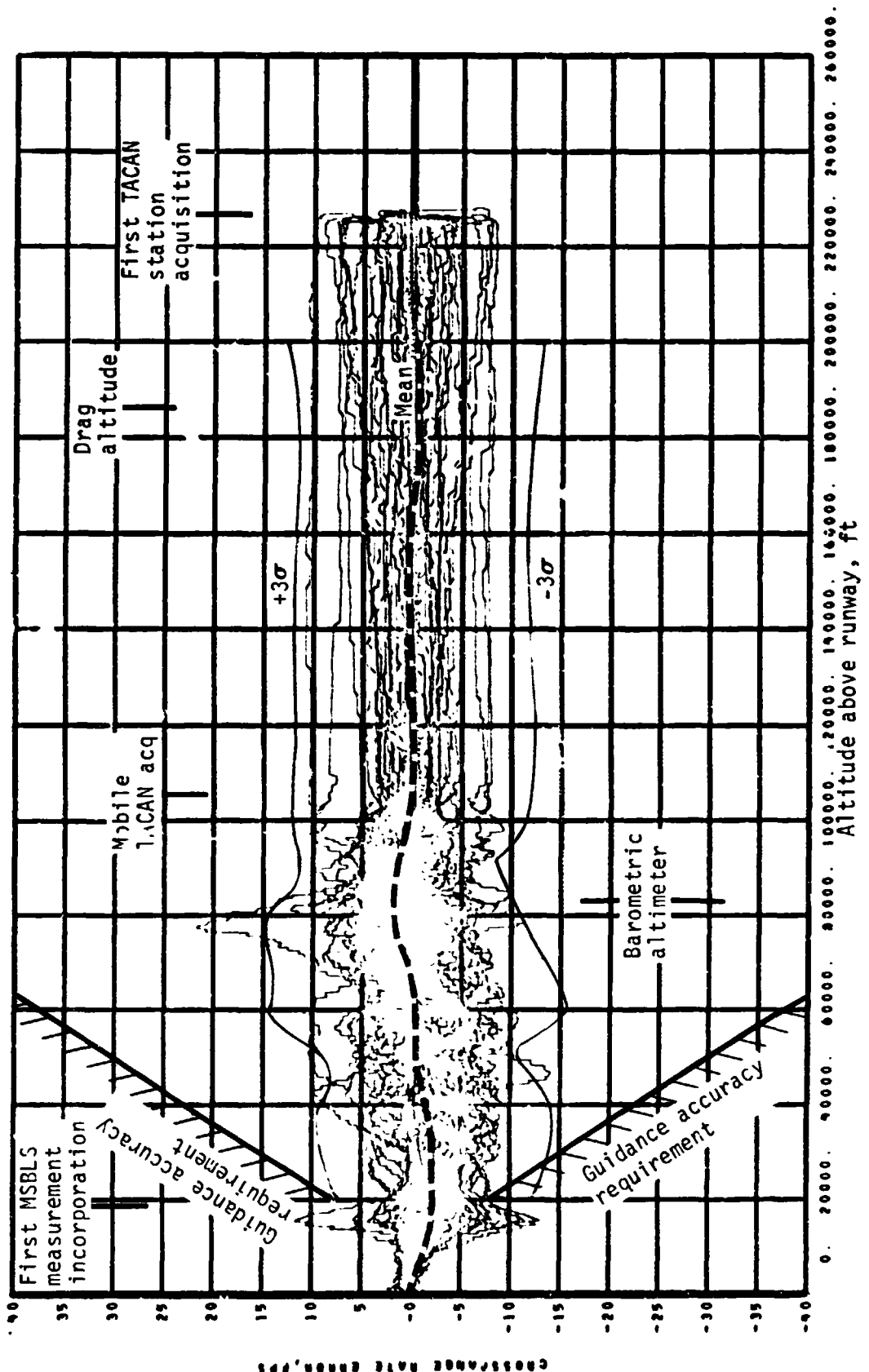
(f) Crossrange rate error.

Figure 4.- Continued.

34
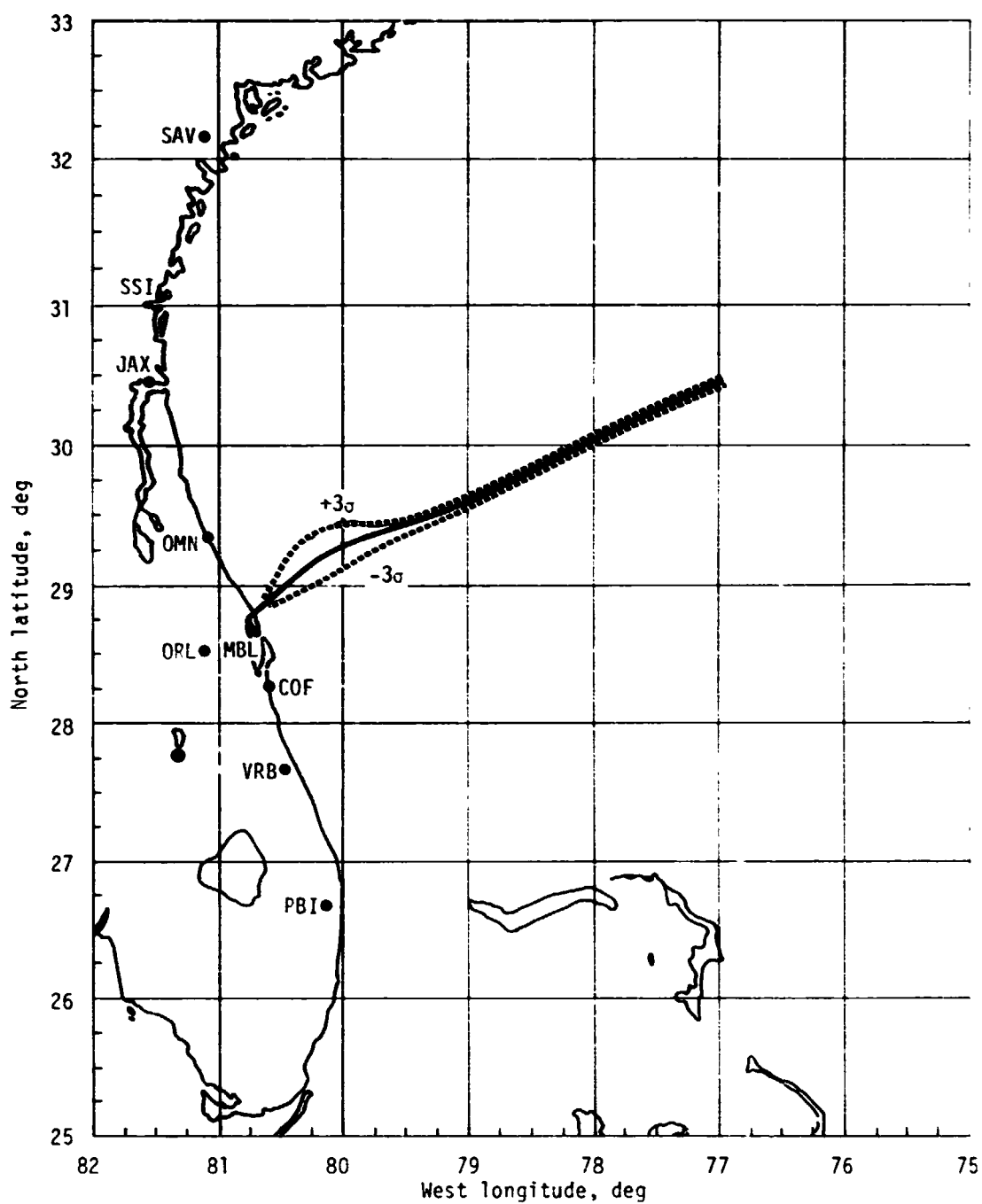
(g) TACAN station locations and groundtrack.

Figure 4.- Concluded.

(a) Elevon deflection.
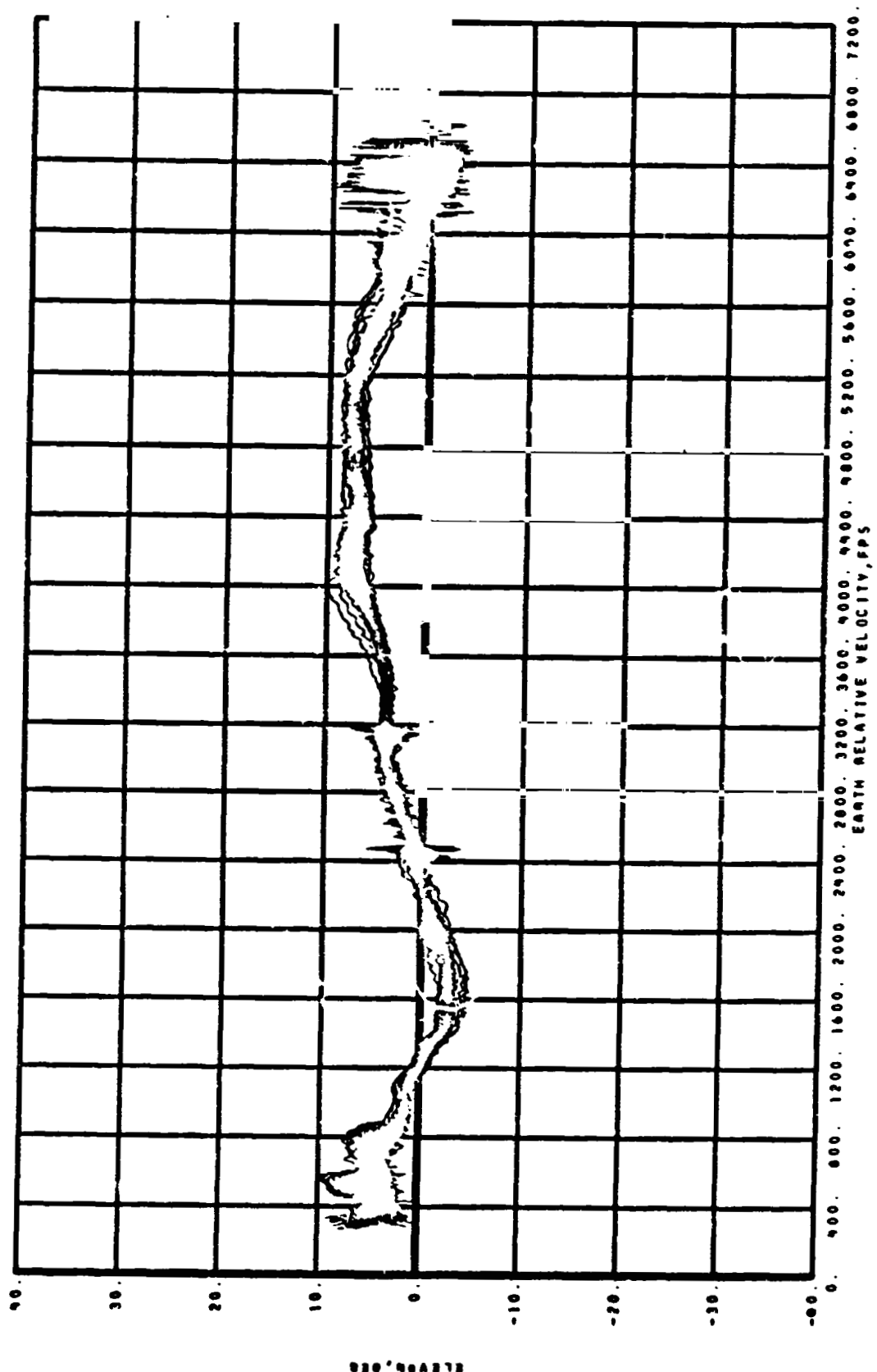
Figure 5.- Control surface deflections - hinge moments - GRTLS.

36
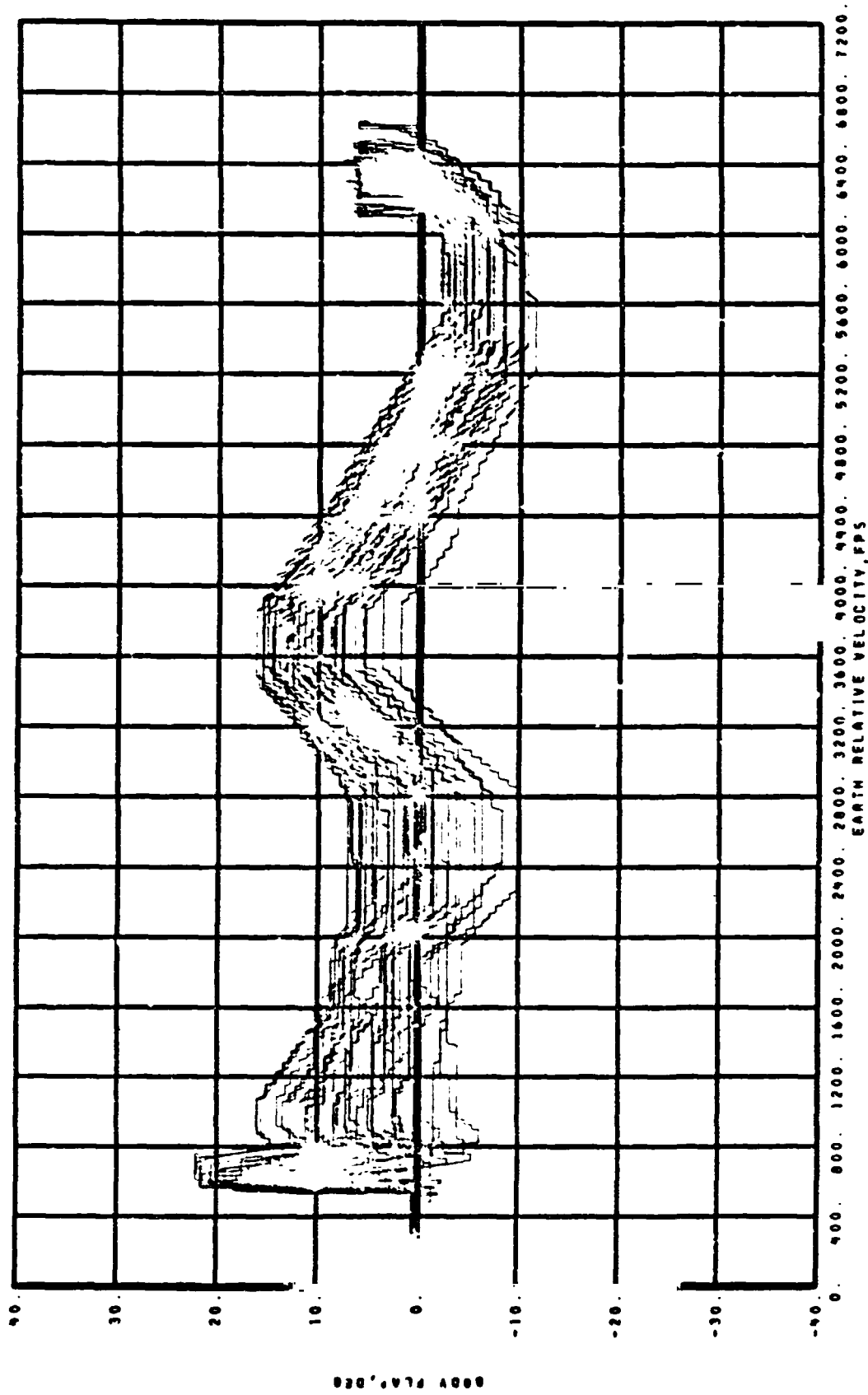
(b) Body-flap deflections.
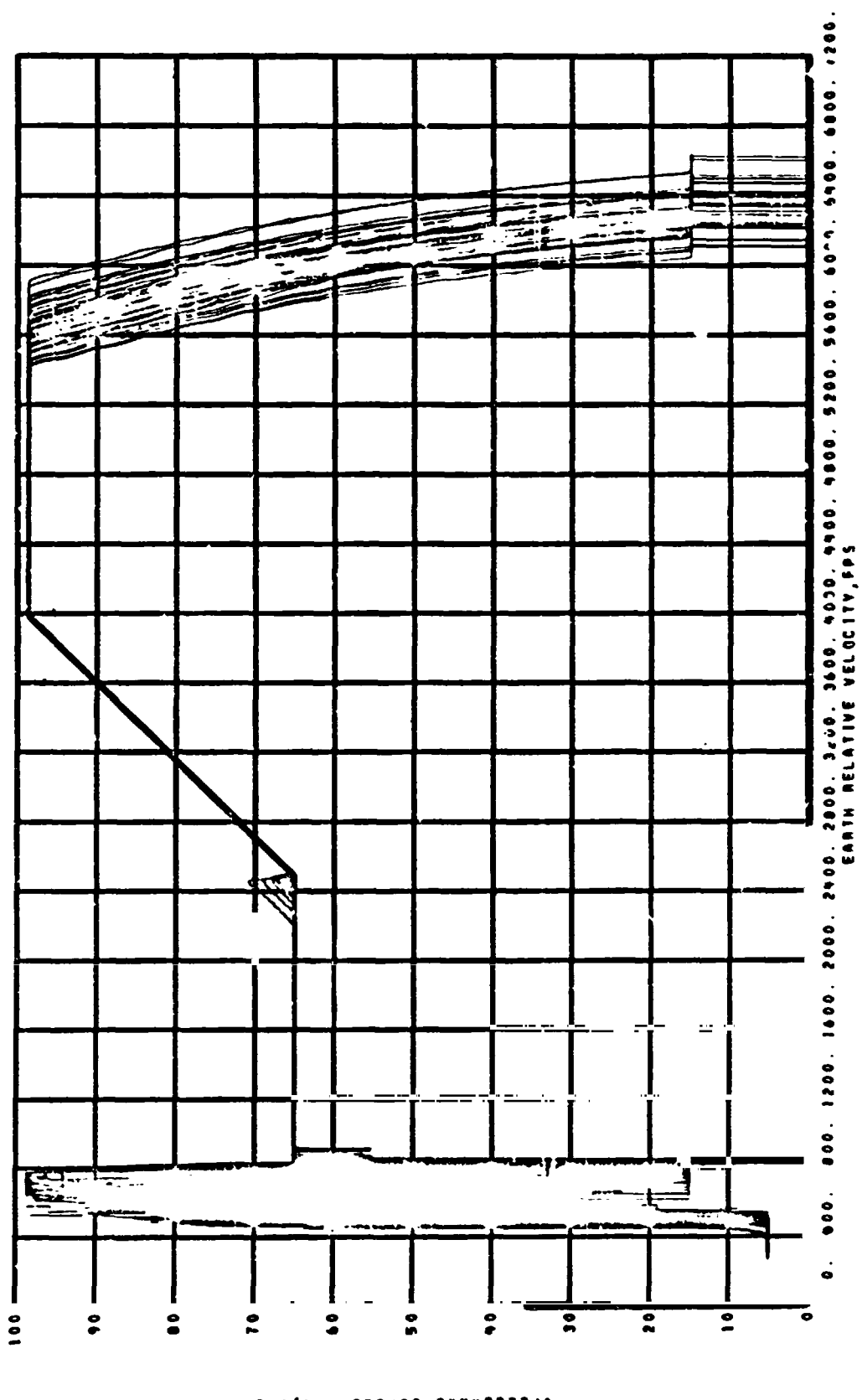
Figure 5.- Continued.

(c) Speedbrake deflections.
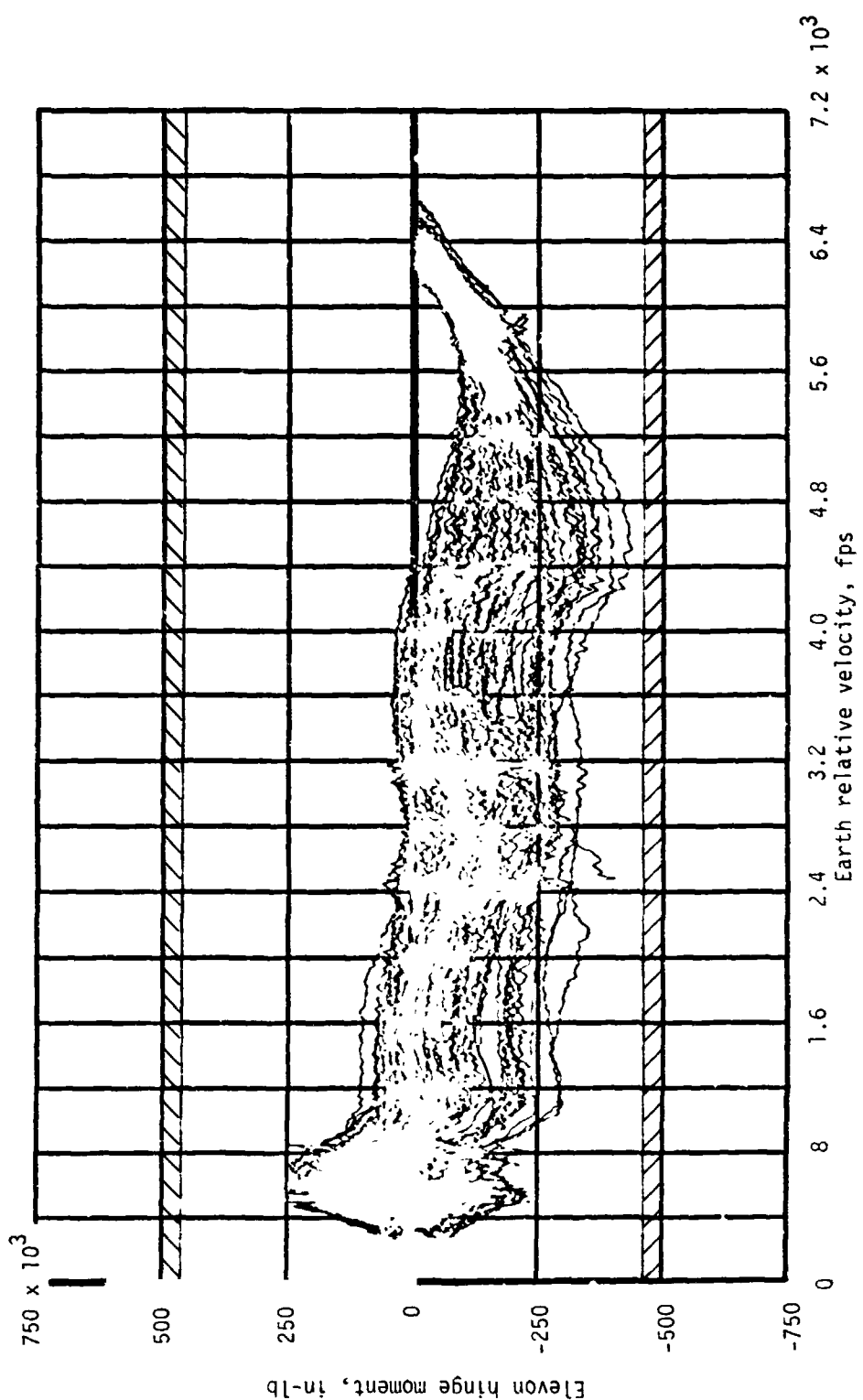
Figure 5.- Continued.

(d) Outboard elevon hinge moments.
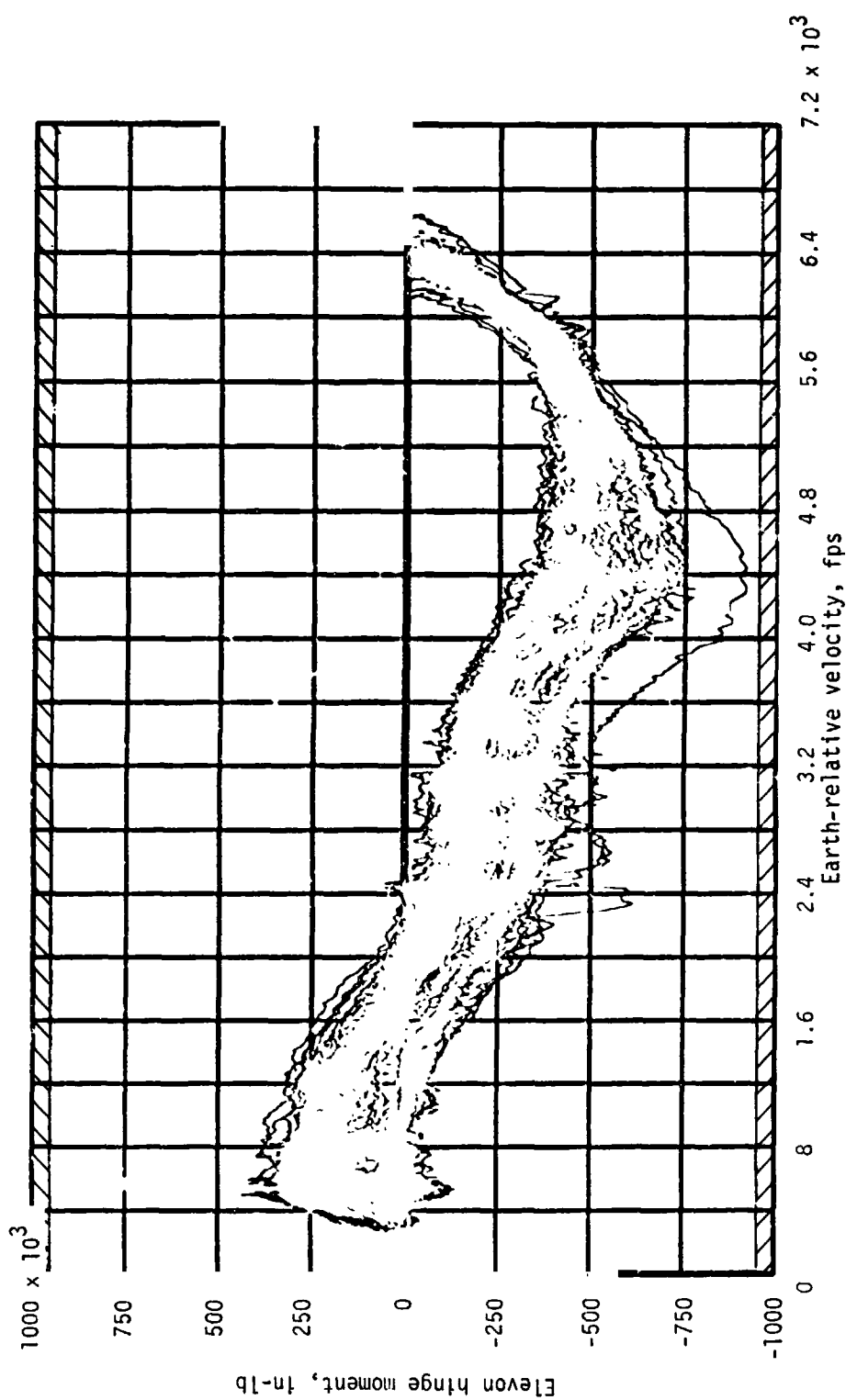
Figure 5.- Continued.

(e) Inboard elevon hinge moments.
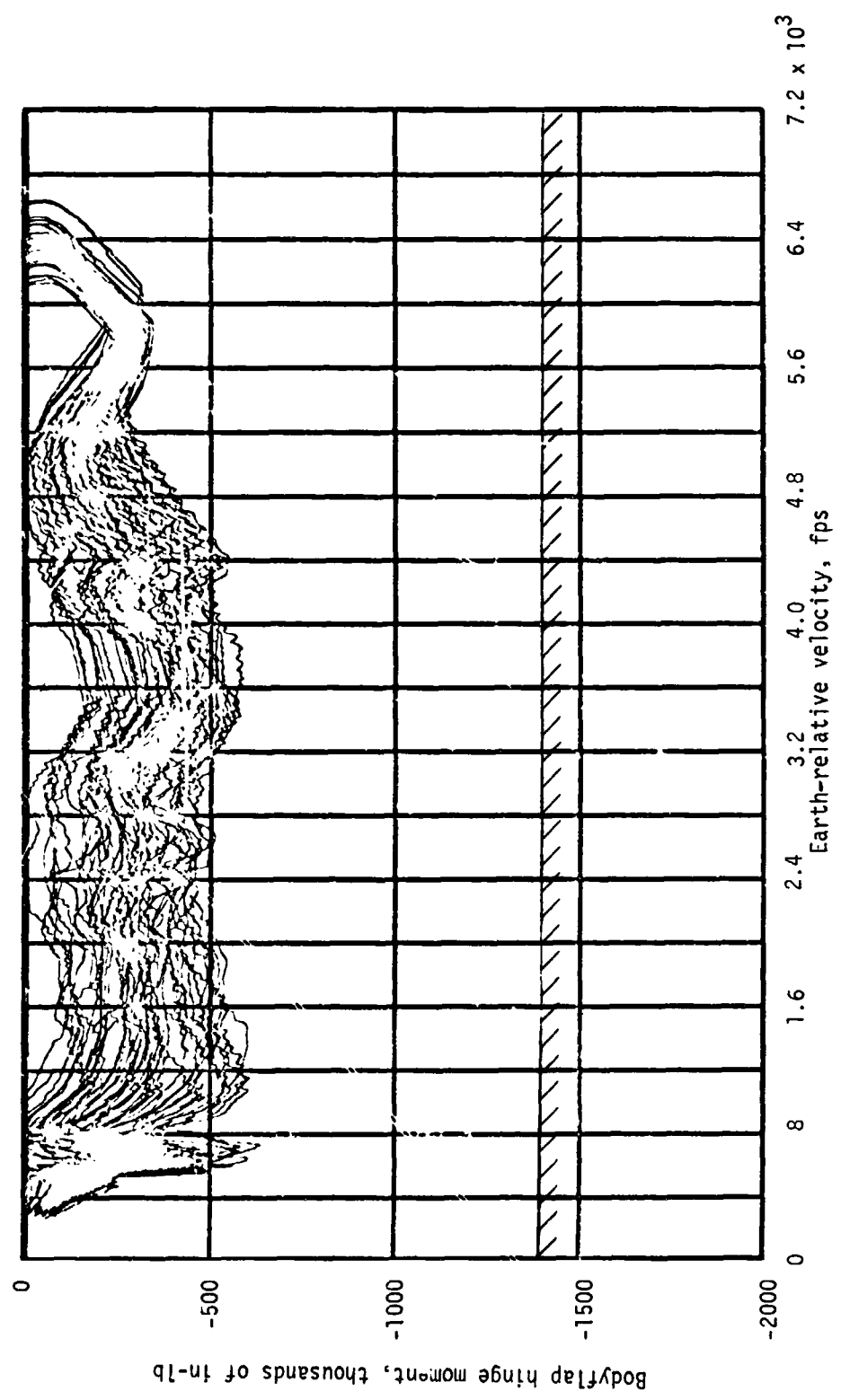
Figure 5.- Continued.

(f) Body-flap hinge moments.
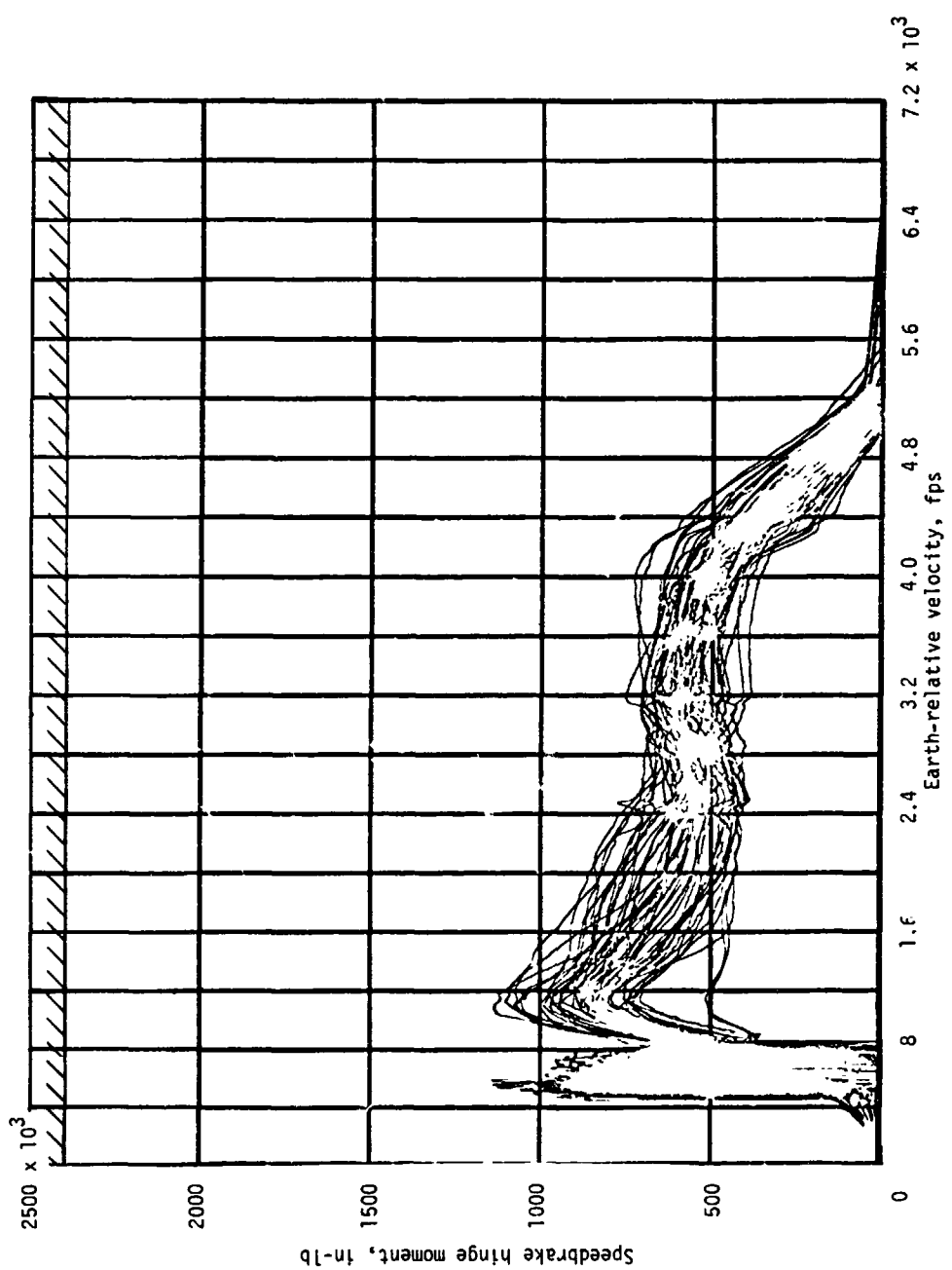
Figure 5.- Continued.

(g) Speedbrake hinge moments.

Figure 5.- Concluded.

42
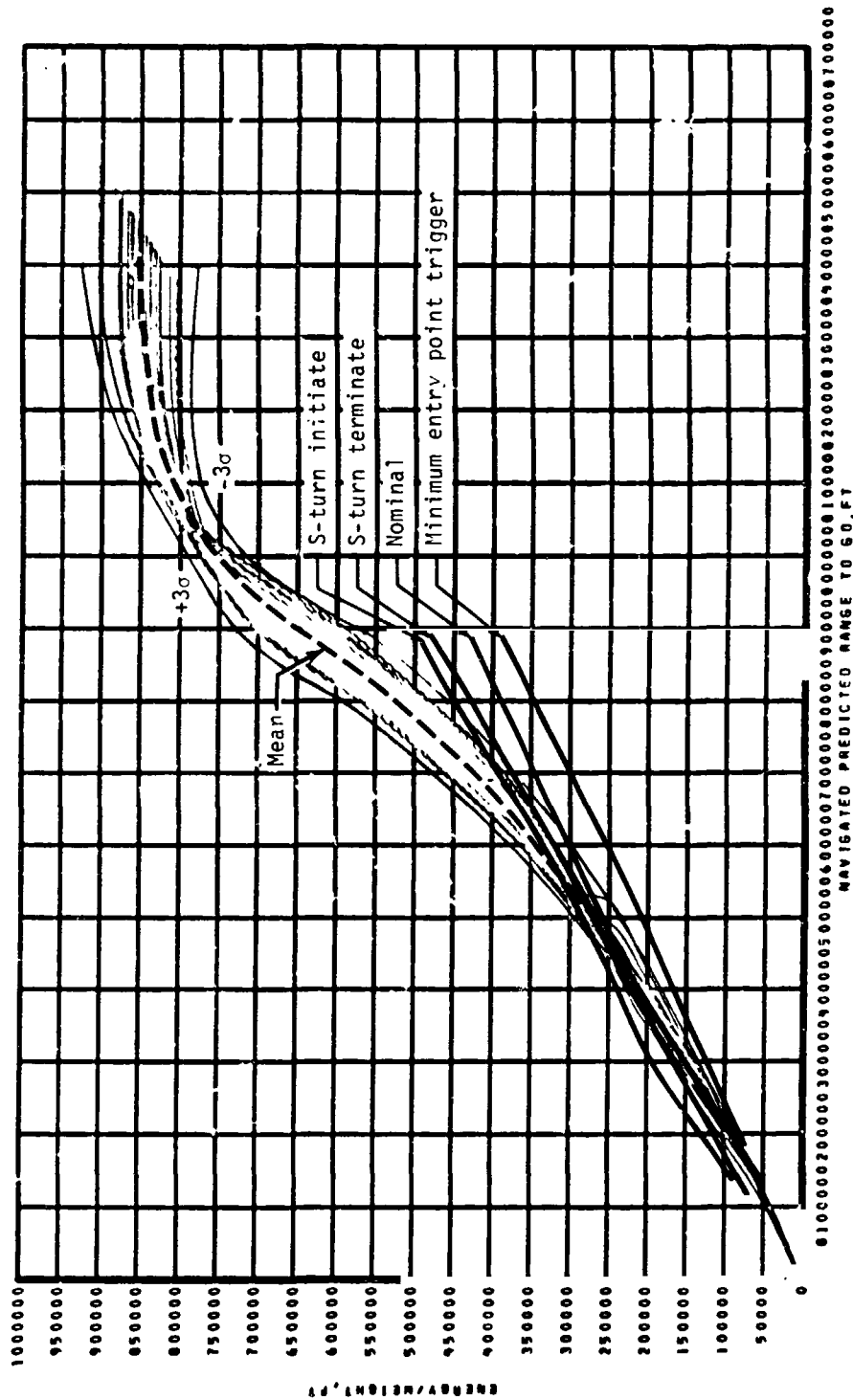
(a) Energy/weight.

Figure 6.- GRTLS guidance performance.

43
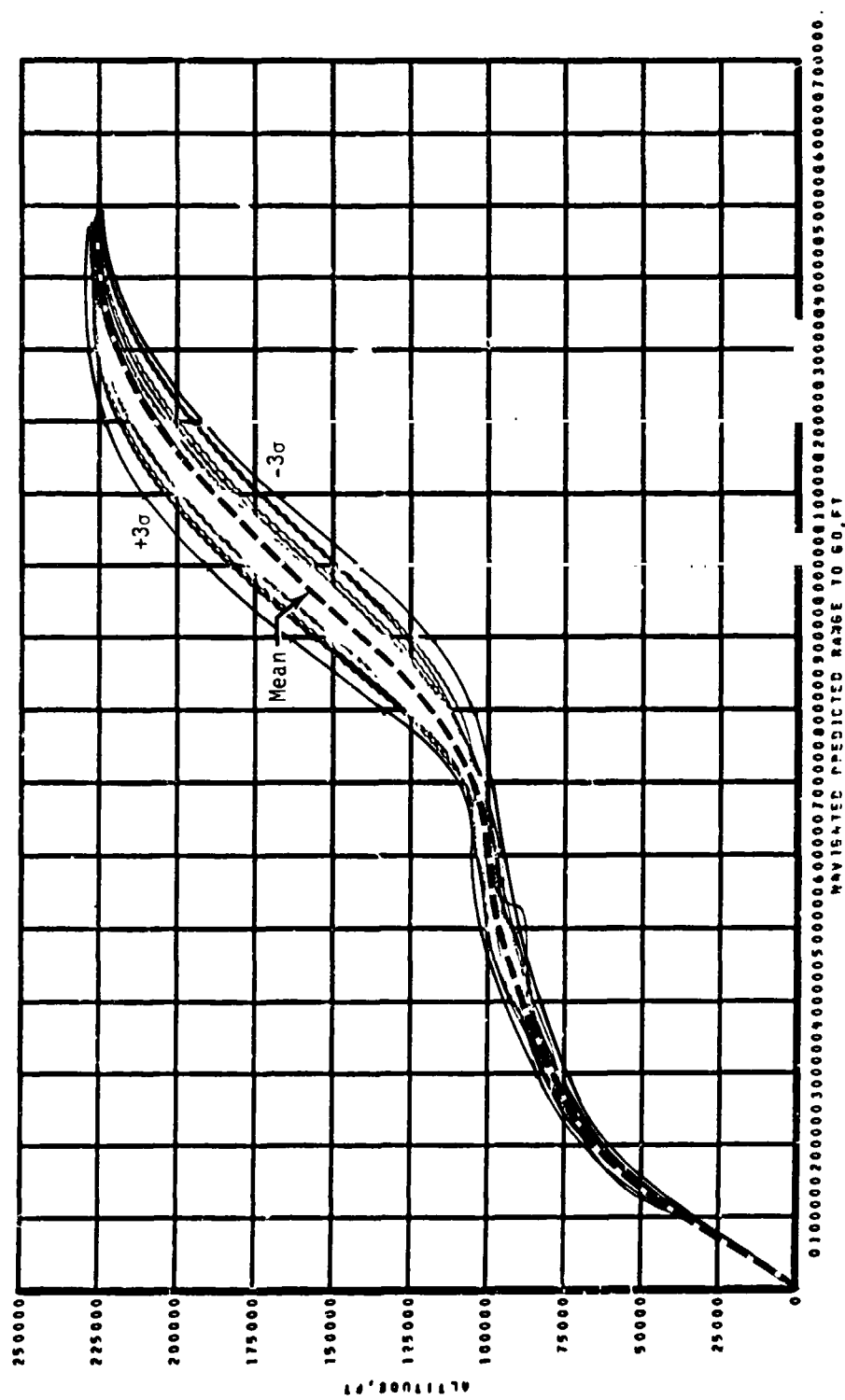
(b) Altitude

Figure 6.- Continued.

44
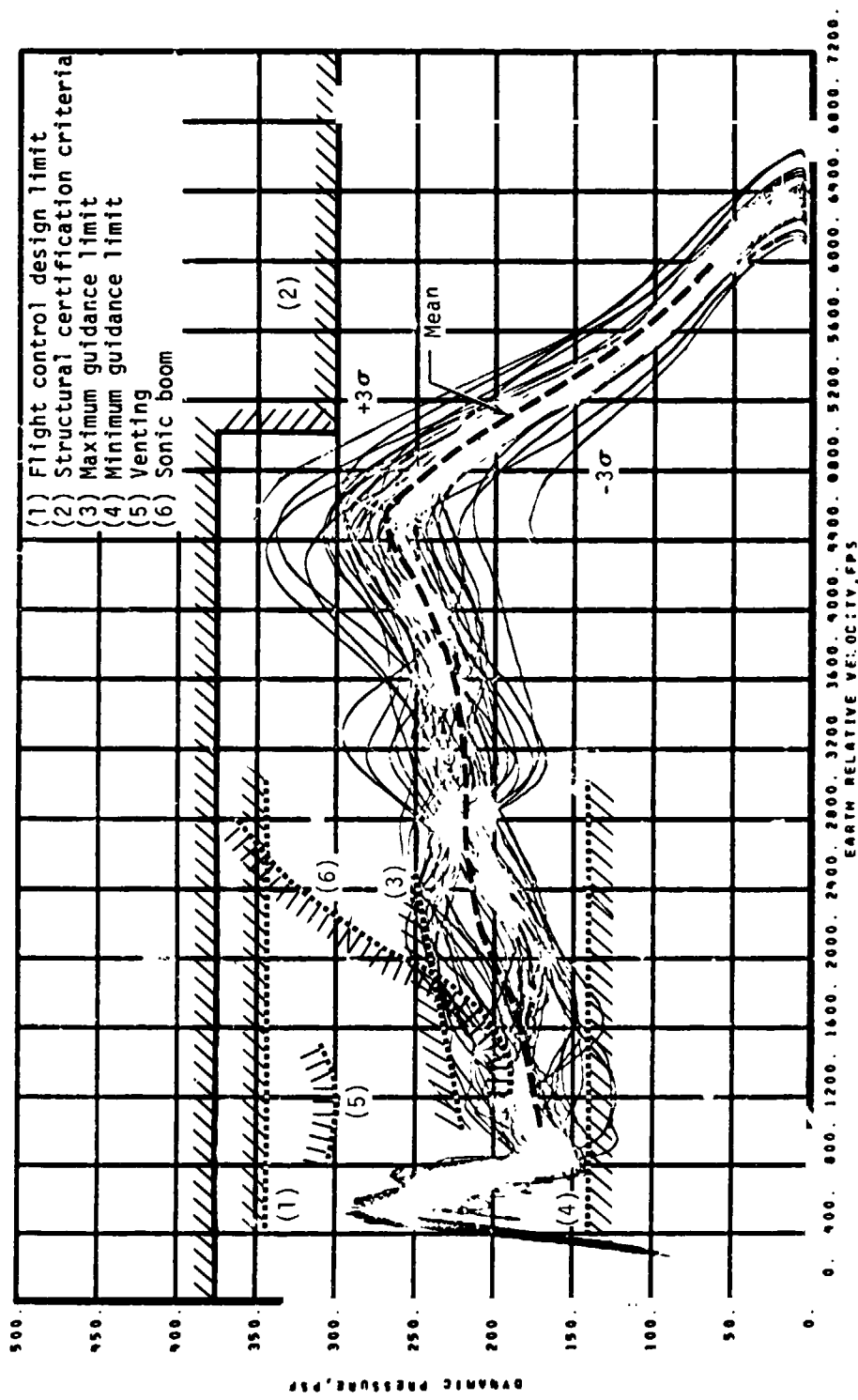
(c) Dynamic pressure.

Figure 6. – Continued.

45
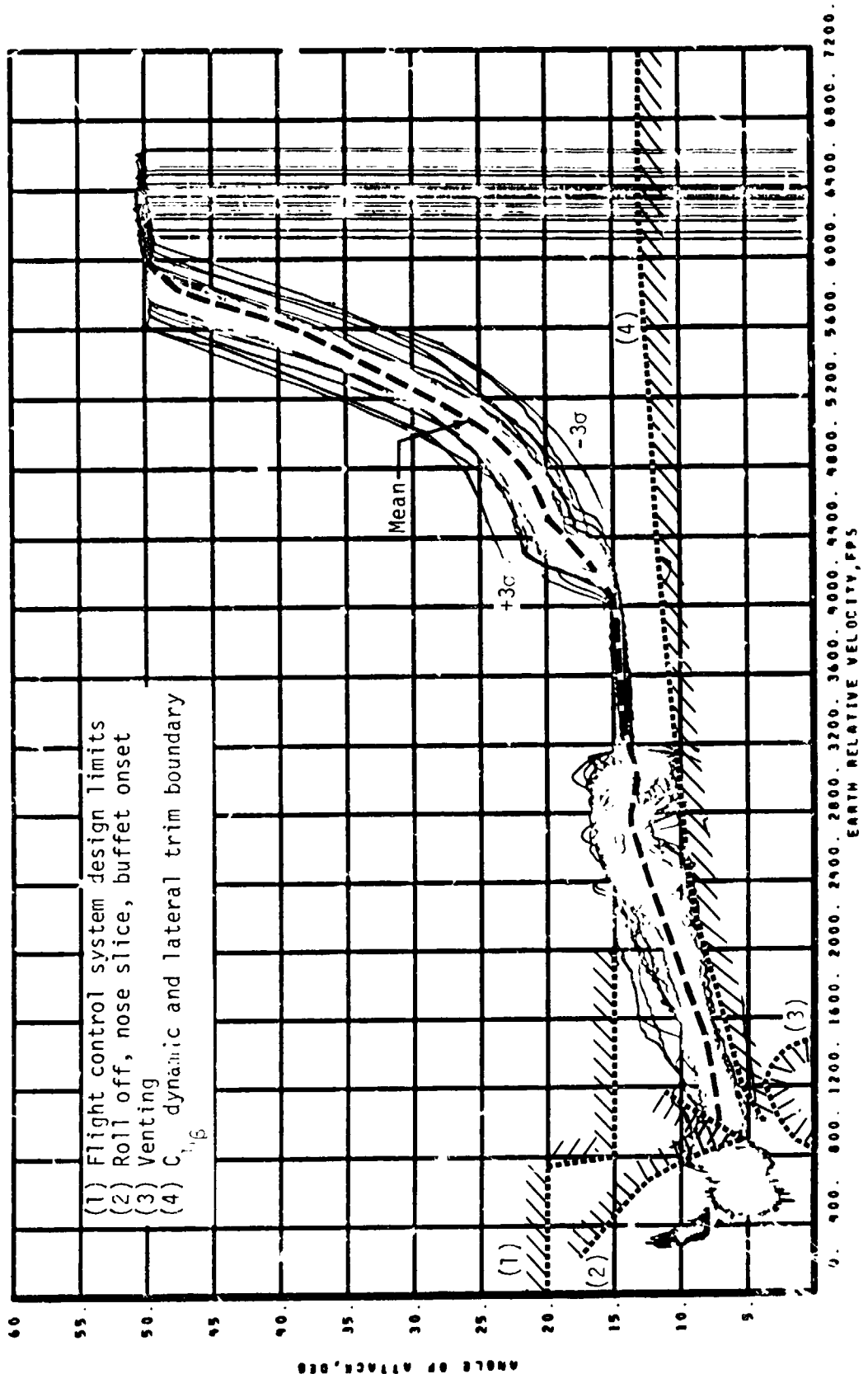
(d) Angle of attack.

Figure 6.- Continued.

46
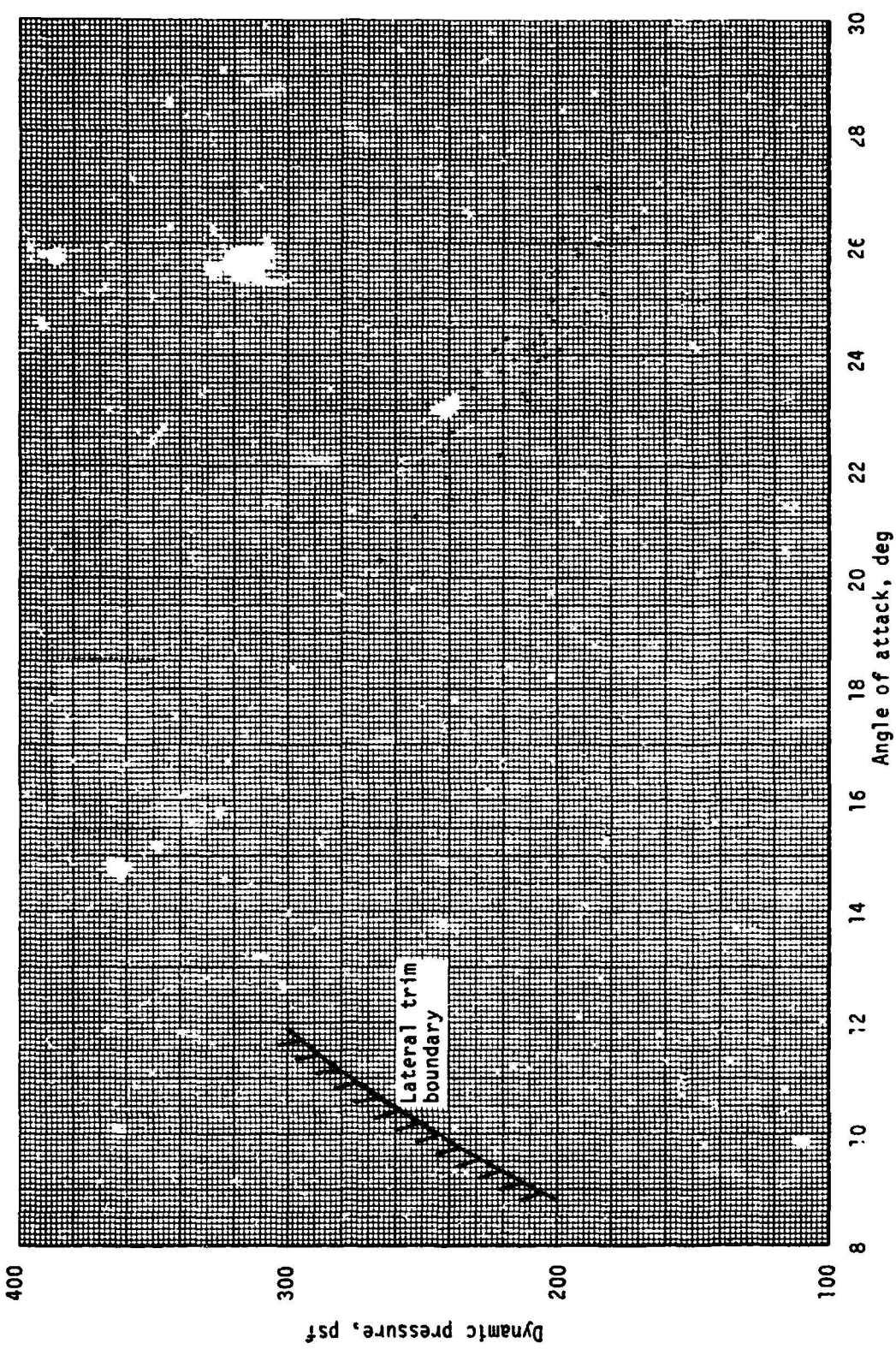
(e) Dynamic pressure - angle-of-attack scatter plot - Mach = 5.0.

Figure 6.- Continued.

47
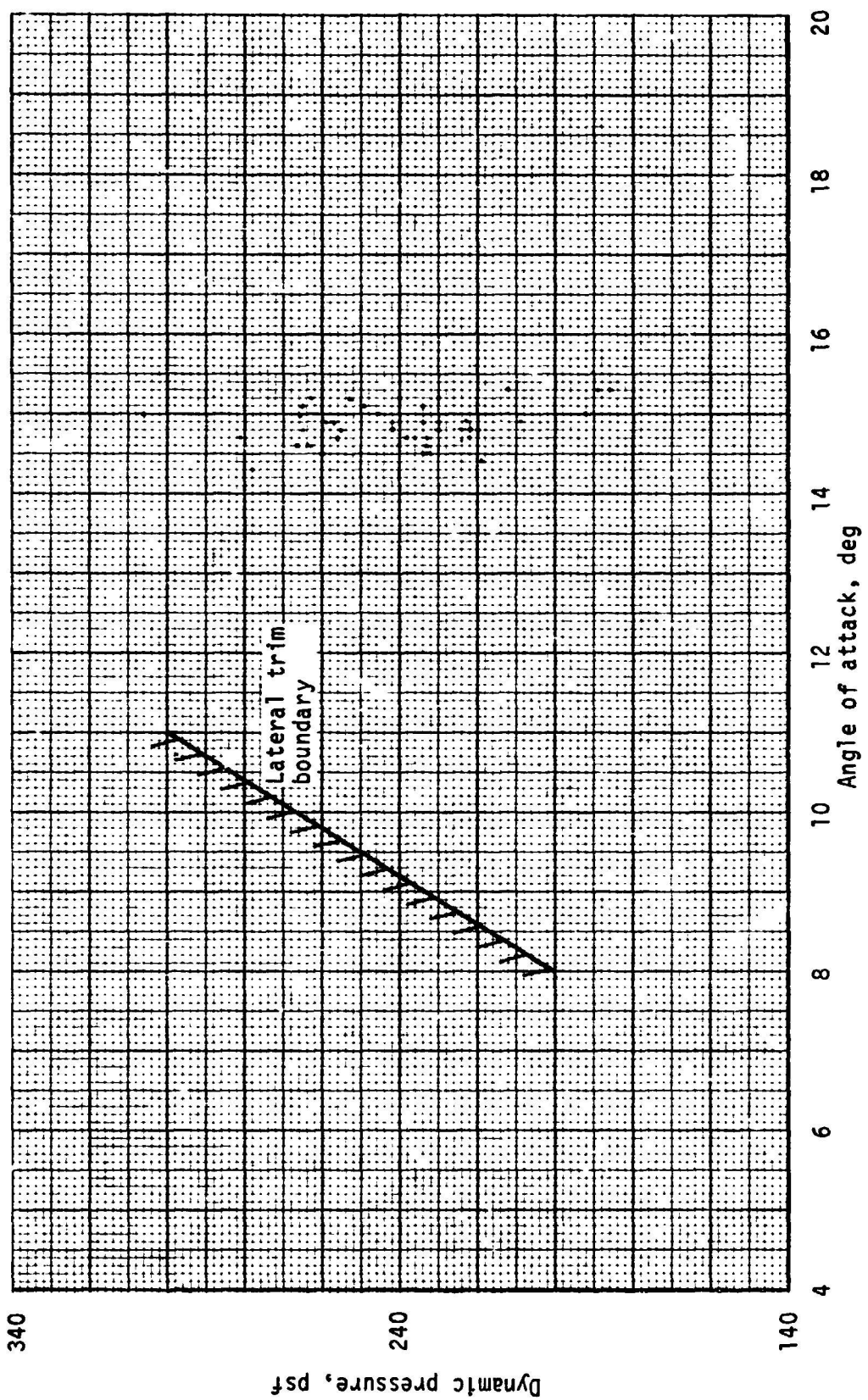
(f) Dynamic pressure - angle of attack - Mach = 4.0

Figure 6.- Continued.
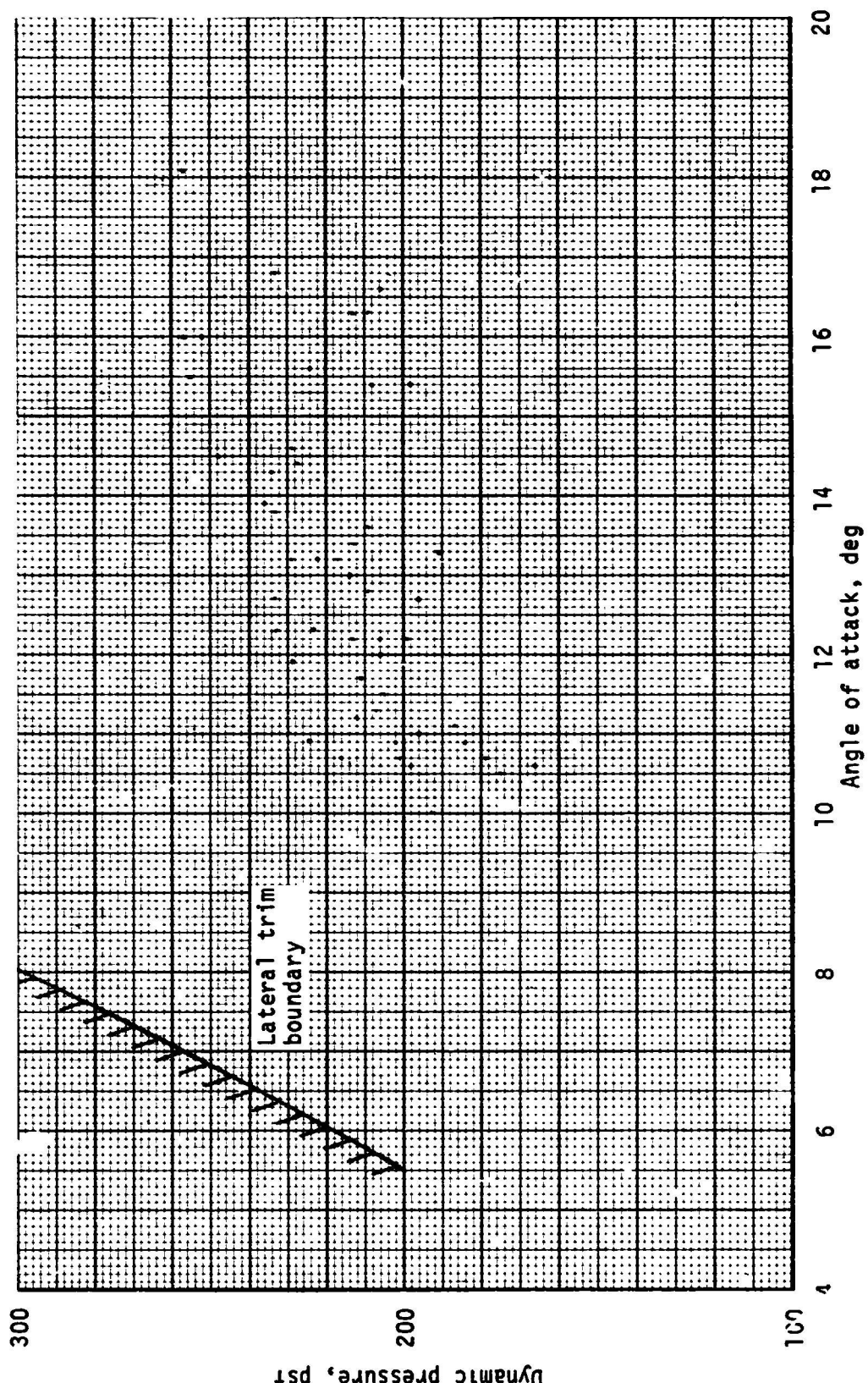
(g) Dynamic pressure - angle of attack - Mach = 3.0.

Figure 6.- Continued.
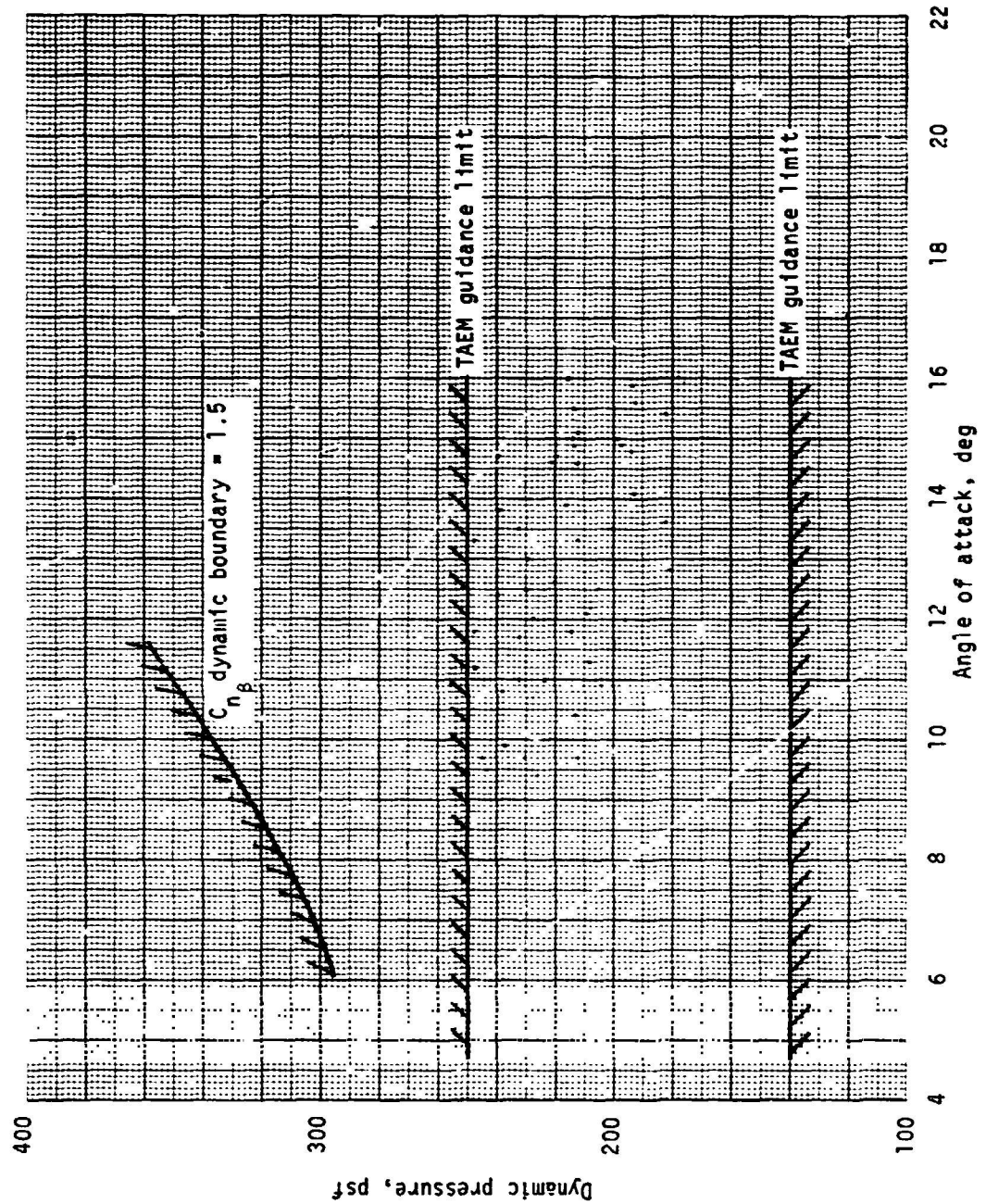
(h) Dynamic pressure - angle of attack - Mach = 2.5

Figure 6.- Continued.
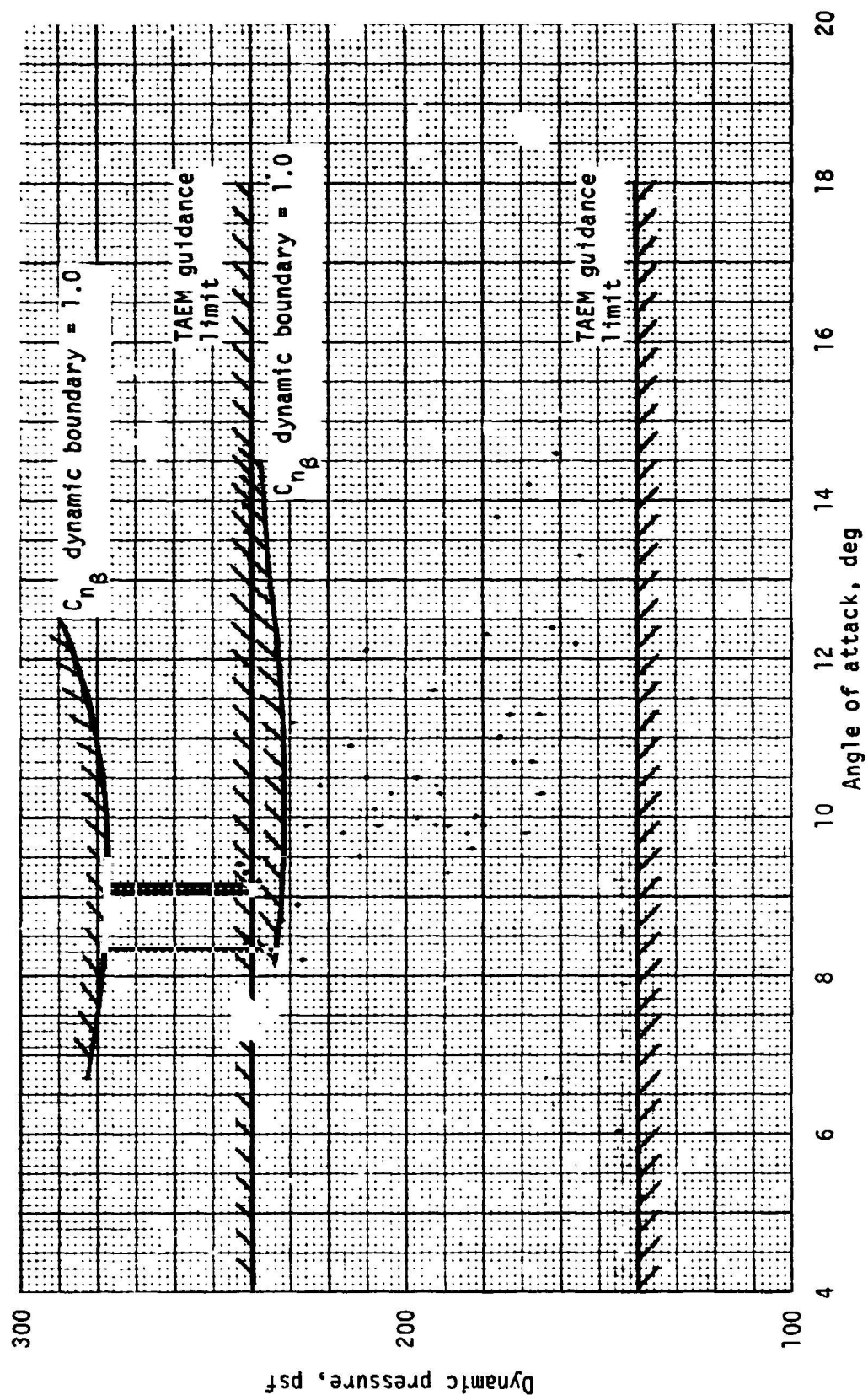
(1) Dynamic pressure - angle-of-attack scatter plot - Mach = 2.0

Figure 6.- Continued.
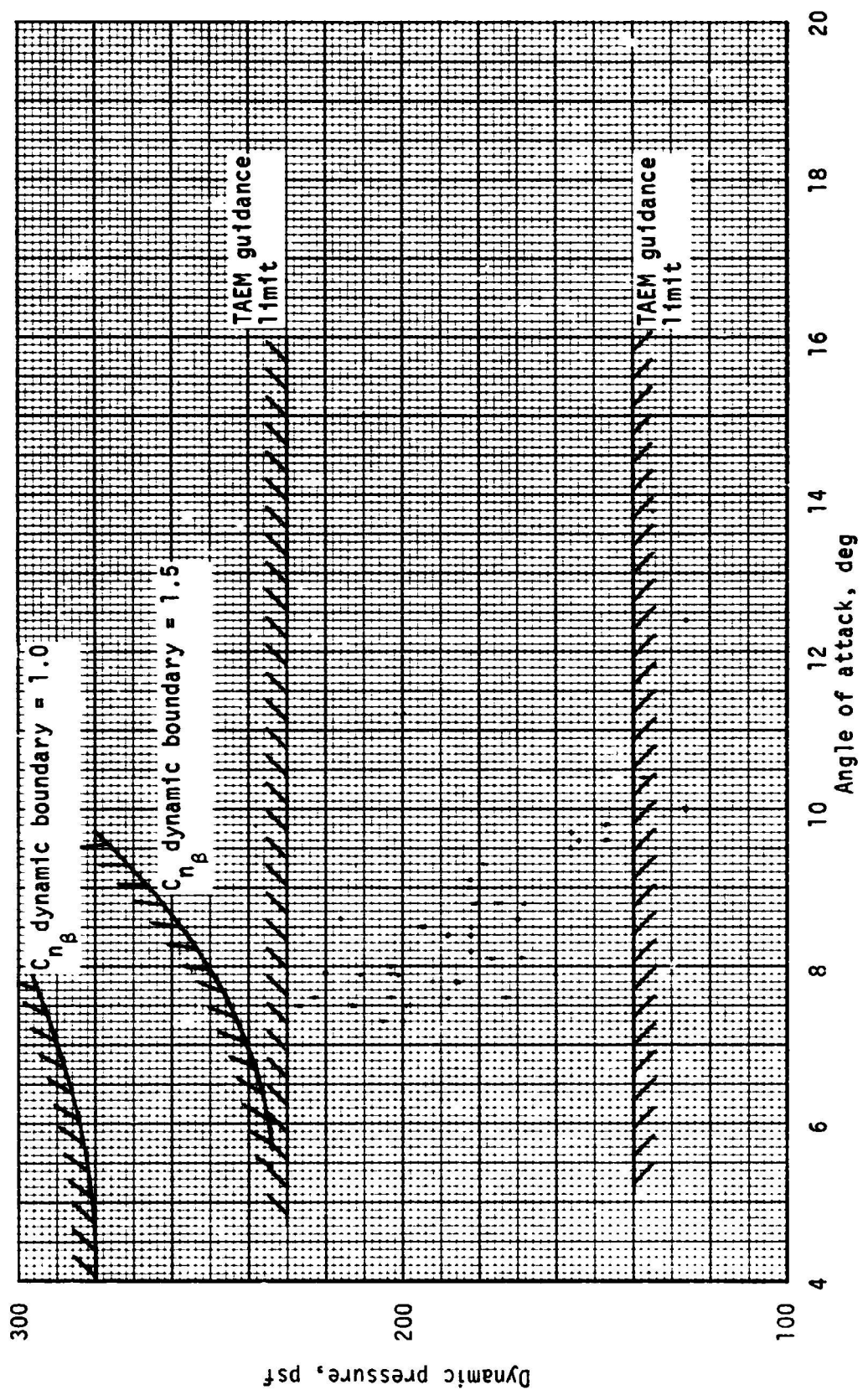
(j) Dynamic pressure - angle-of-attack scatter plot - Mach = 1.5.

Figure 6.- Continued.
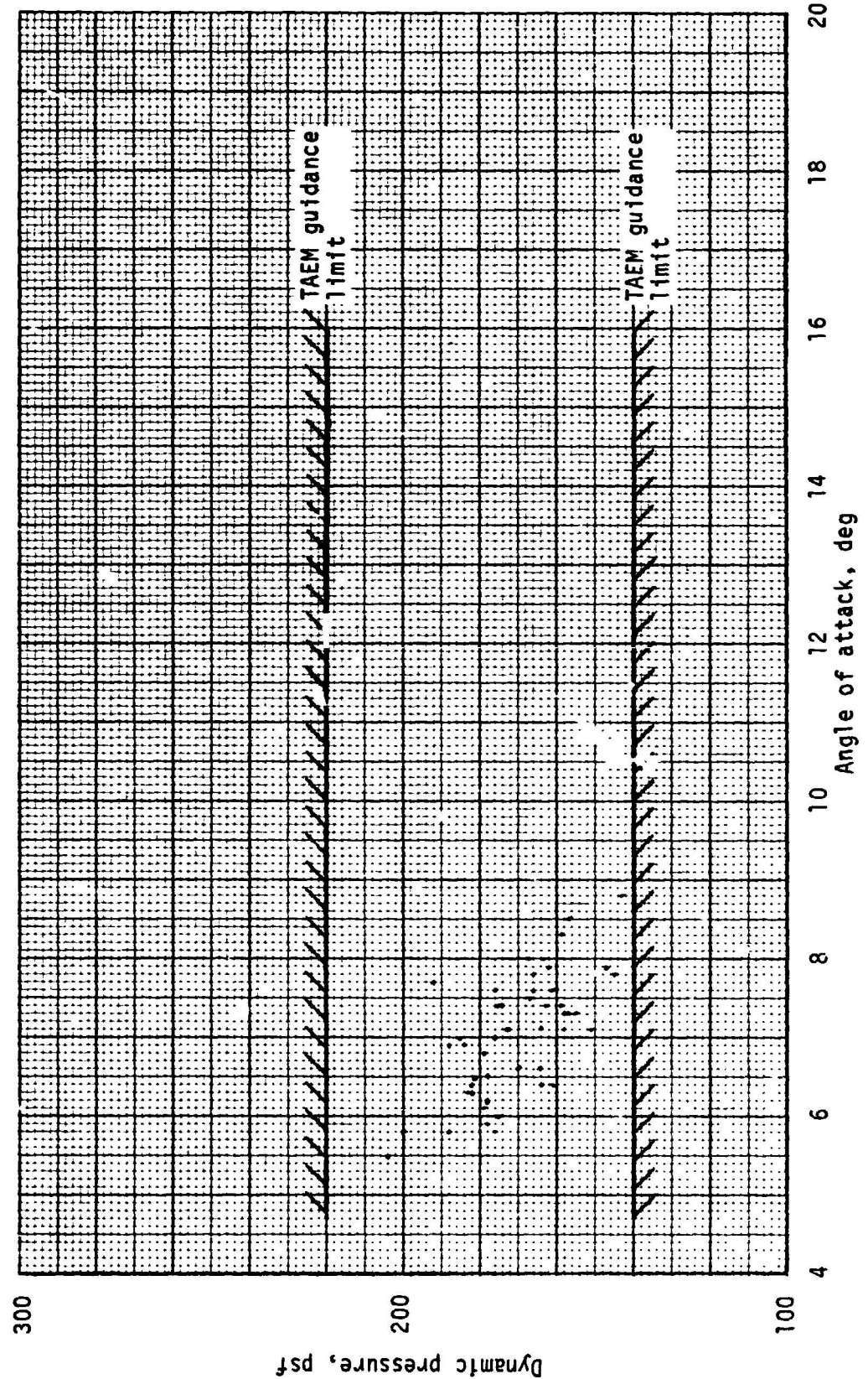
(k) Dynamic pressure - angle-of-attack scatter plot - Mach = 1.0.

Figure 6.- Continued.
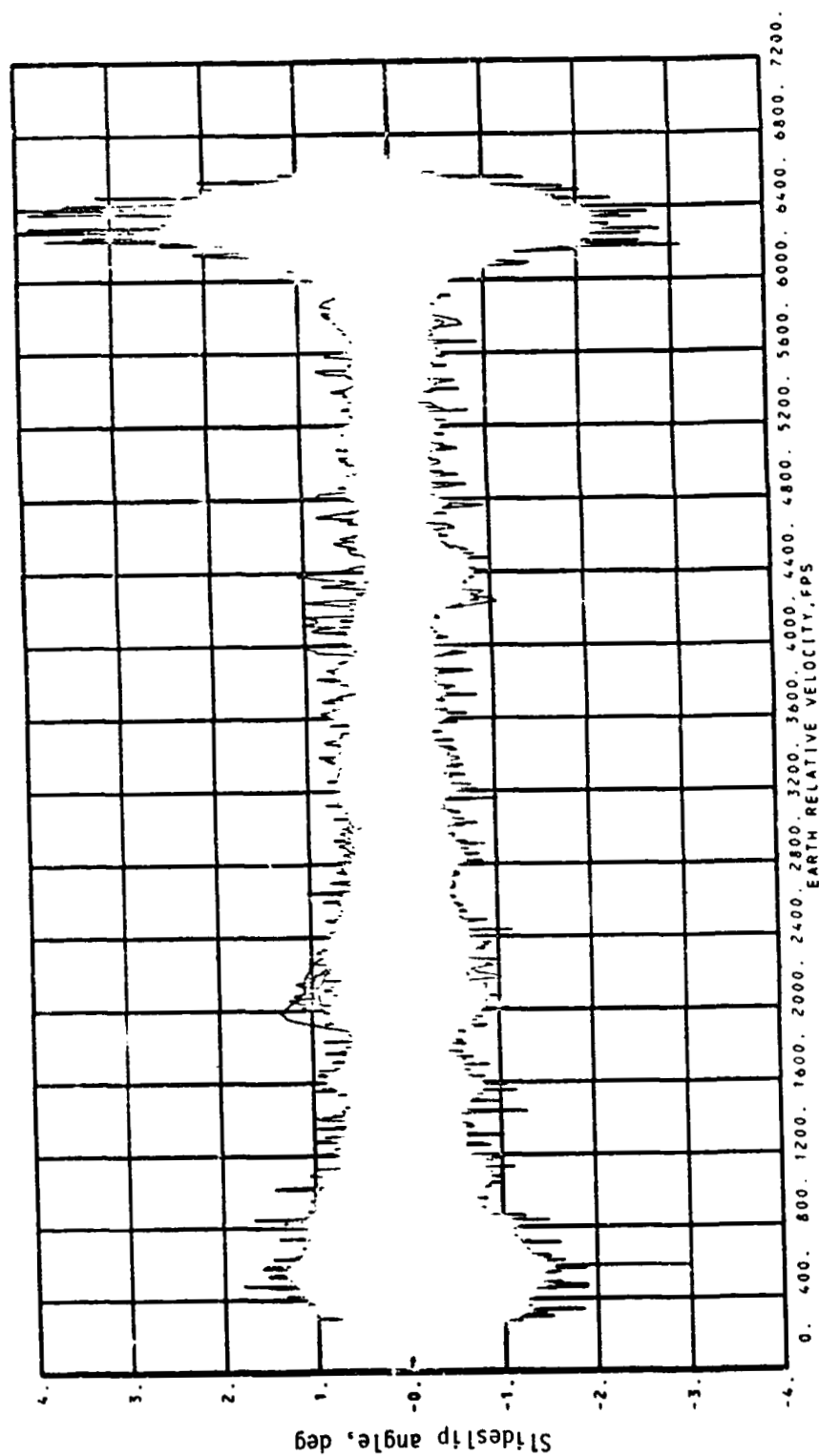
(1) Sideslip angle.

Figure 6.- Continued.

54
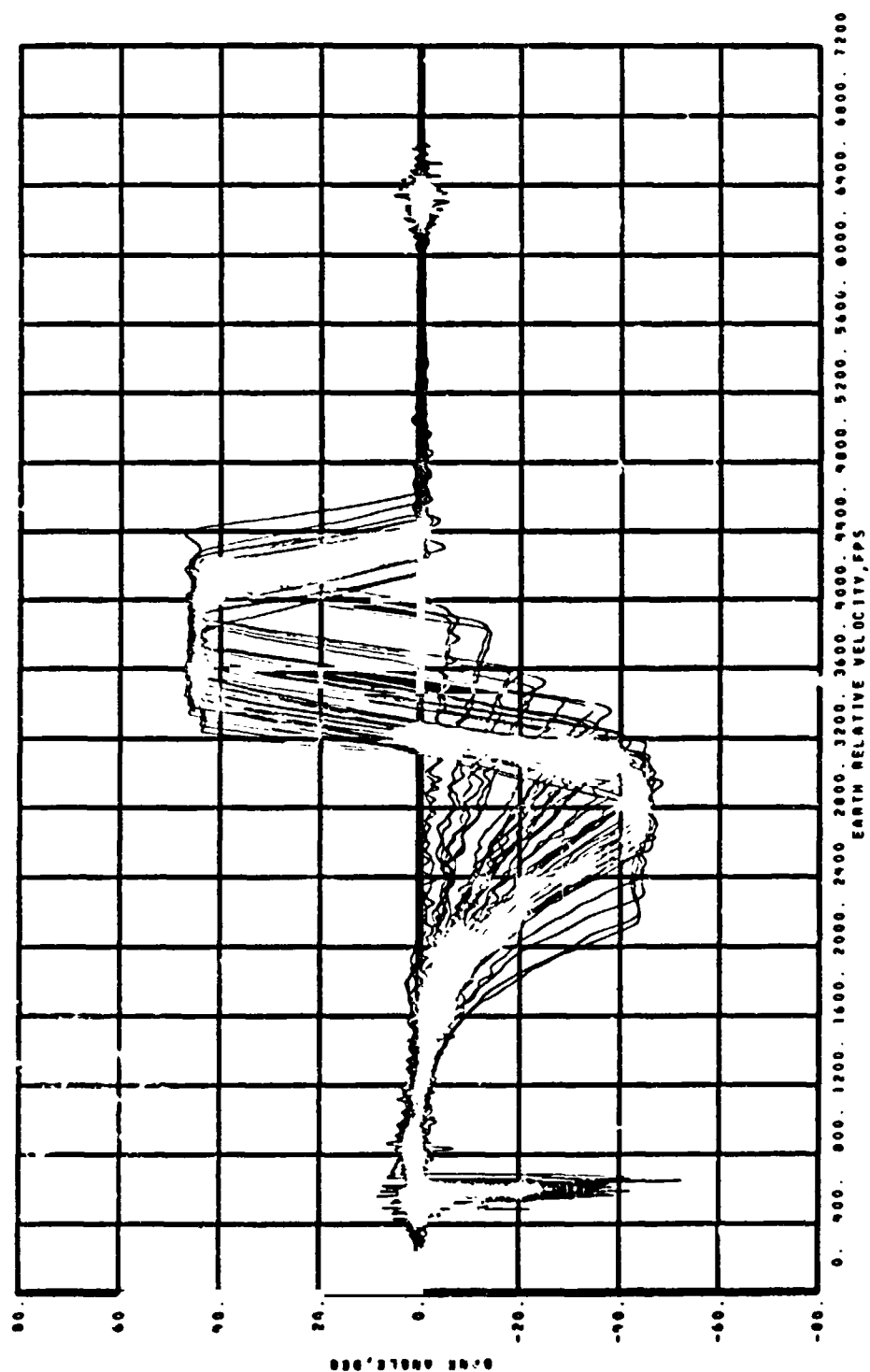
(m) Bank angle.

Figure 6.- Continued.

55
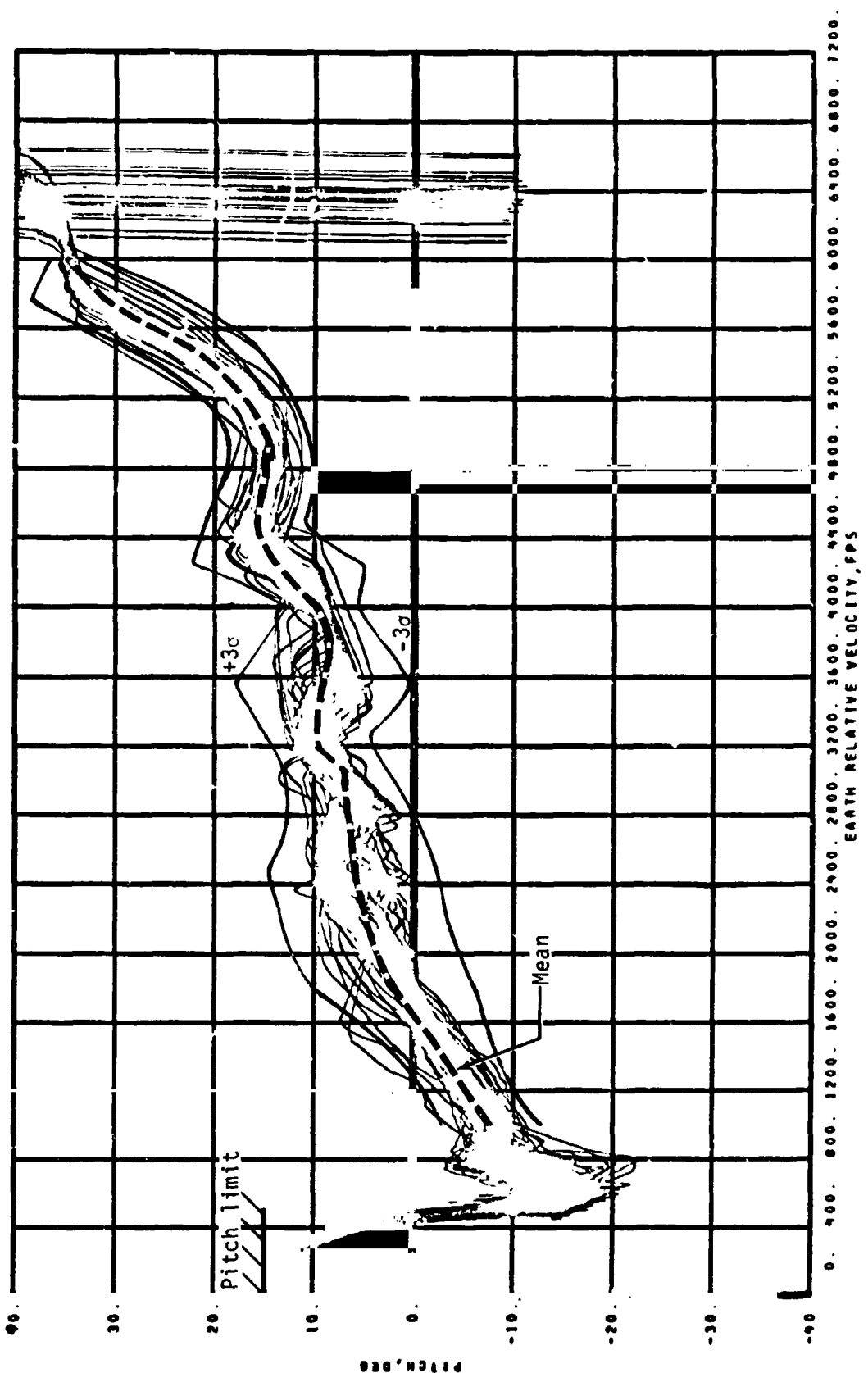
(n) Pitch angle.

Figure 6.- Continued.

56
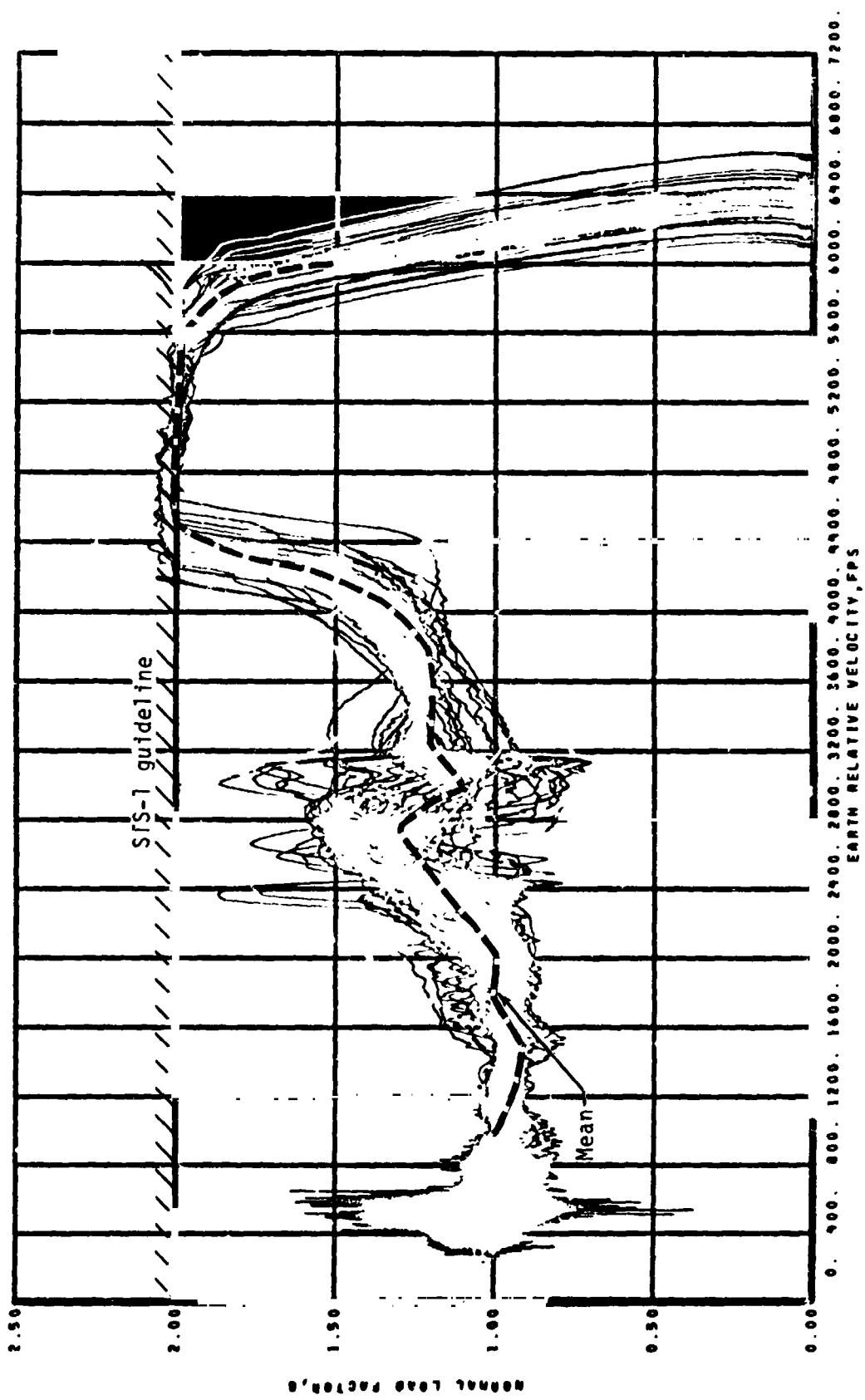
(o) Normal load factor.

Figure 6.- Continued.
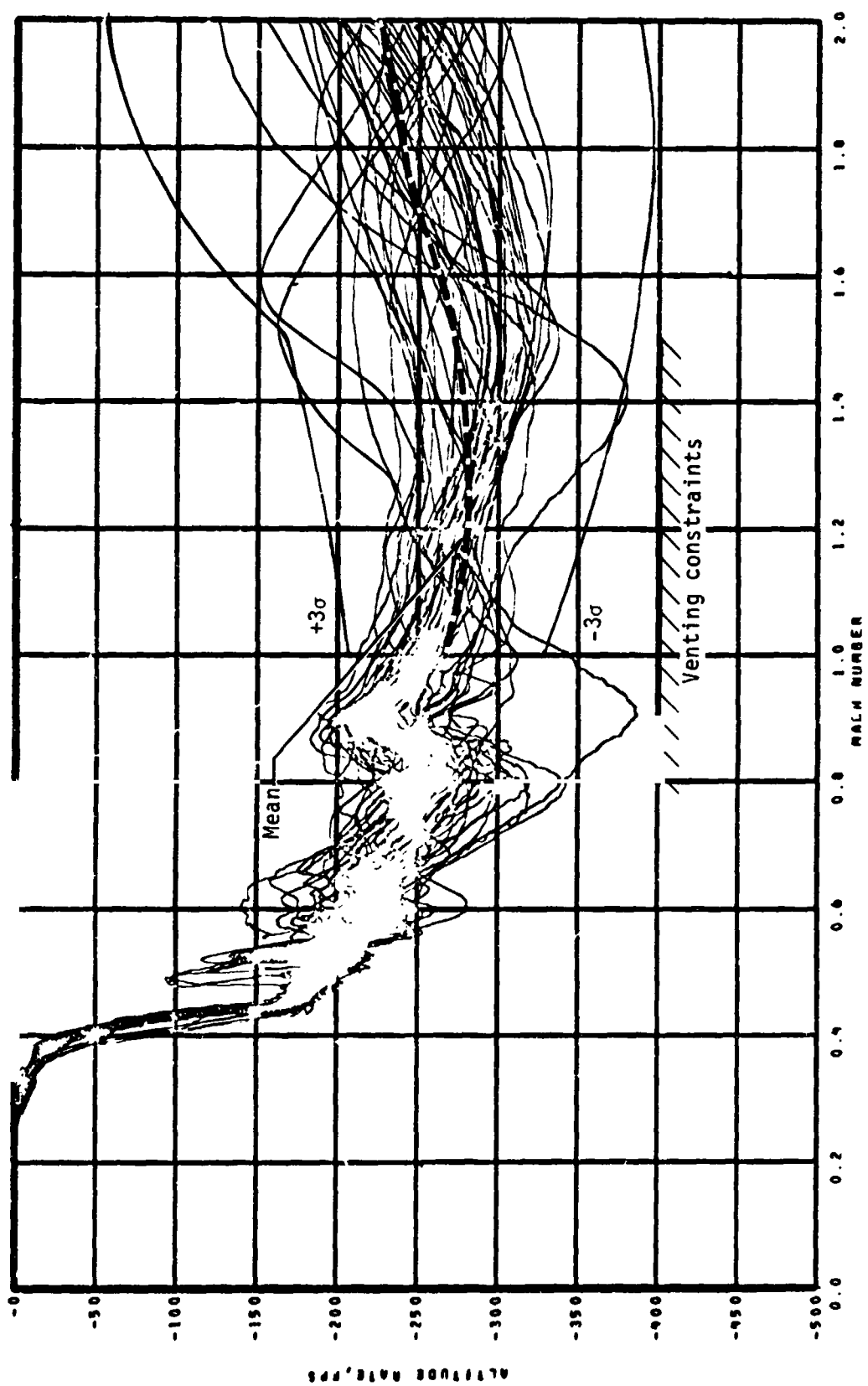
(p) Altitude rate.

Figure 6.- Continued.
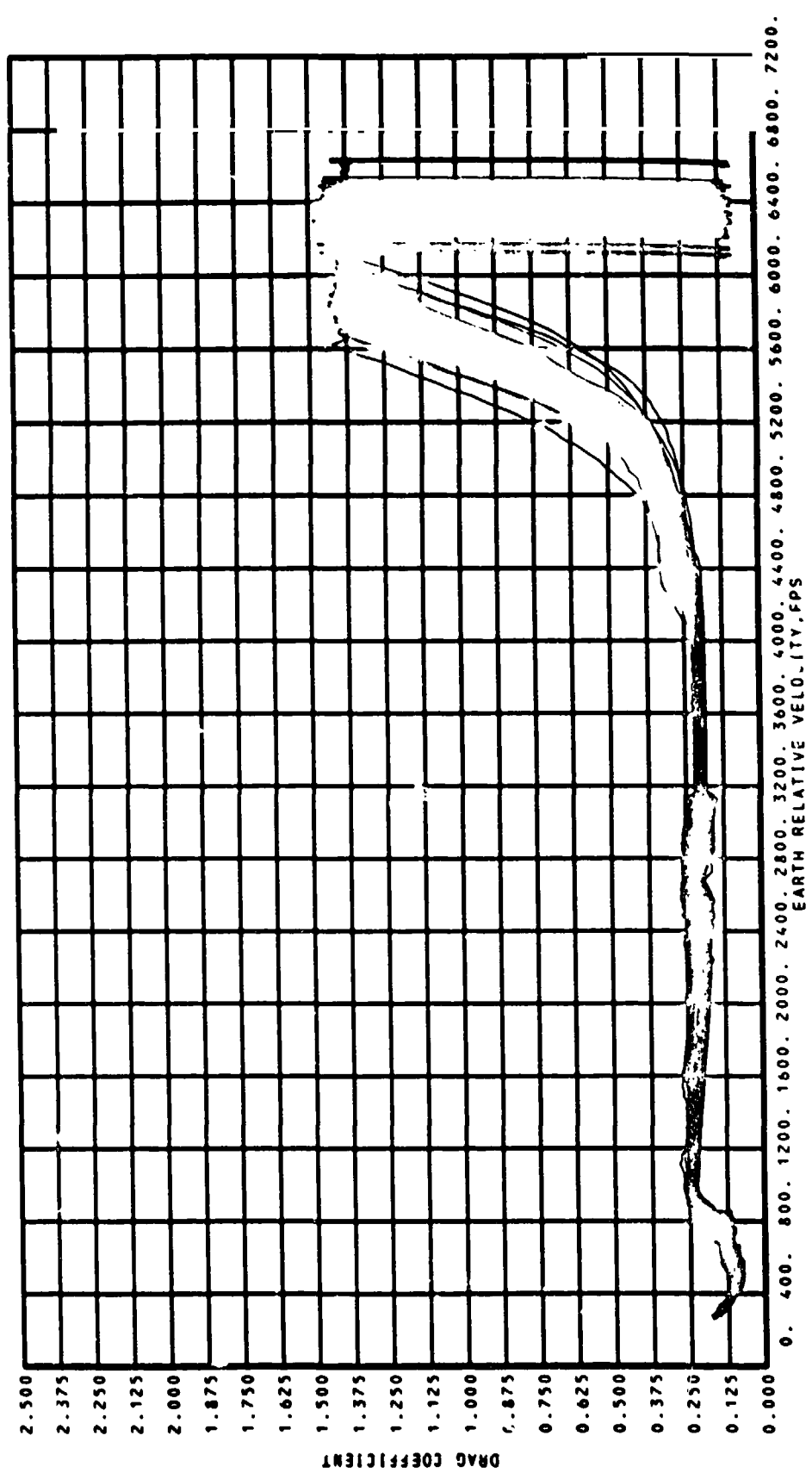
(q) Drag coefficient.

Figure 6.- Continued.
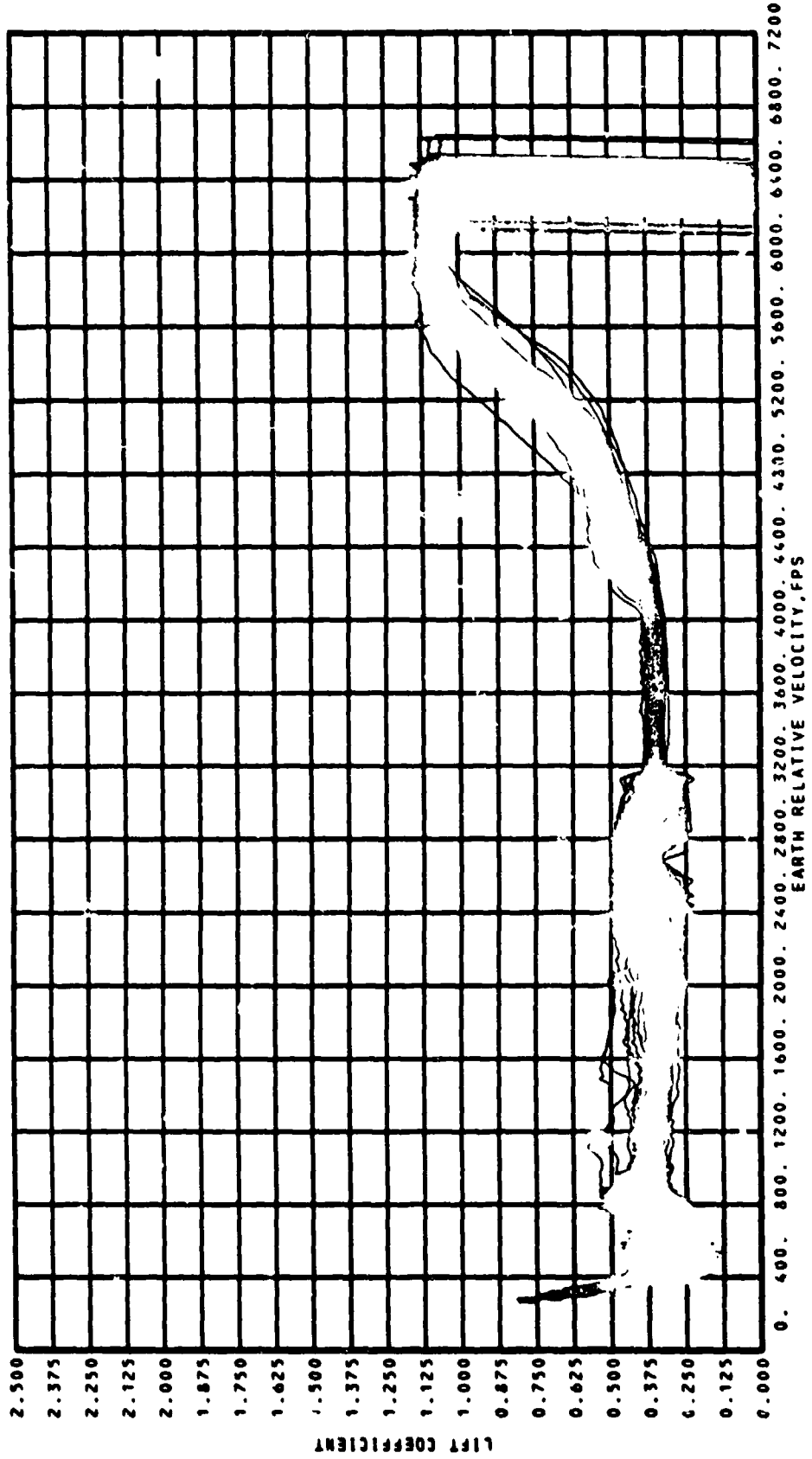
(r) Lift coefficient.

Figure 6.- Continued.

60
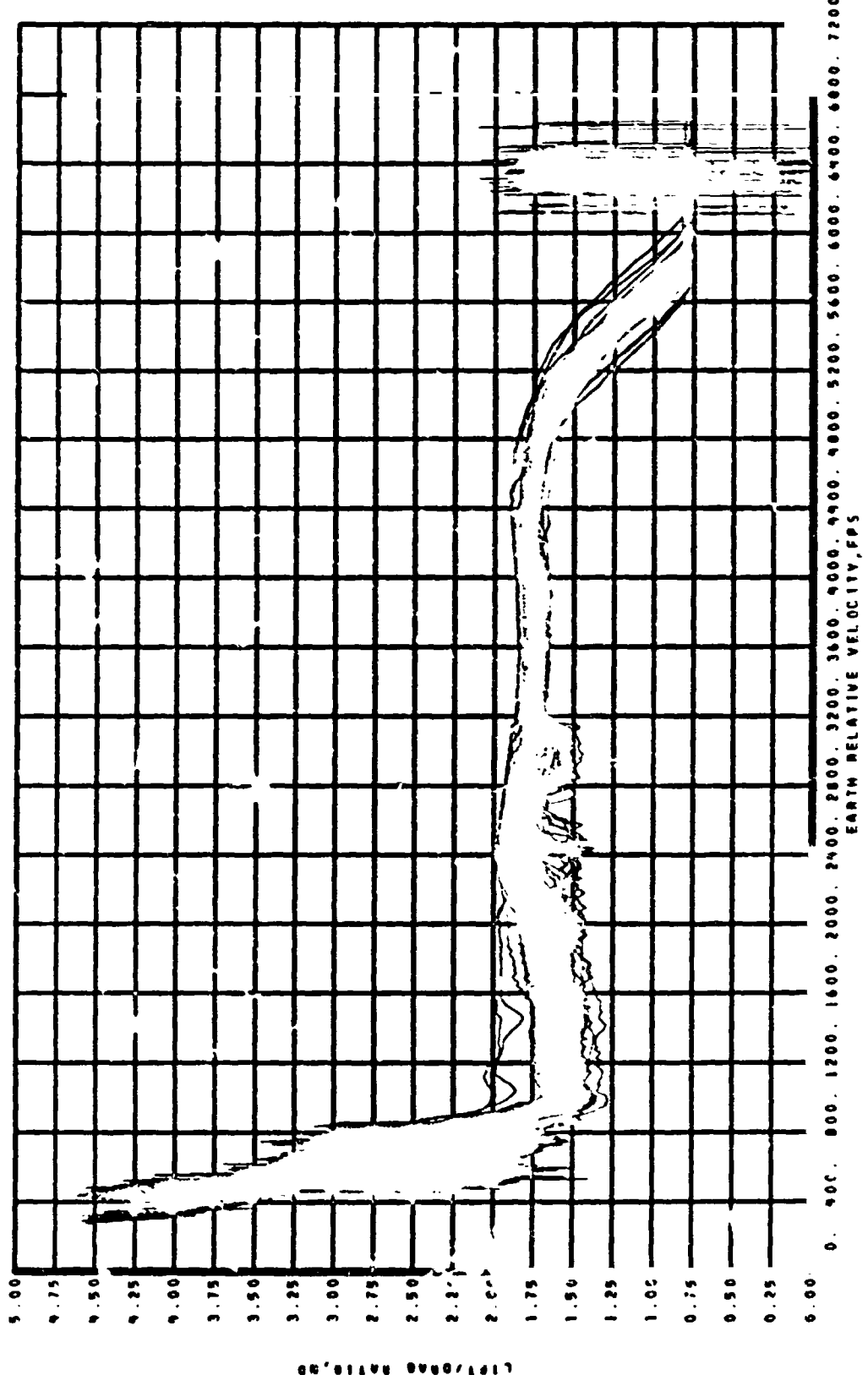
(s) Lift/drag ratio.

Figure 6.- Continued.

(t) Normal force coefficient.

Figure 6.- Continued.

62
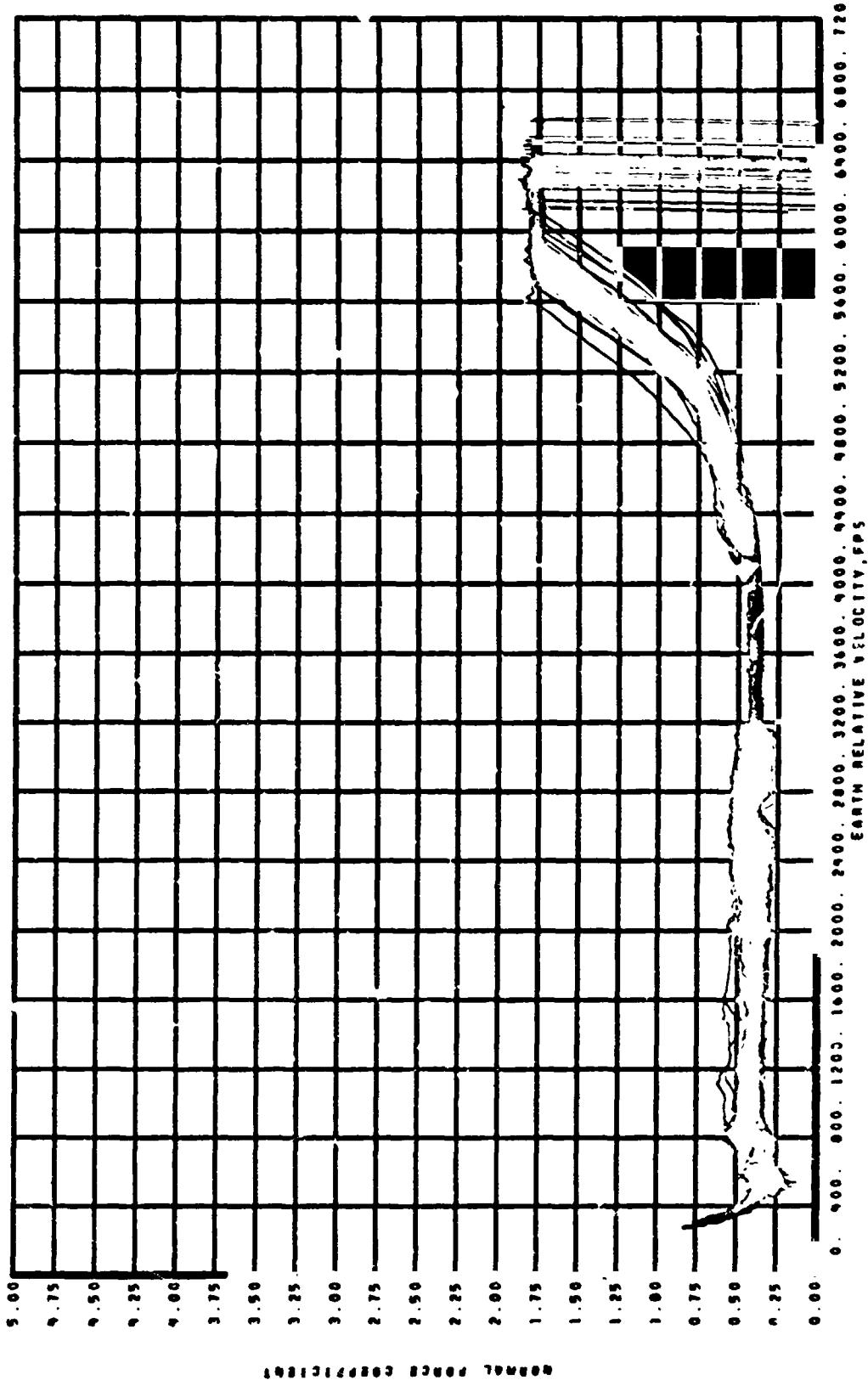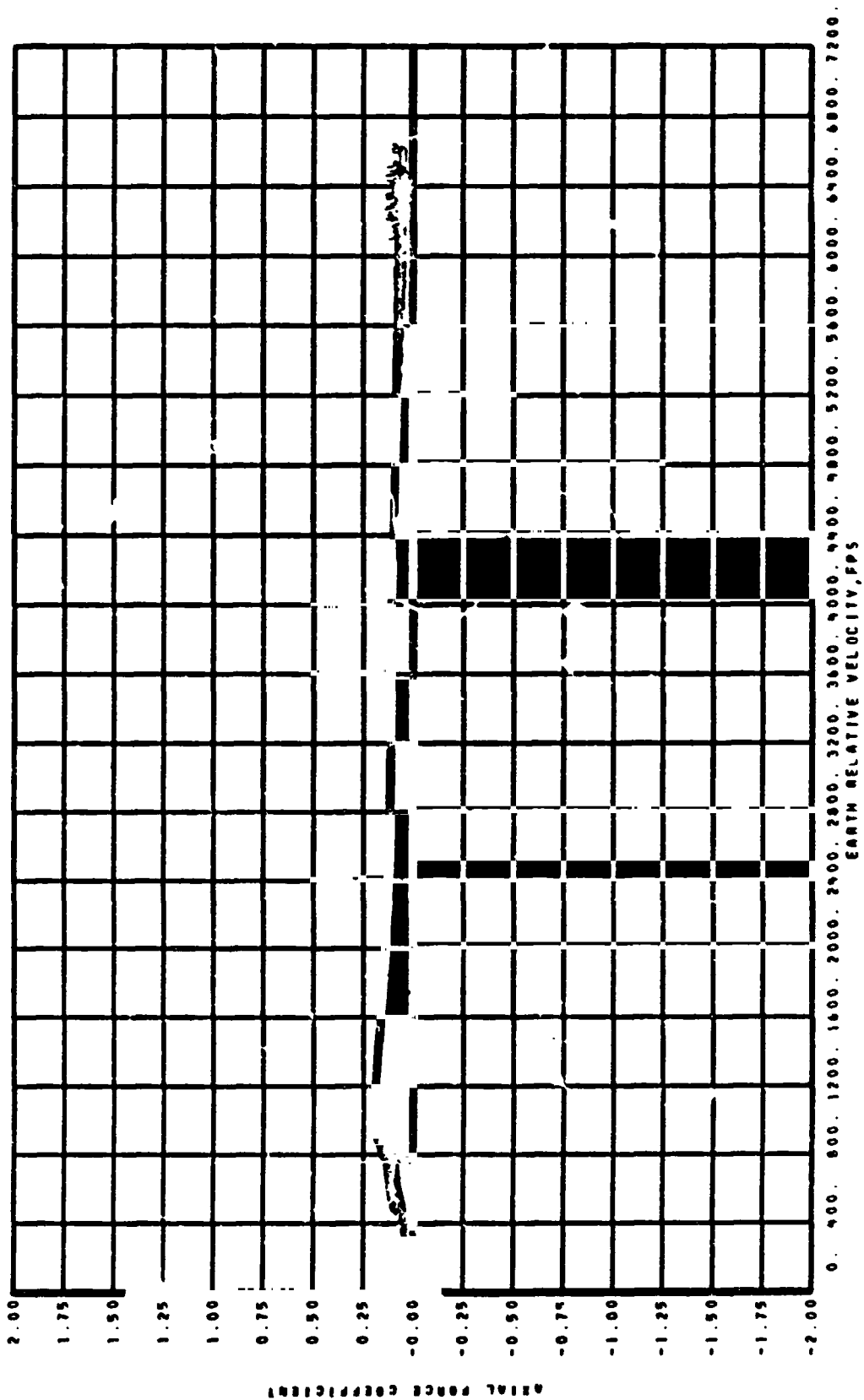
(u) Axial force coefficient.

Figure 6.- Continued.

63
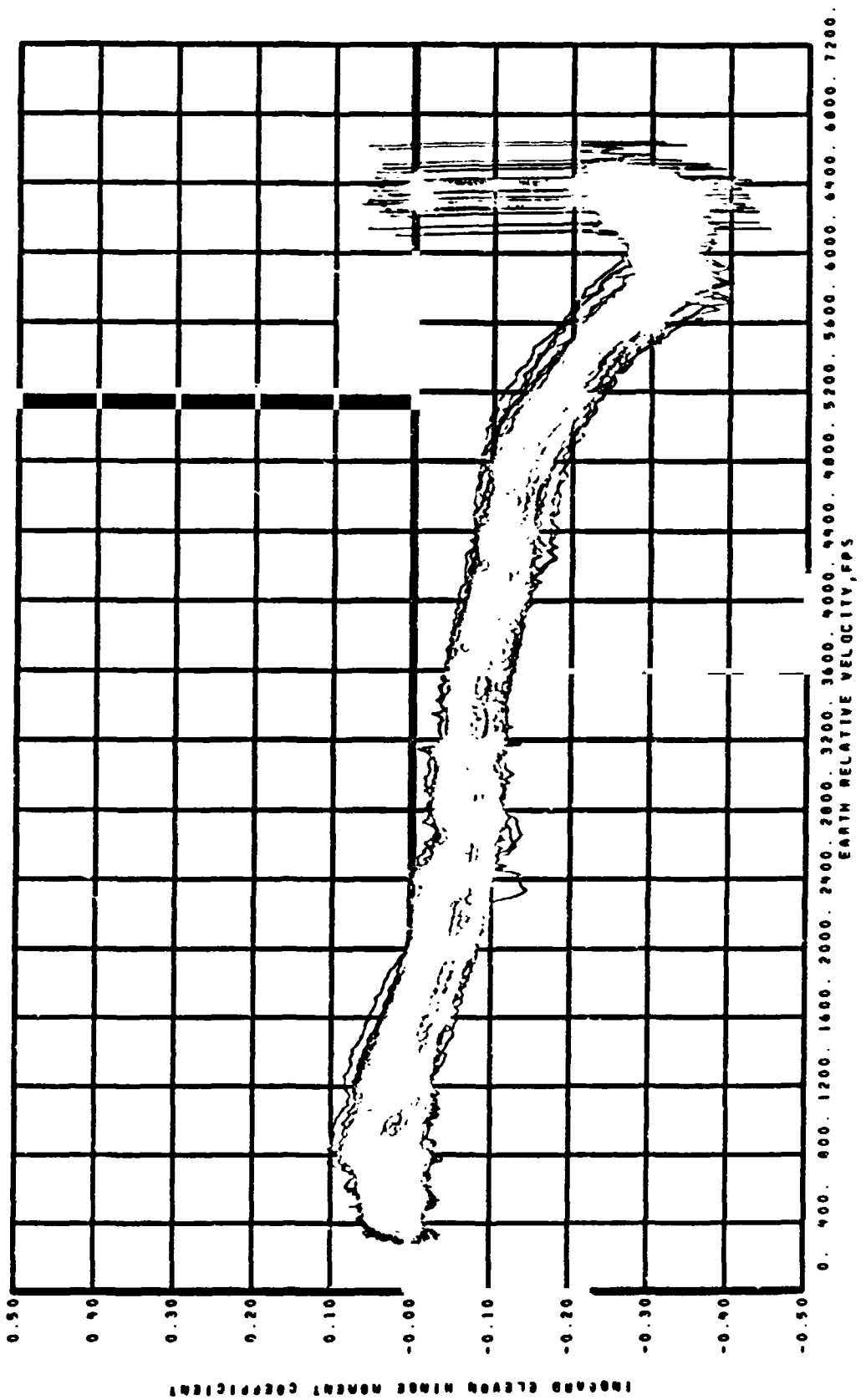
(v) Inboard elevon hinge-moment coefficient.
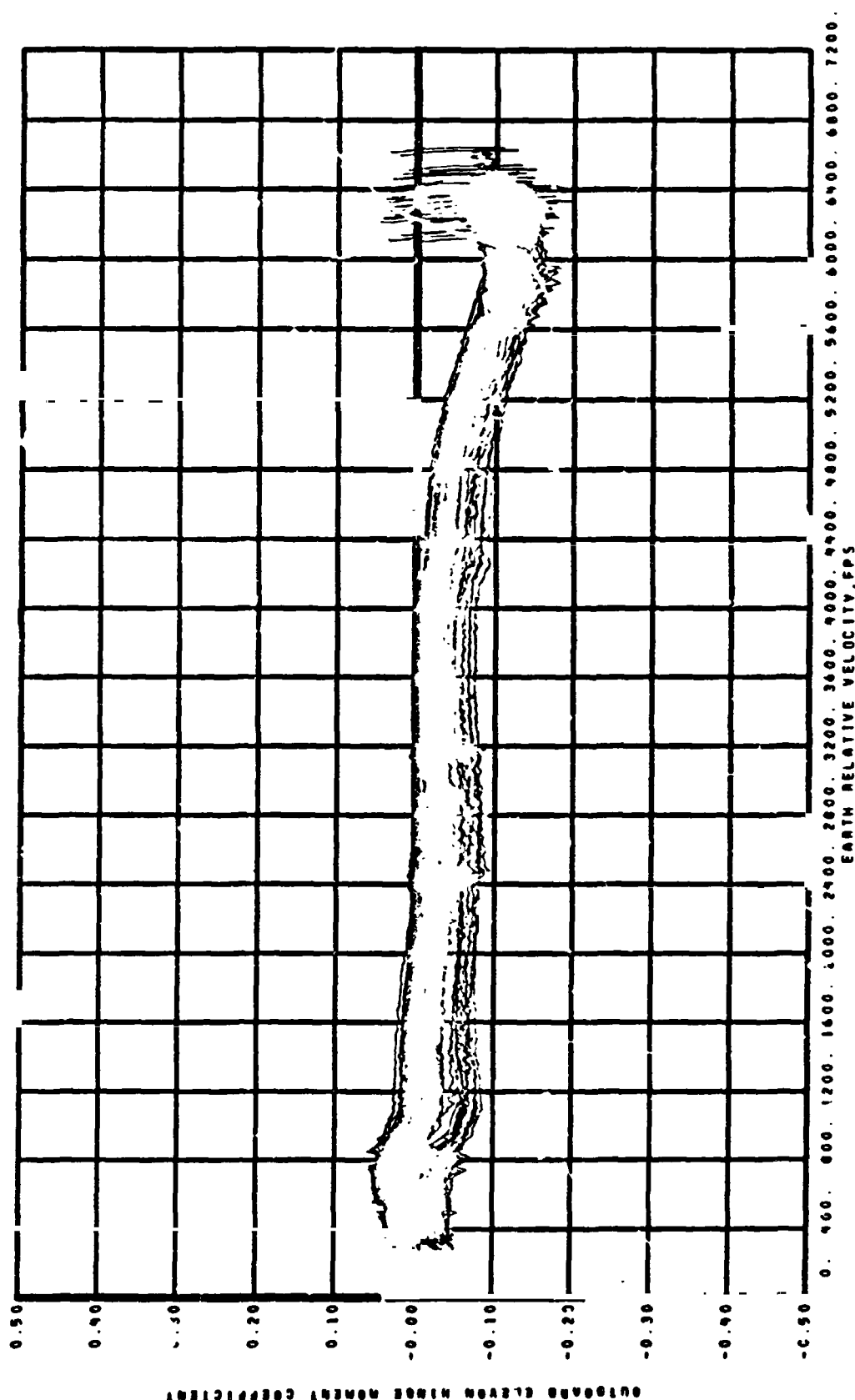
Figure 6.- Continued.

(w) Outboard elevon hinge-moment coefficient.
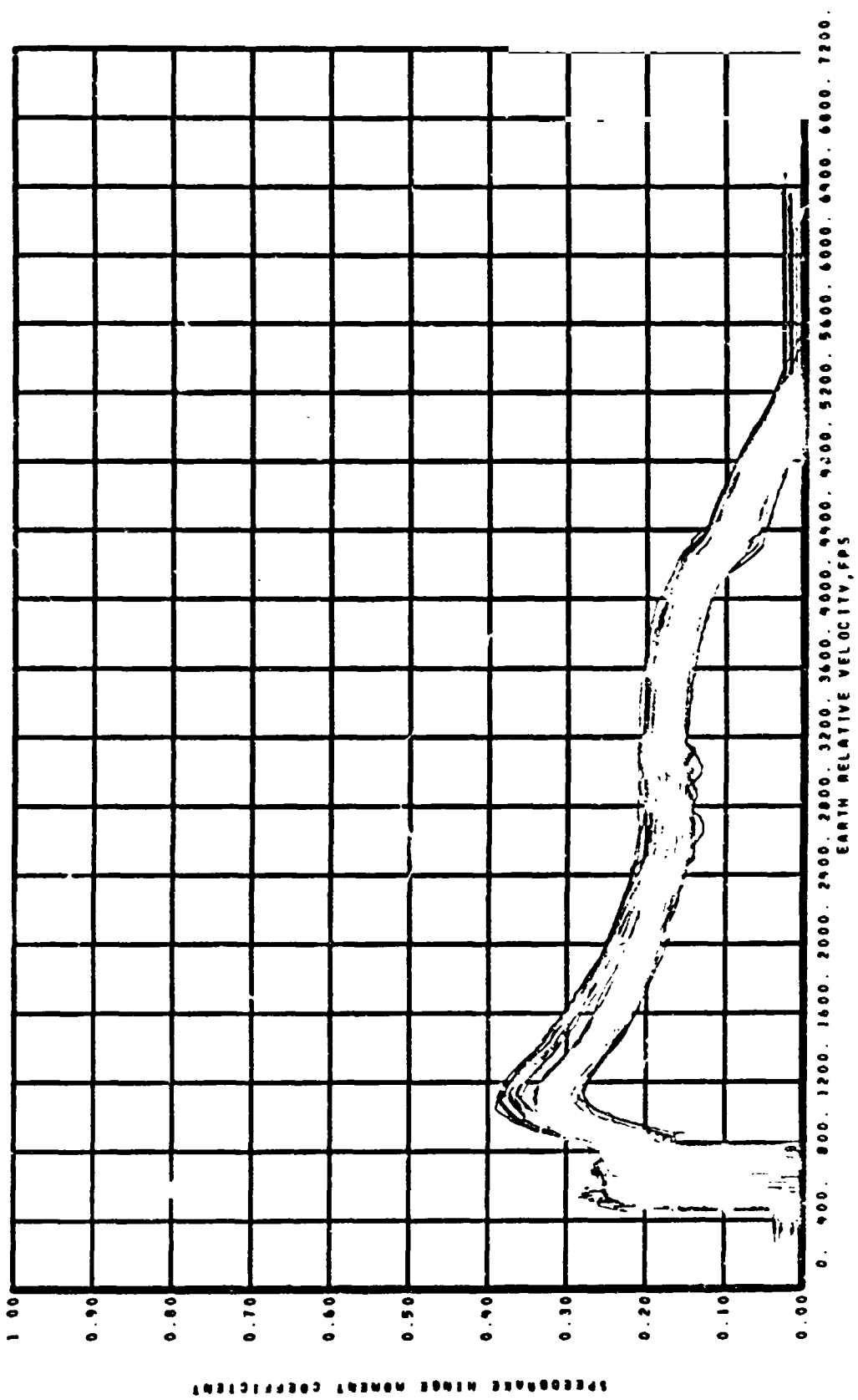
Figure 6.- Continued.

(x) Speedbrake hinge-moment coefficient.
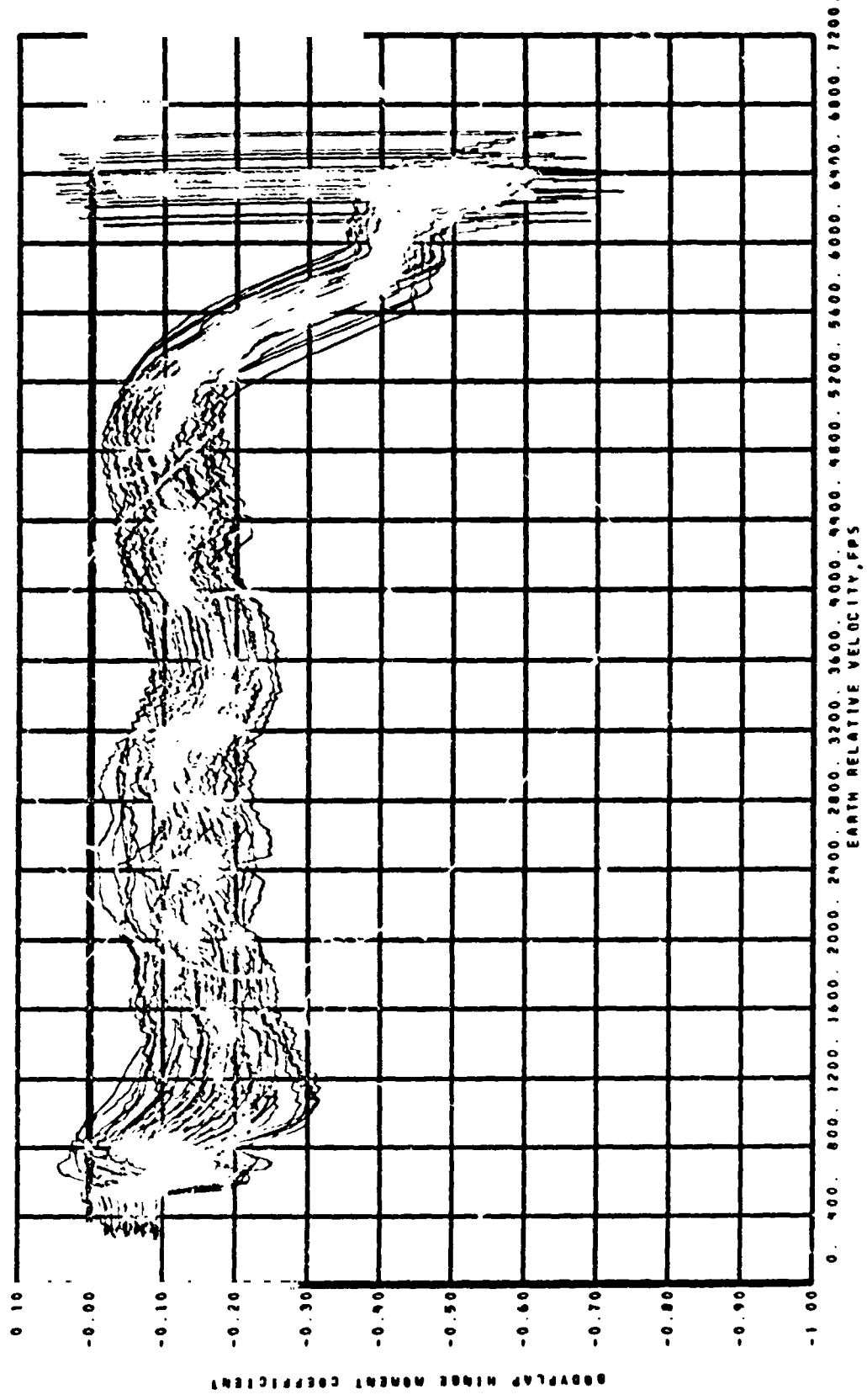
Figure 6.- Continued.

(y) Body-flap hinge-moment coefficient.
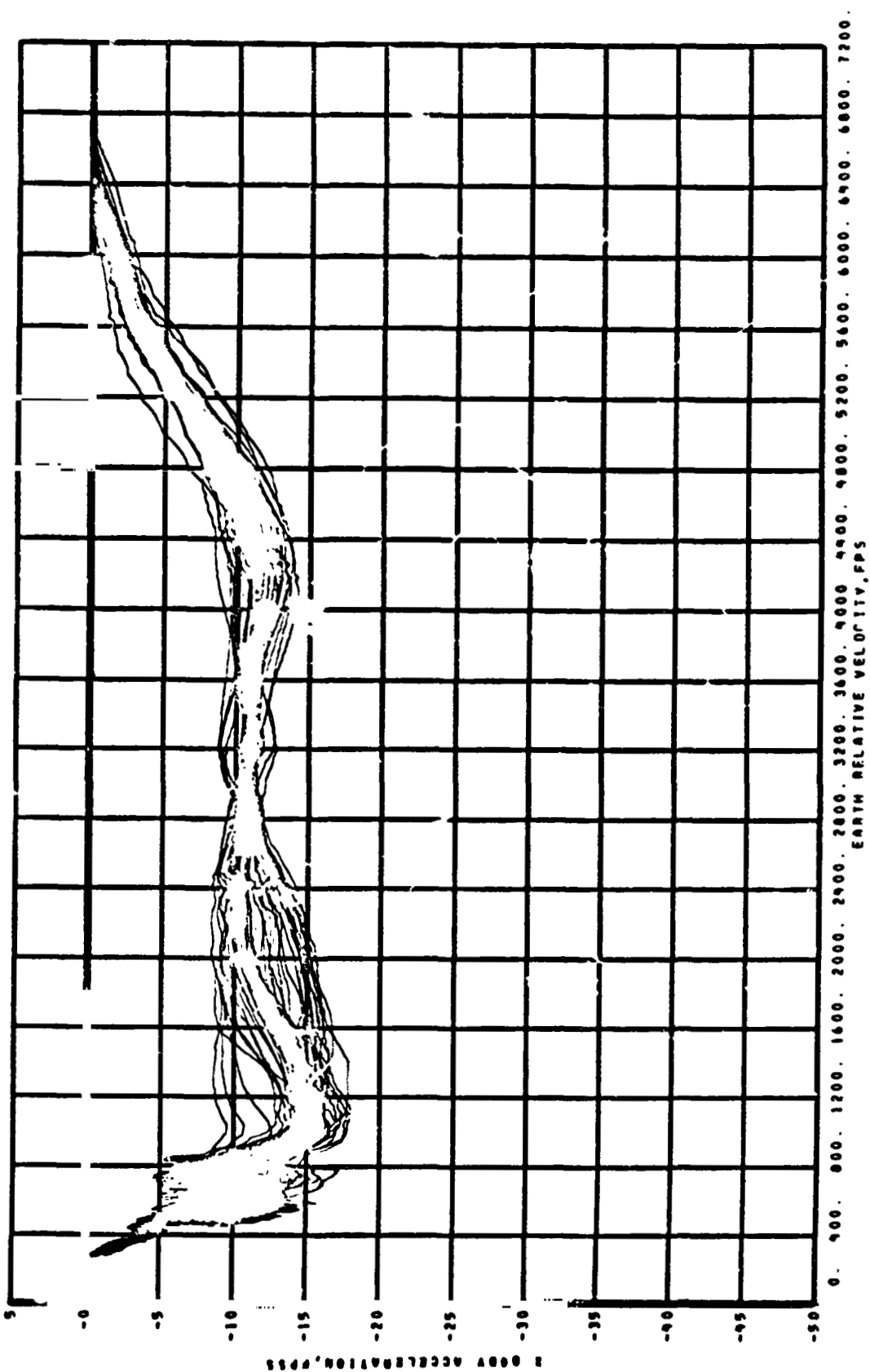
Figure 6.- Continued.

(z) X-body acceleration.
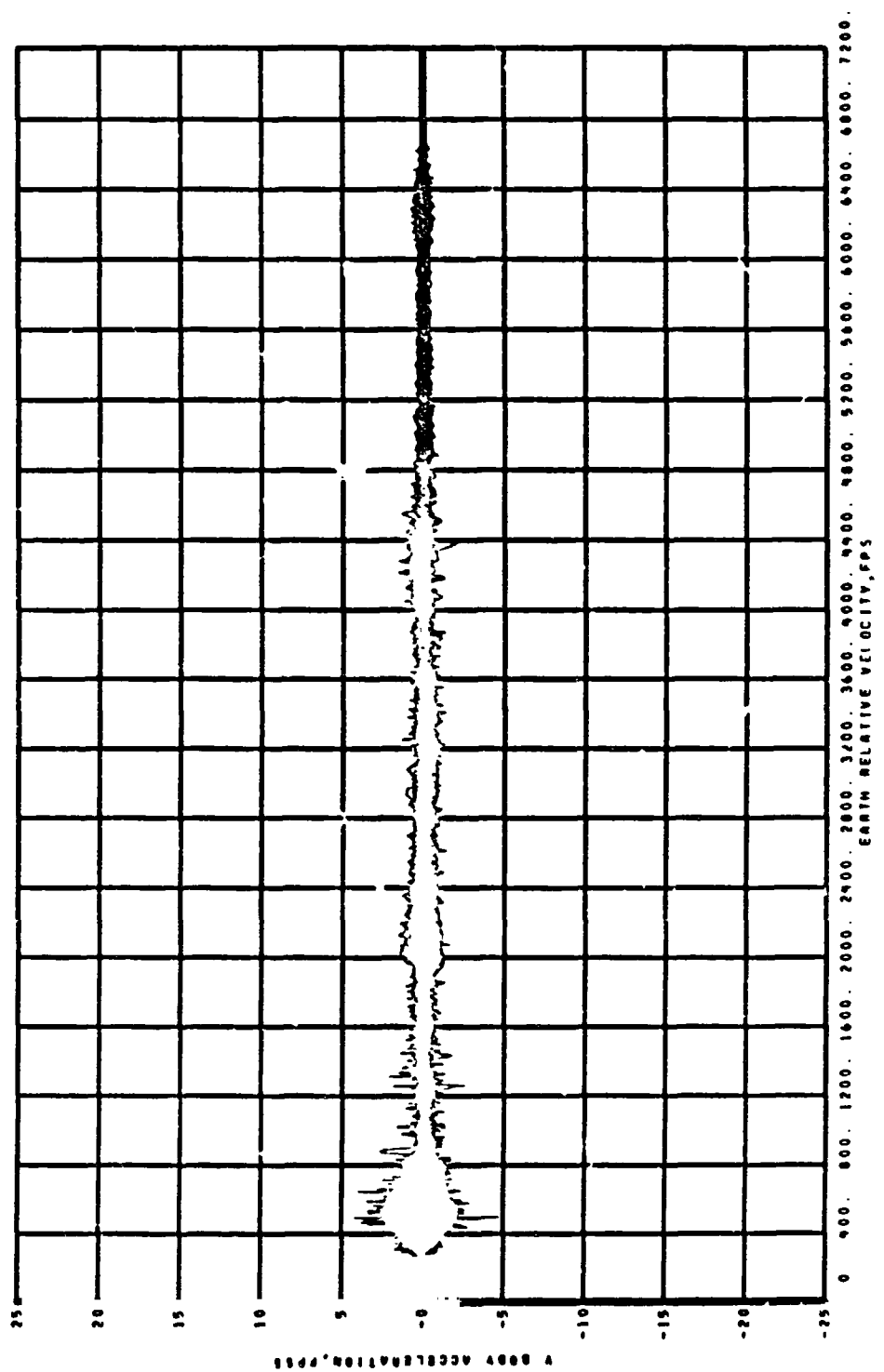
Figure 6.- Continued.

(aa) Y-body acceleration.

Figure 6.- Continued.

69
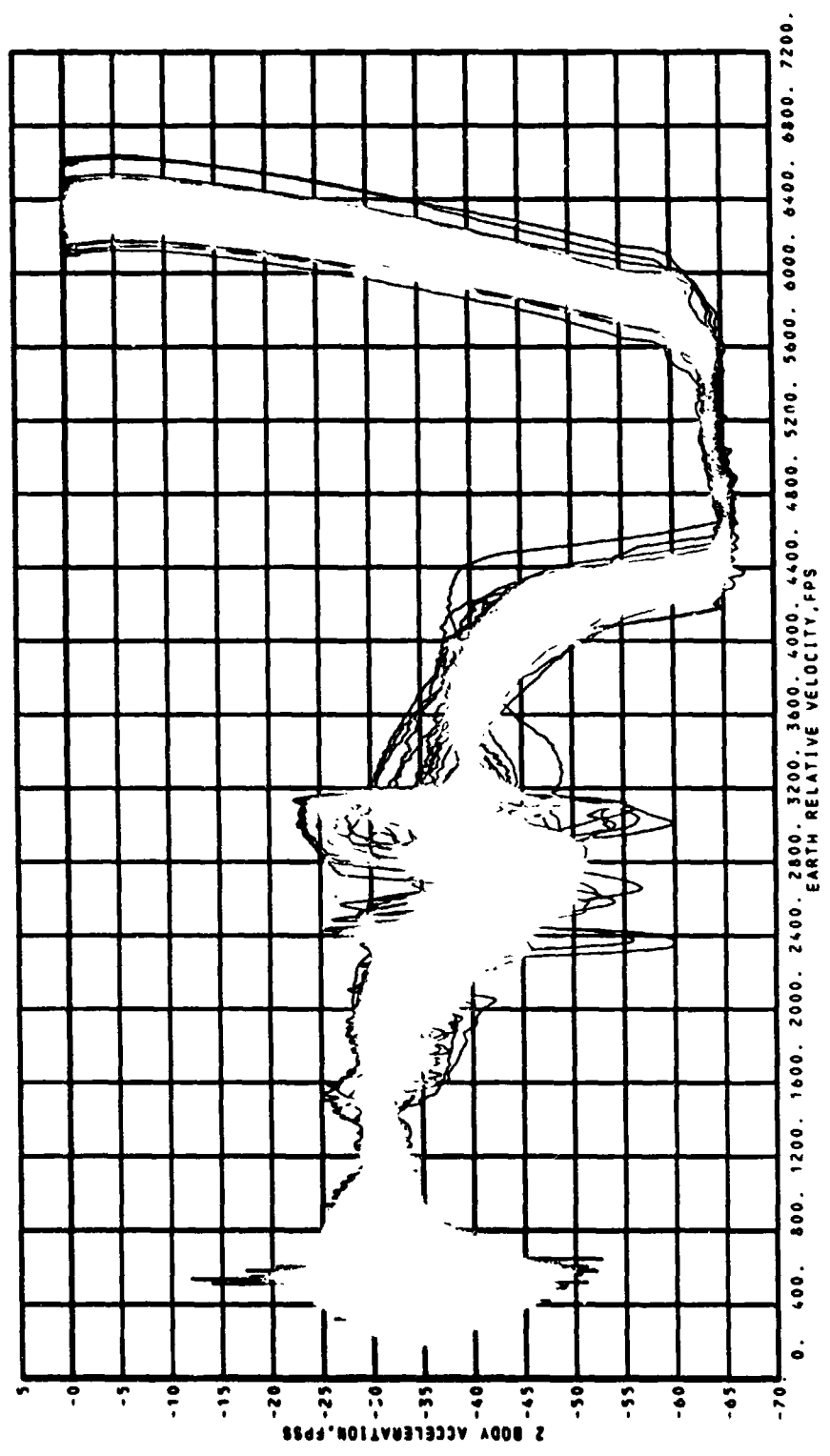
(bb) Z-body acceleration.

Figure 6.- Concluded.

70
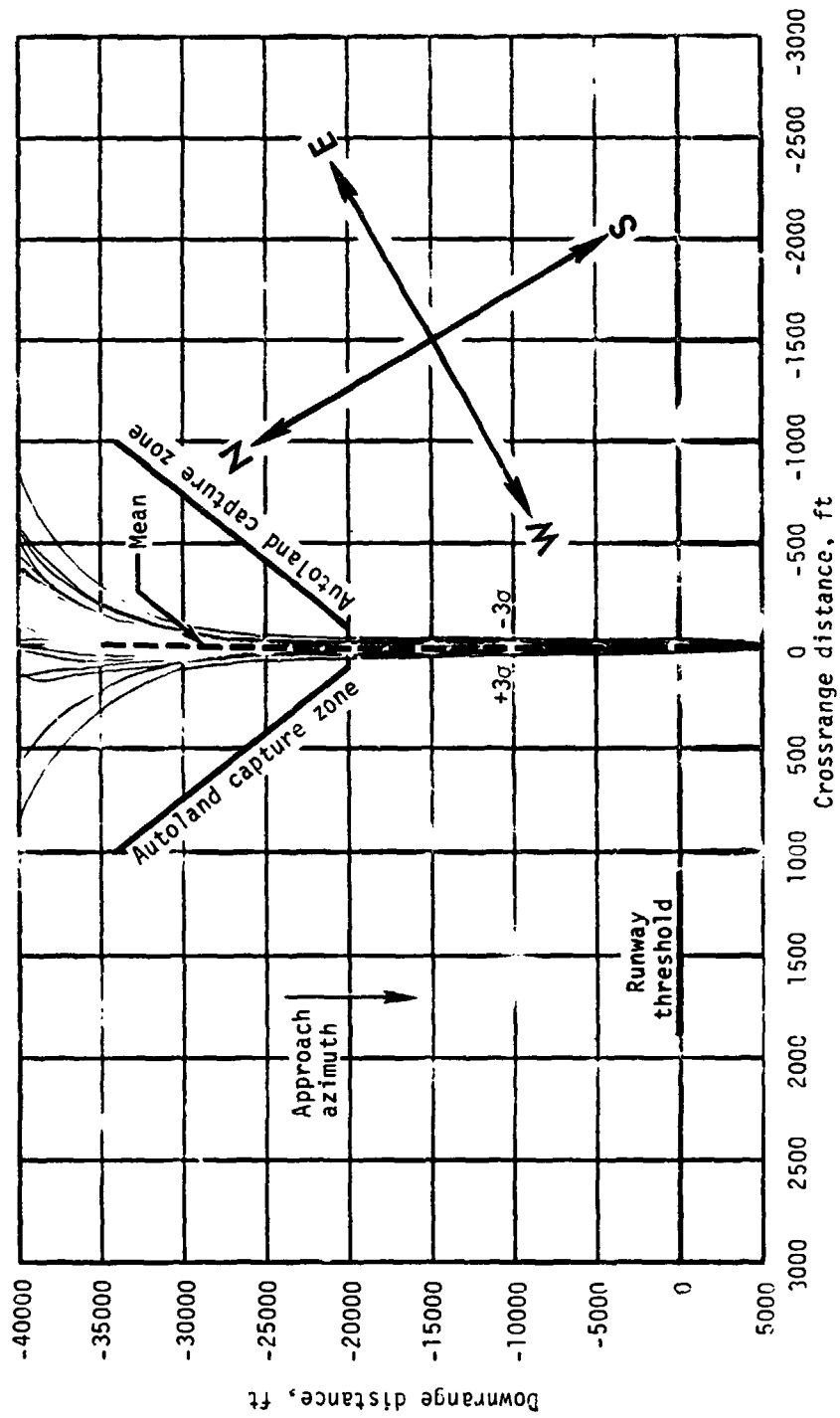
(a) Groundtrack.

Figure 7.- Autoland guidance performance parameters.

71
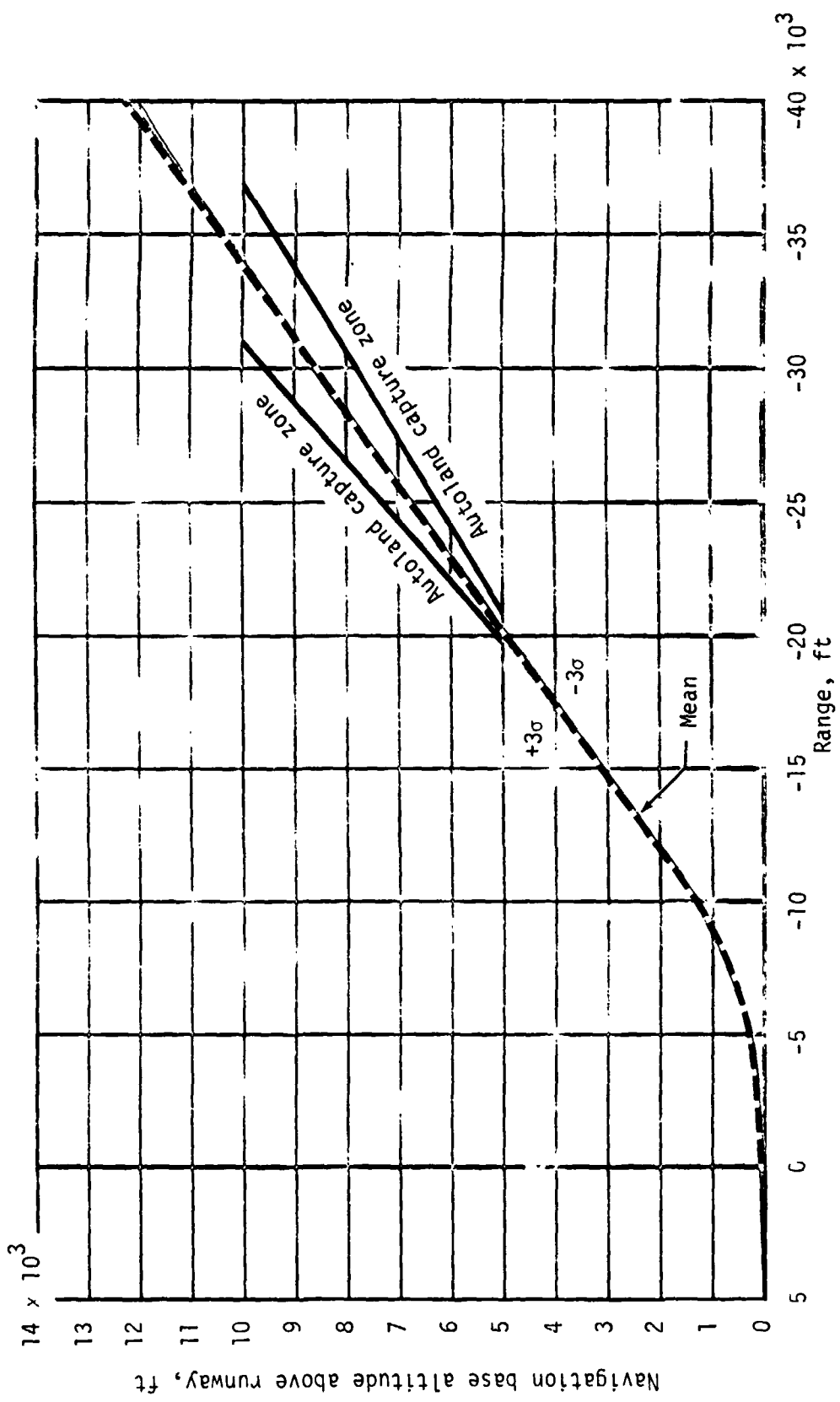
(b) Navigation base altitude (12 000 feet to landing).

Figure 7.- Continued.
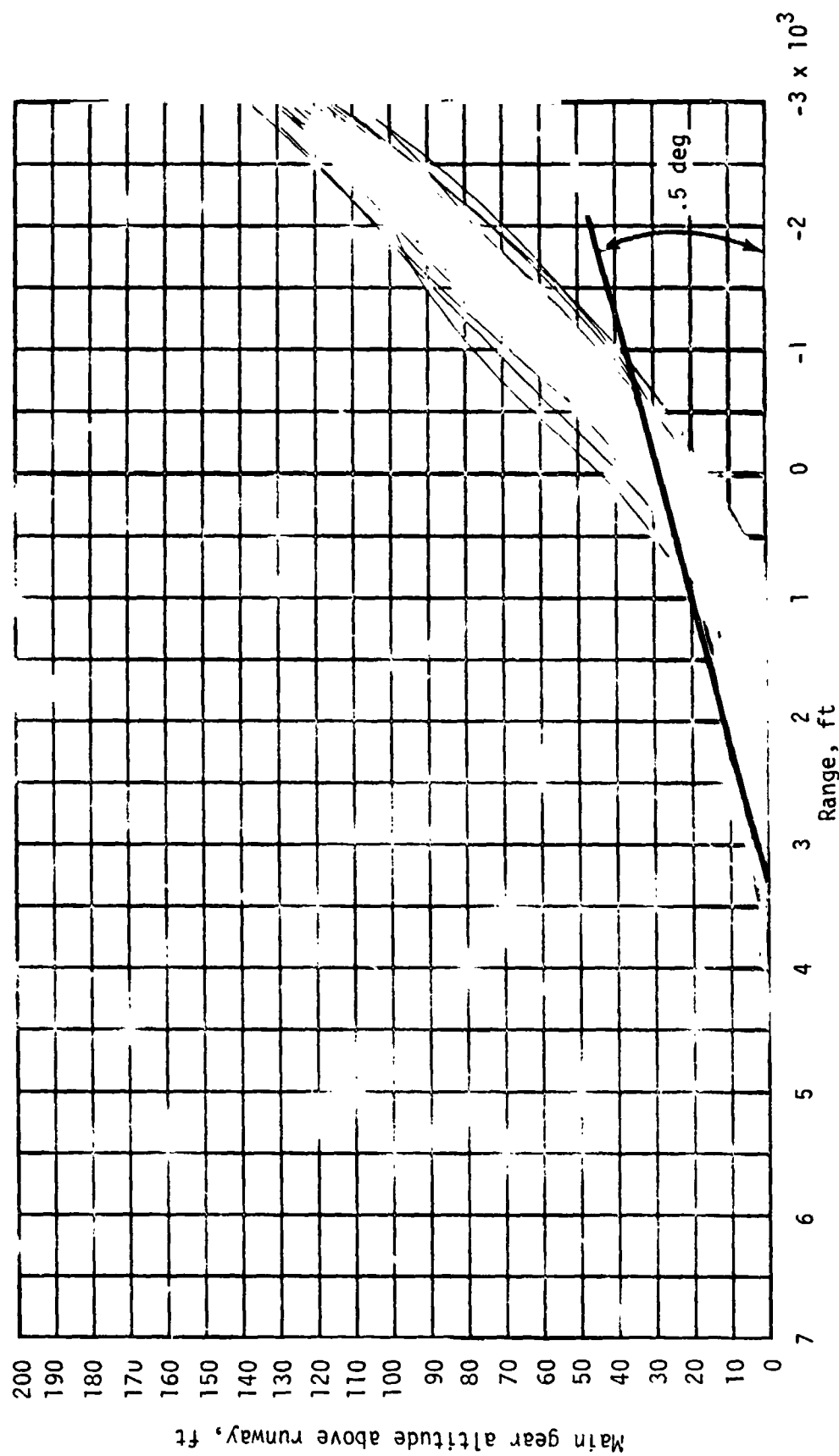
(c) Main gear altitude (130 feet to landing).

Figure 7.- Continued.

73

Altitude rate, fps

Final flare altitude rate line

Altitude above runway, ft
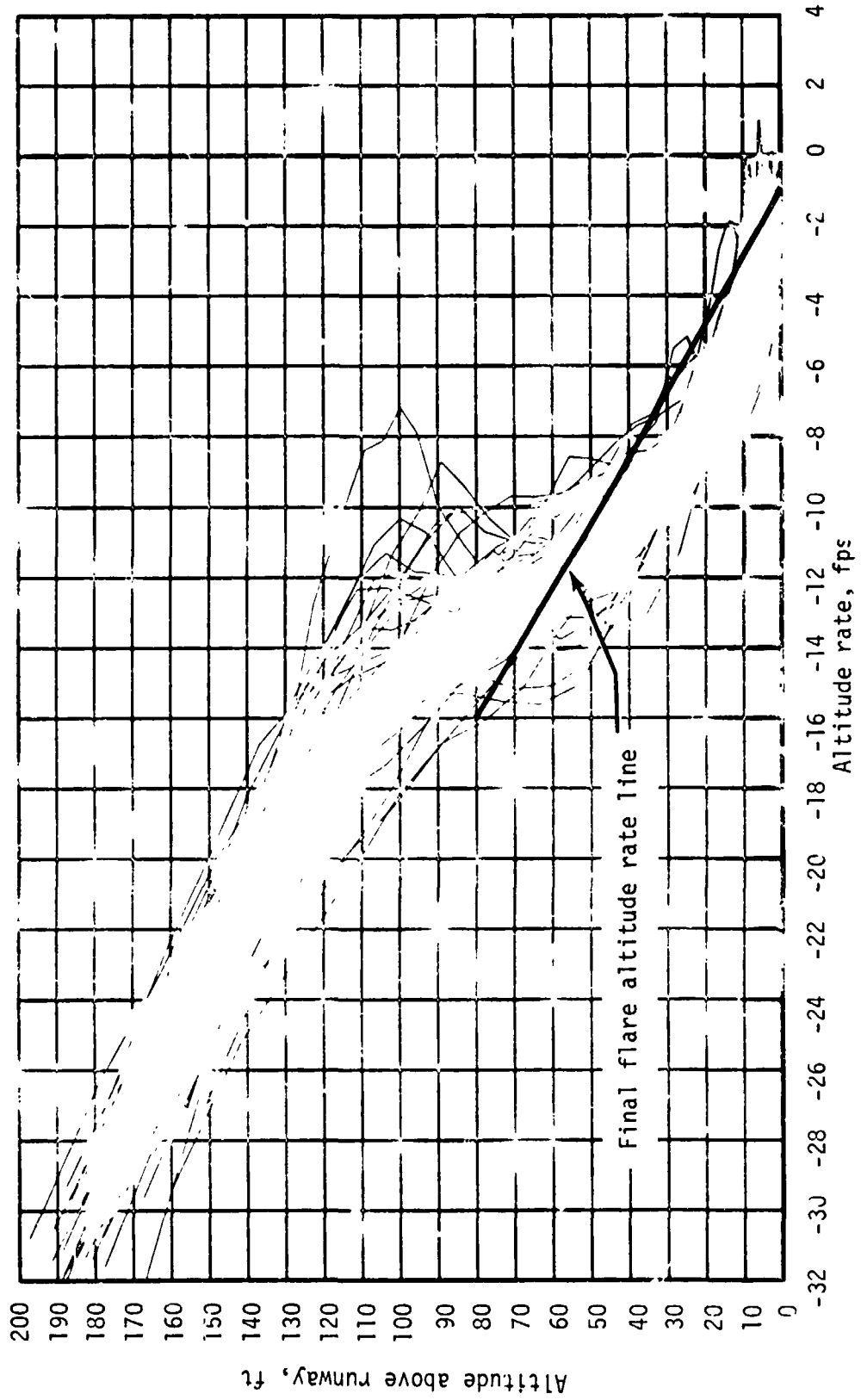
(d) Final flare altitude and altitude rate.

Figure '.- Continued.

74
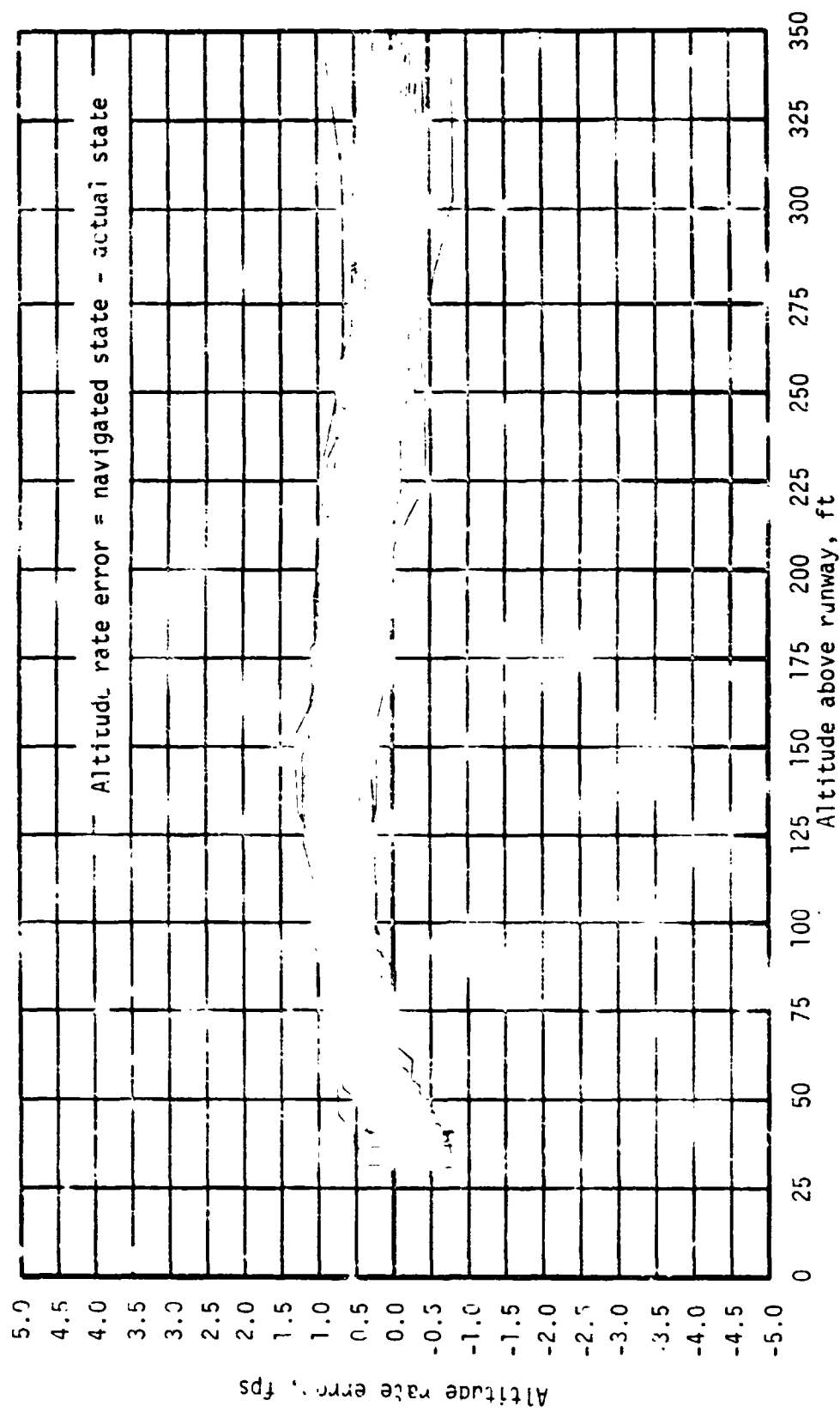
(e) Altitude rate errors.

Figure 7.- Continued.

75
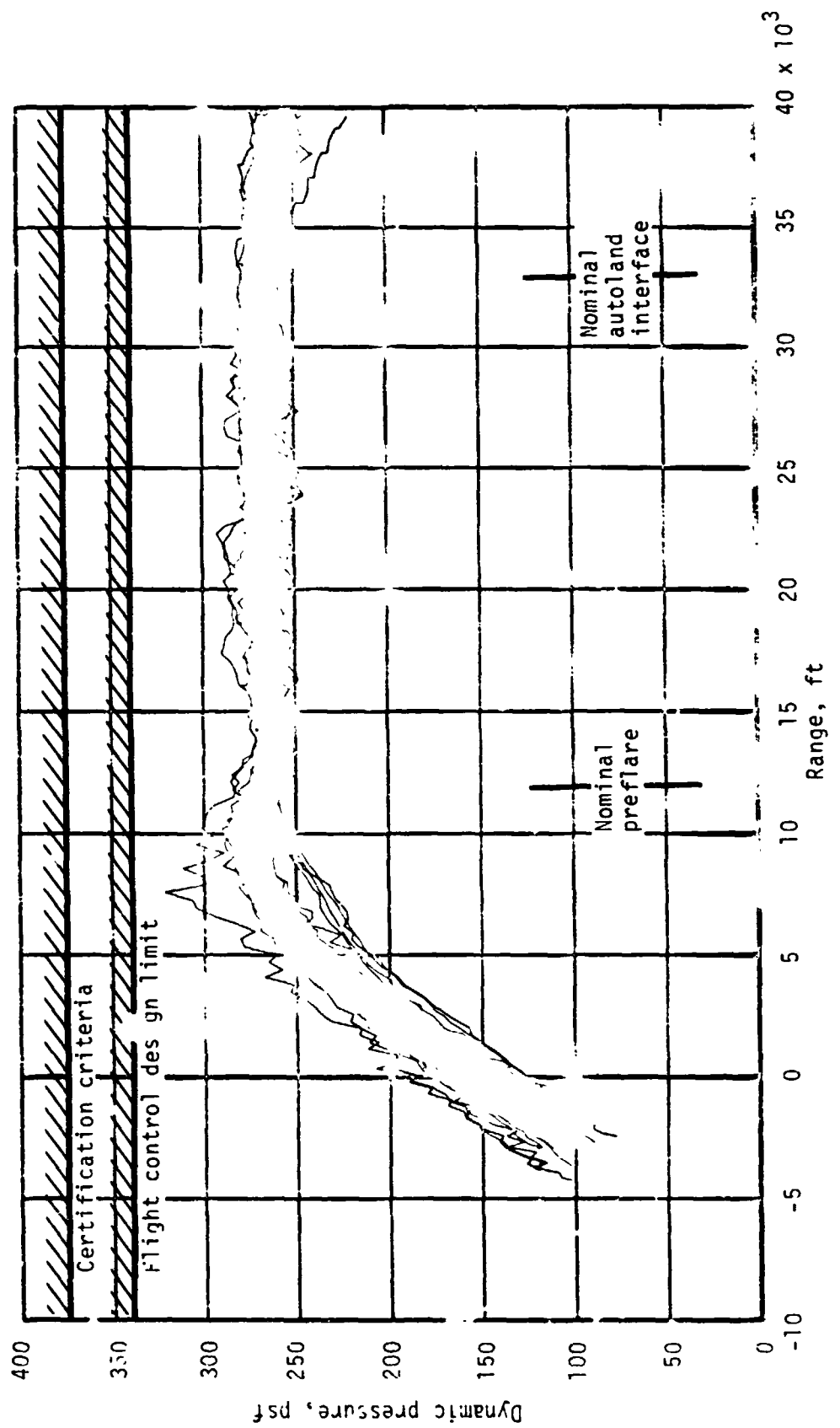
(f) Dynamic pressure.

Figure 7.- Continued.
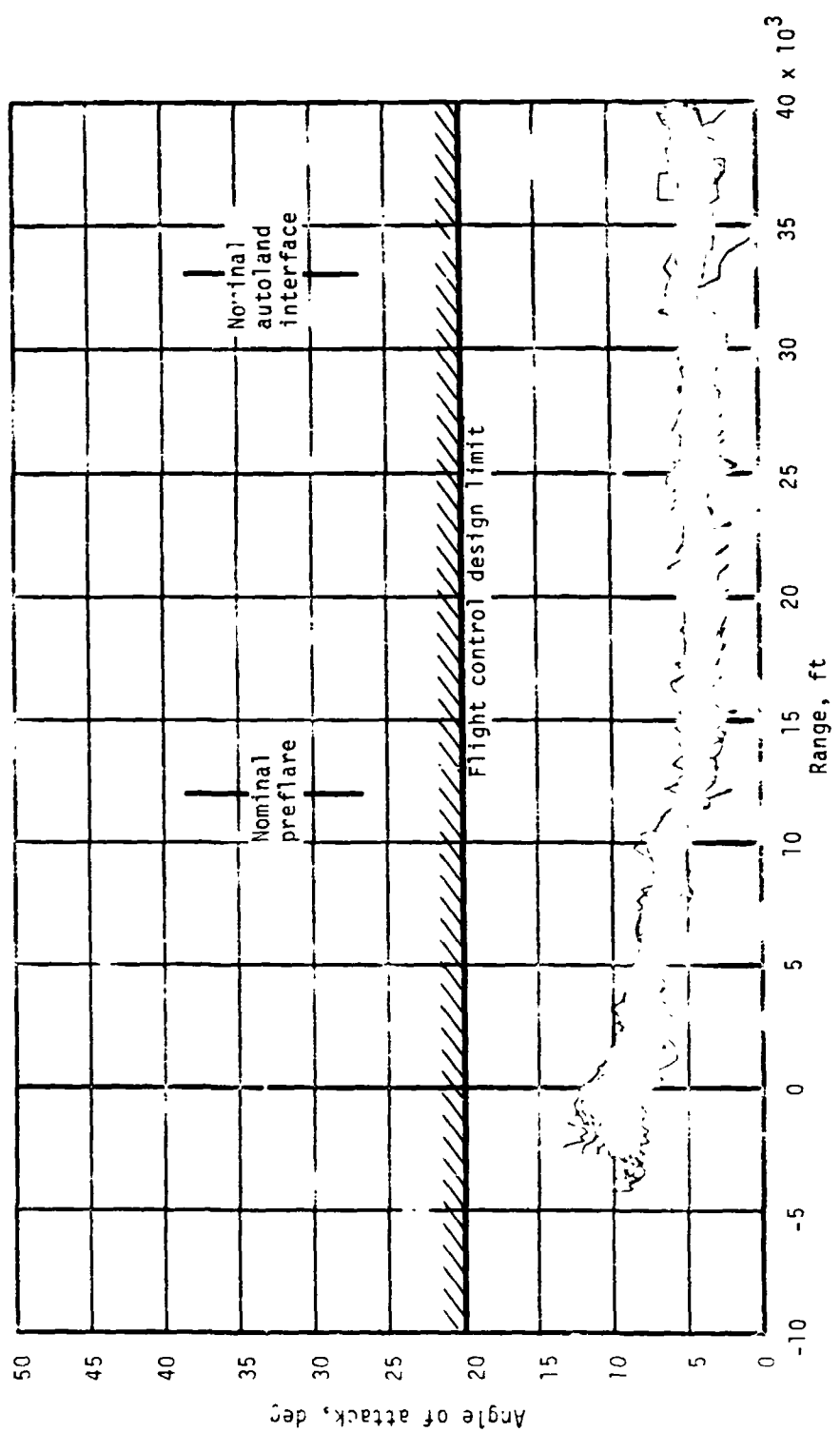
(g) Angle of attack.

Figure 7.- Continued.
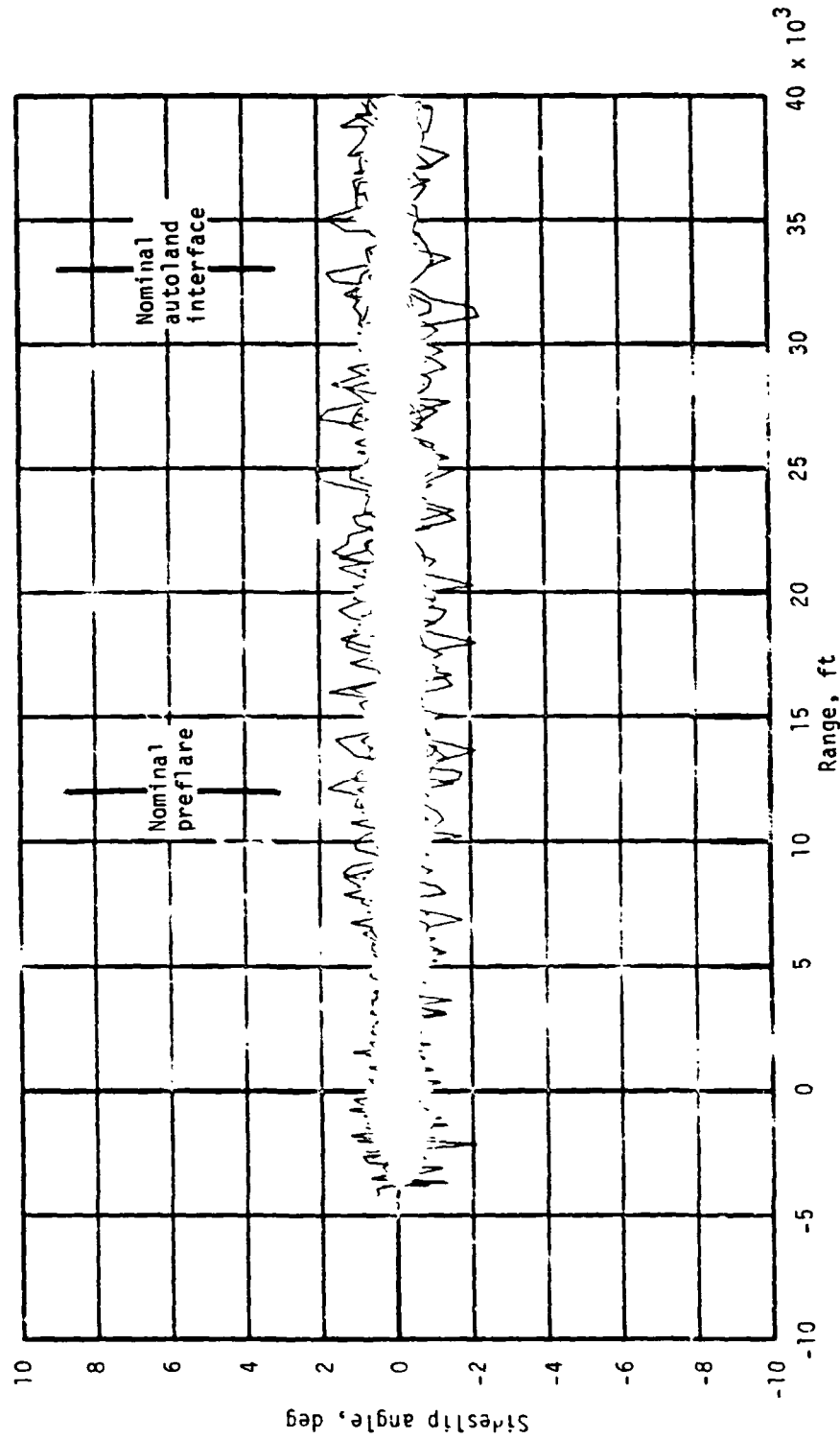
(h) Sideslip angle.

Figure 7.- Continued.
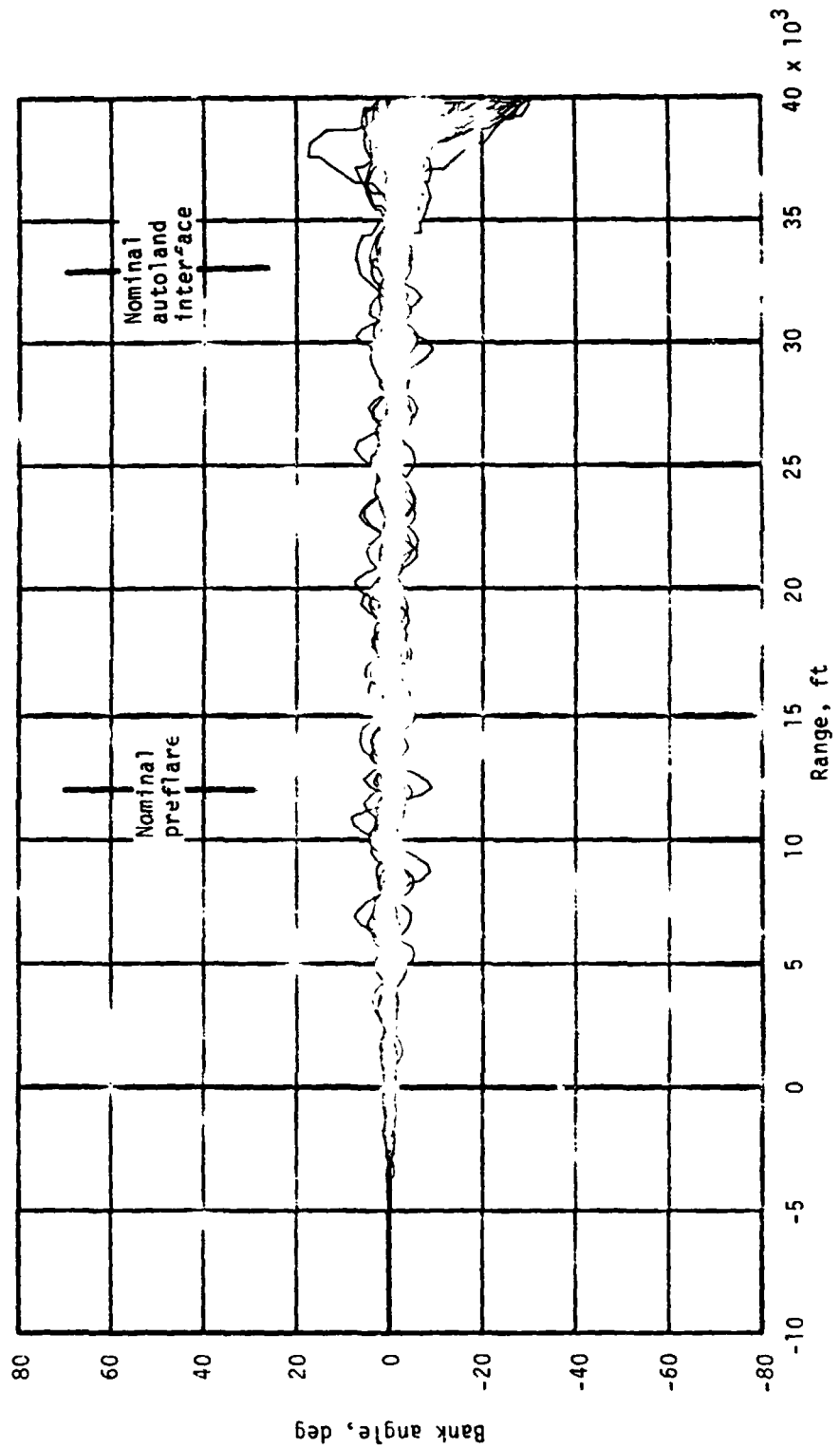
(i) Bank angle.

Figure 7.- Continued.
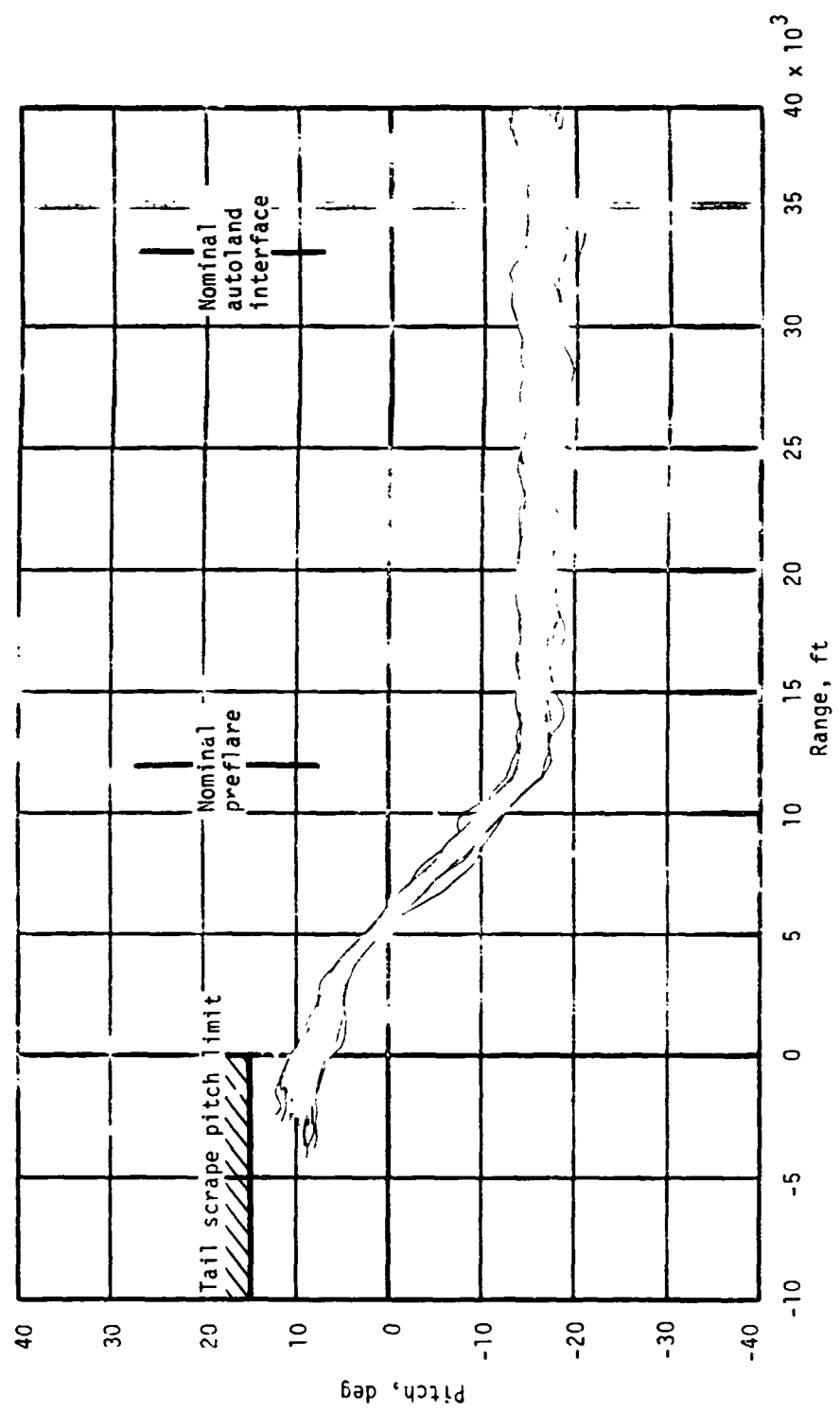
(j) Pitch.

Figure 7.- Continued.
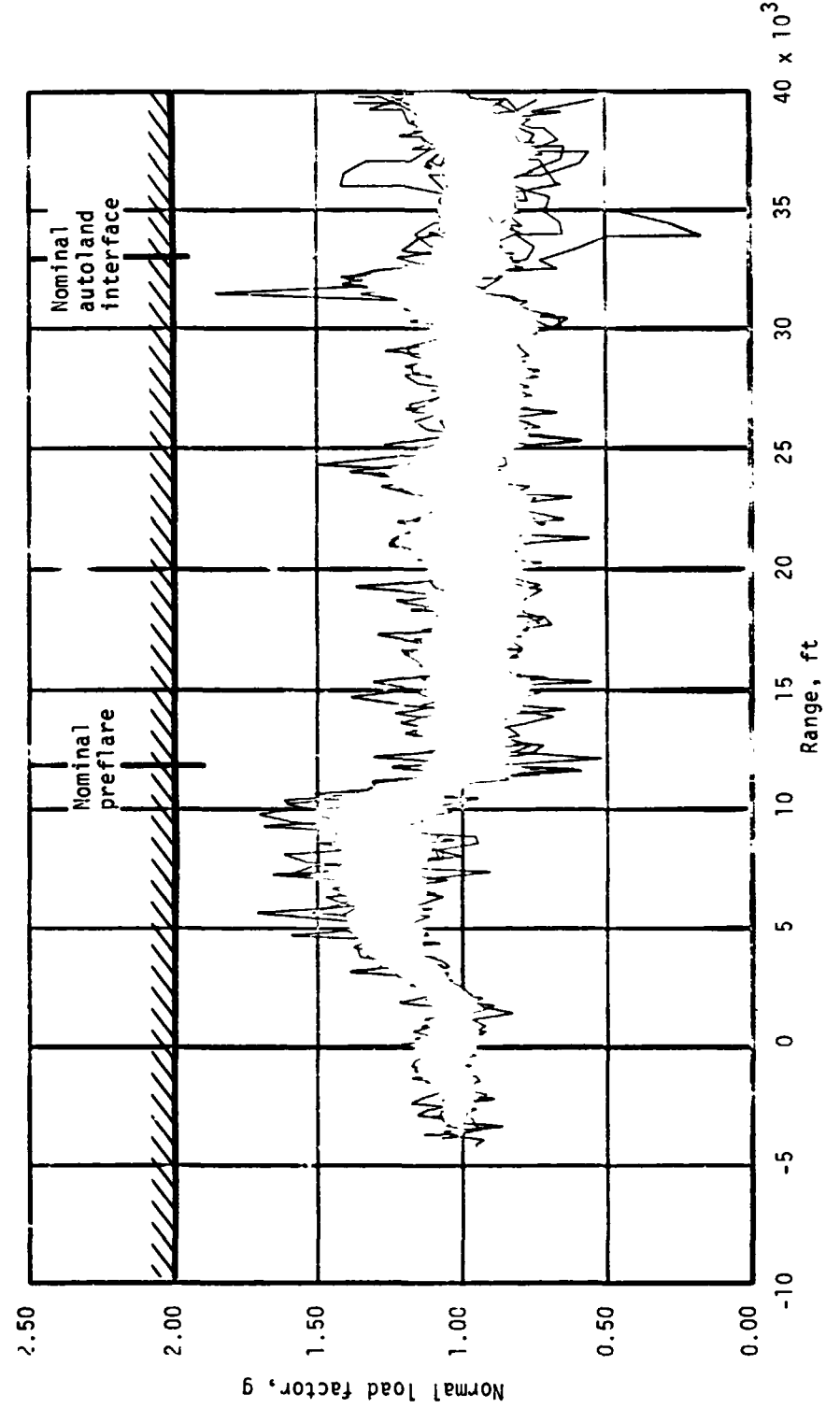
(k) Normal load factor.

Figure 7.- Continued.

81
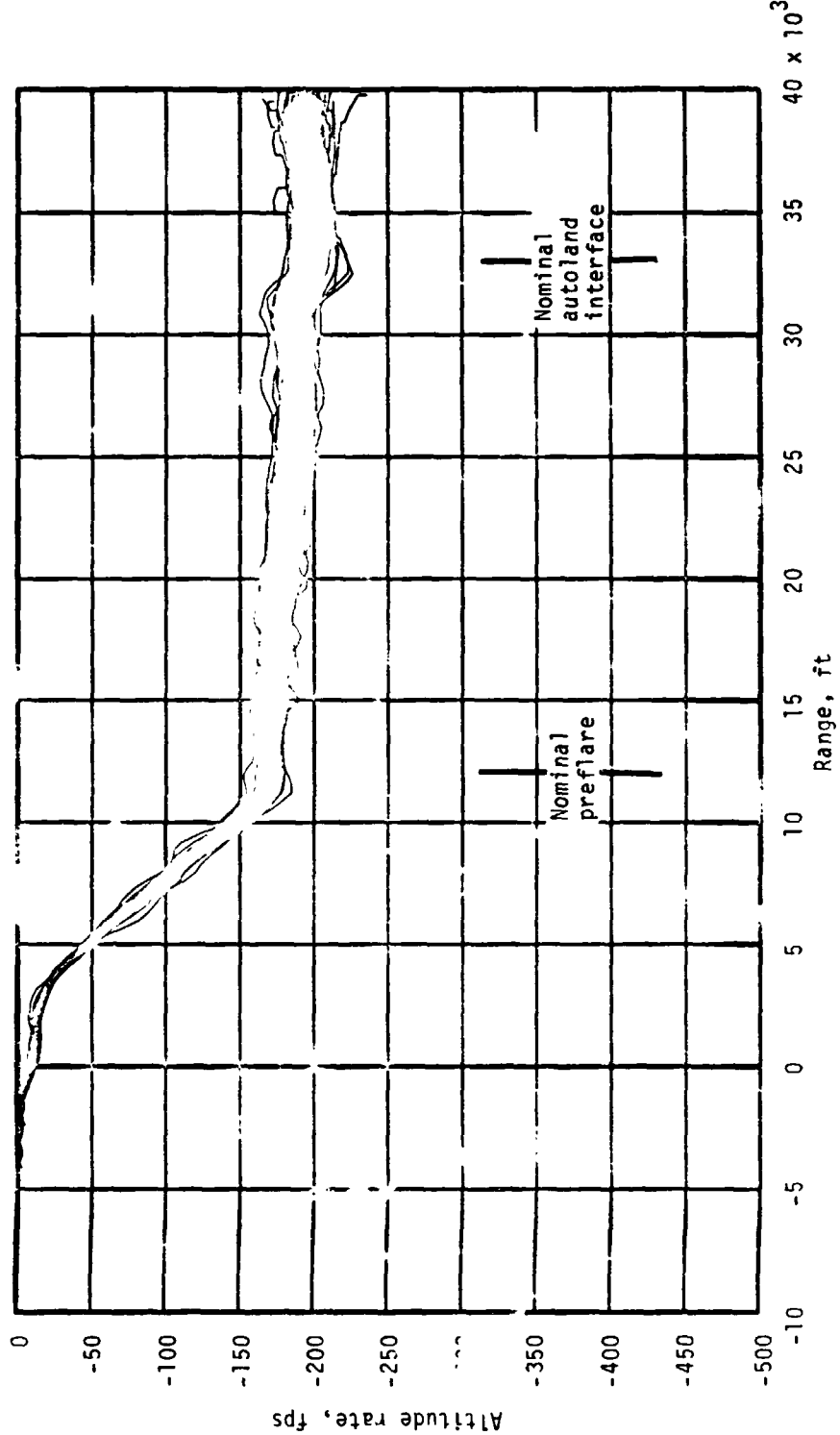
(1) Altitude rate.

Figure 7.- Continued.
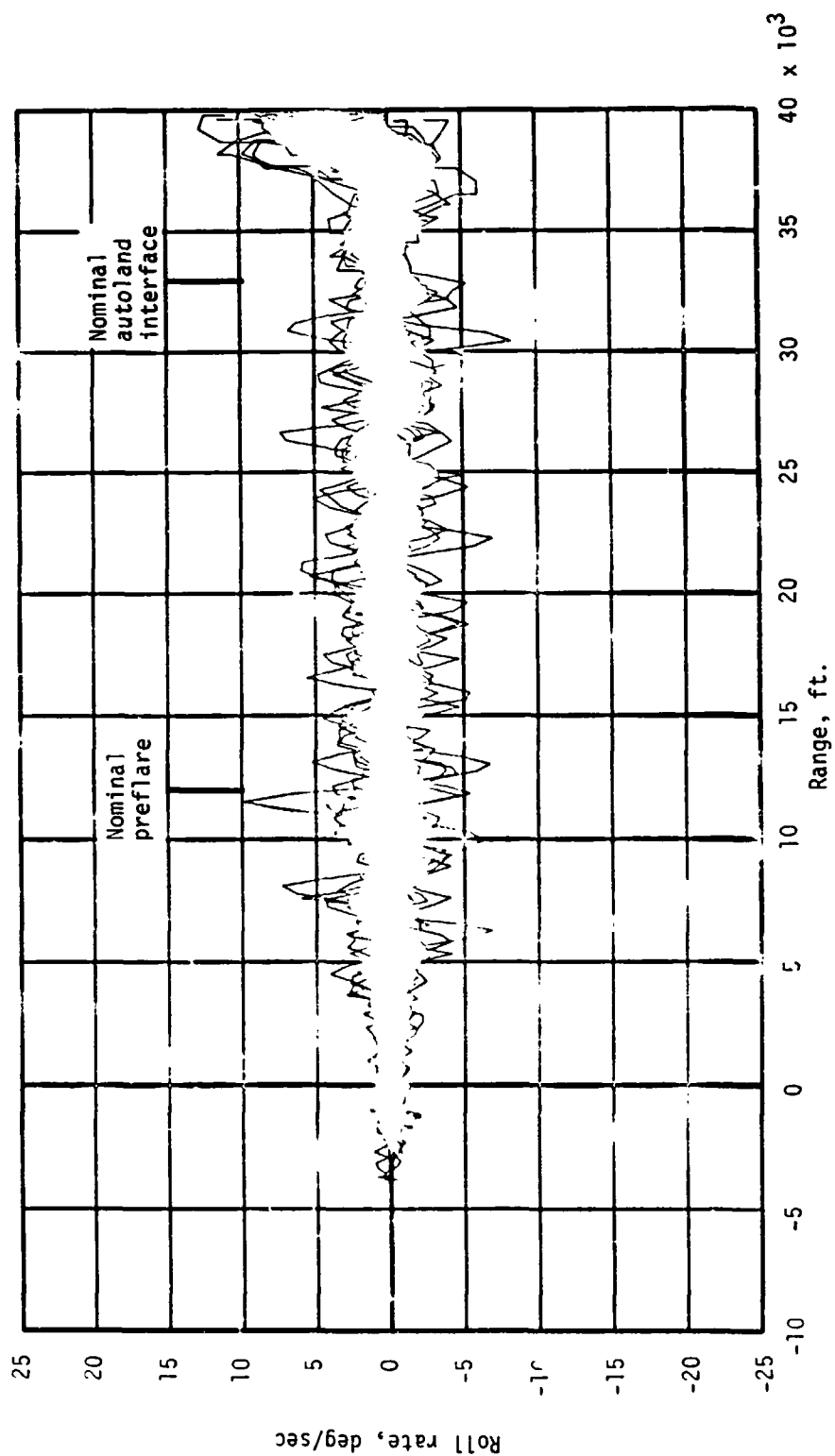
(m) Roll rate.

Figure 7.- Continued.
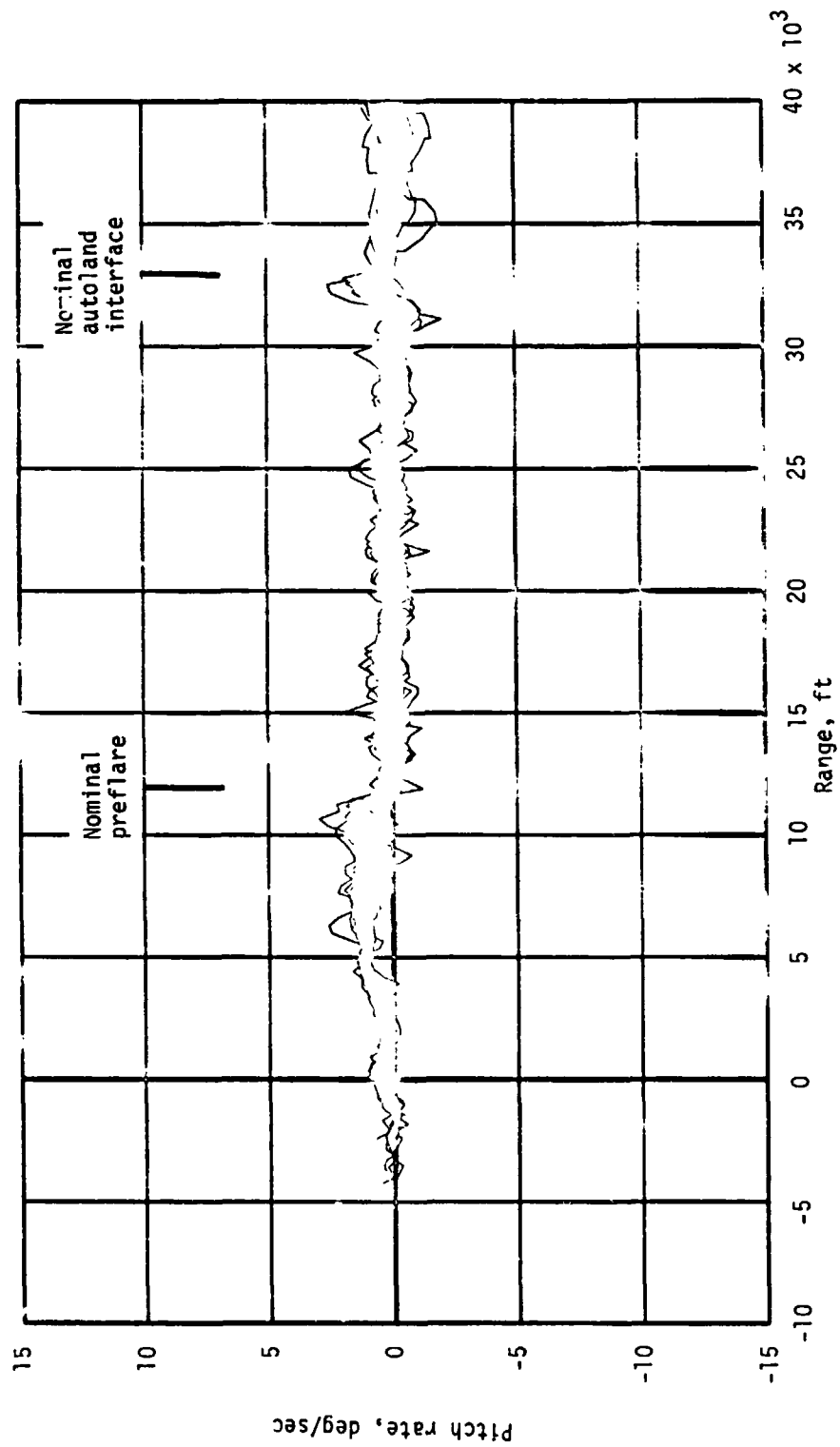
(n) Pitch rate.

Figure 7.- Continued.
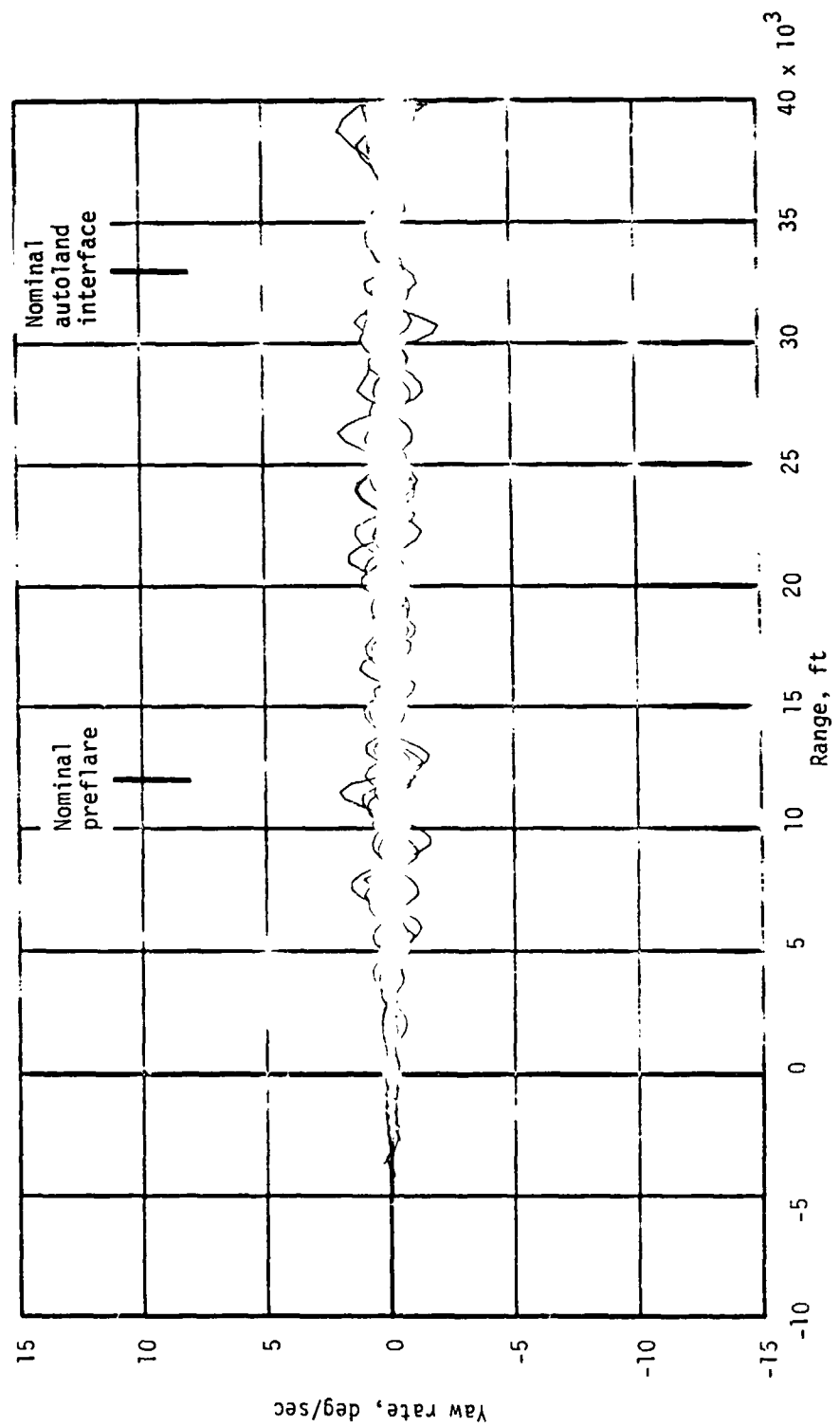
(o) Yaw rate.

Figure 7.- Continued.
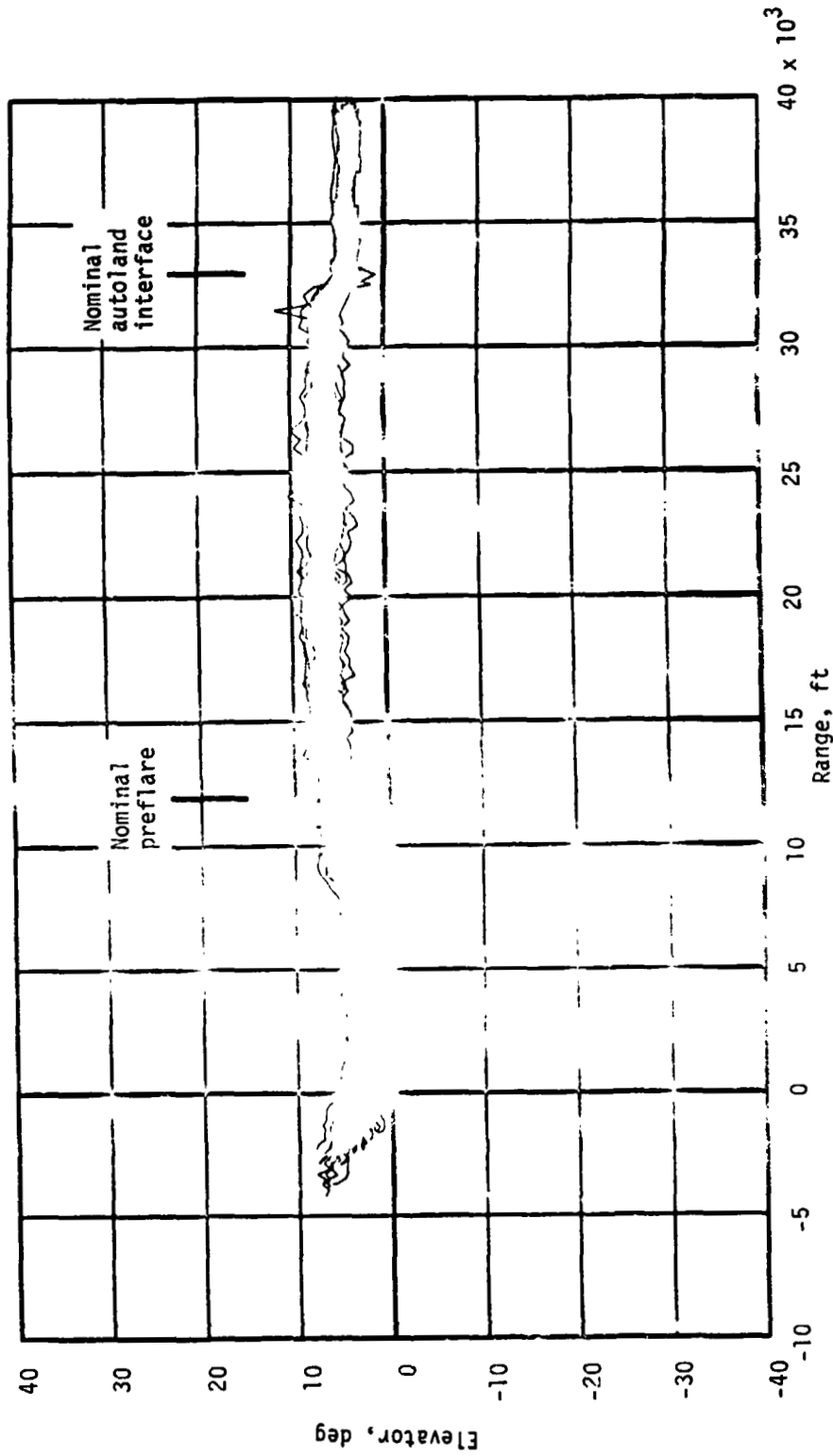
(p) Elevator deflections.

Figure 7.- Continued.
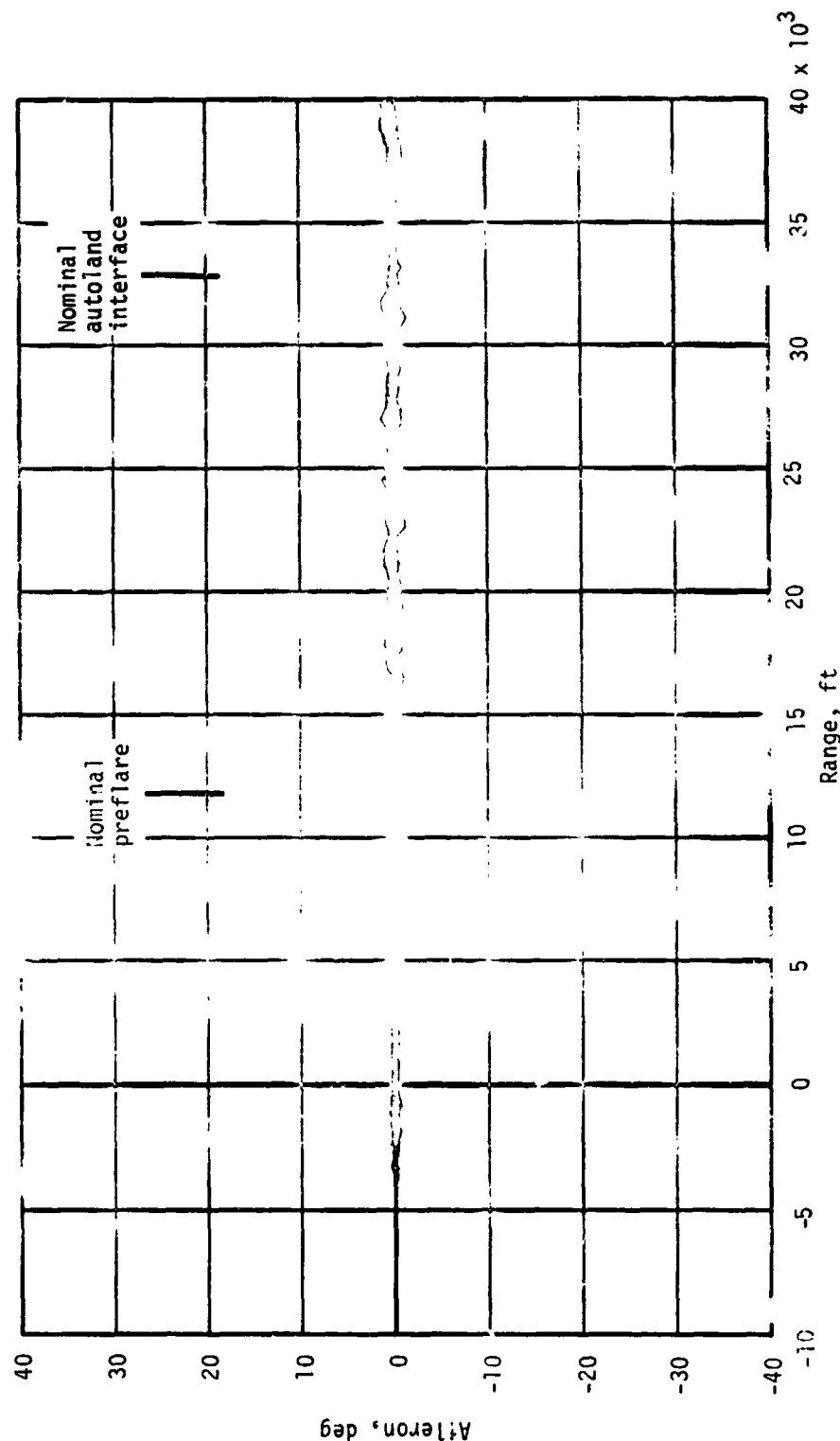
(q) Aileron deflections.

Figure 7.- Continued.
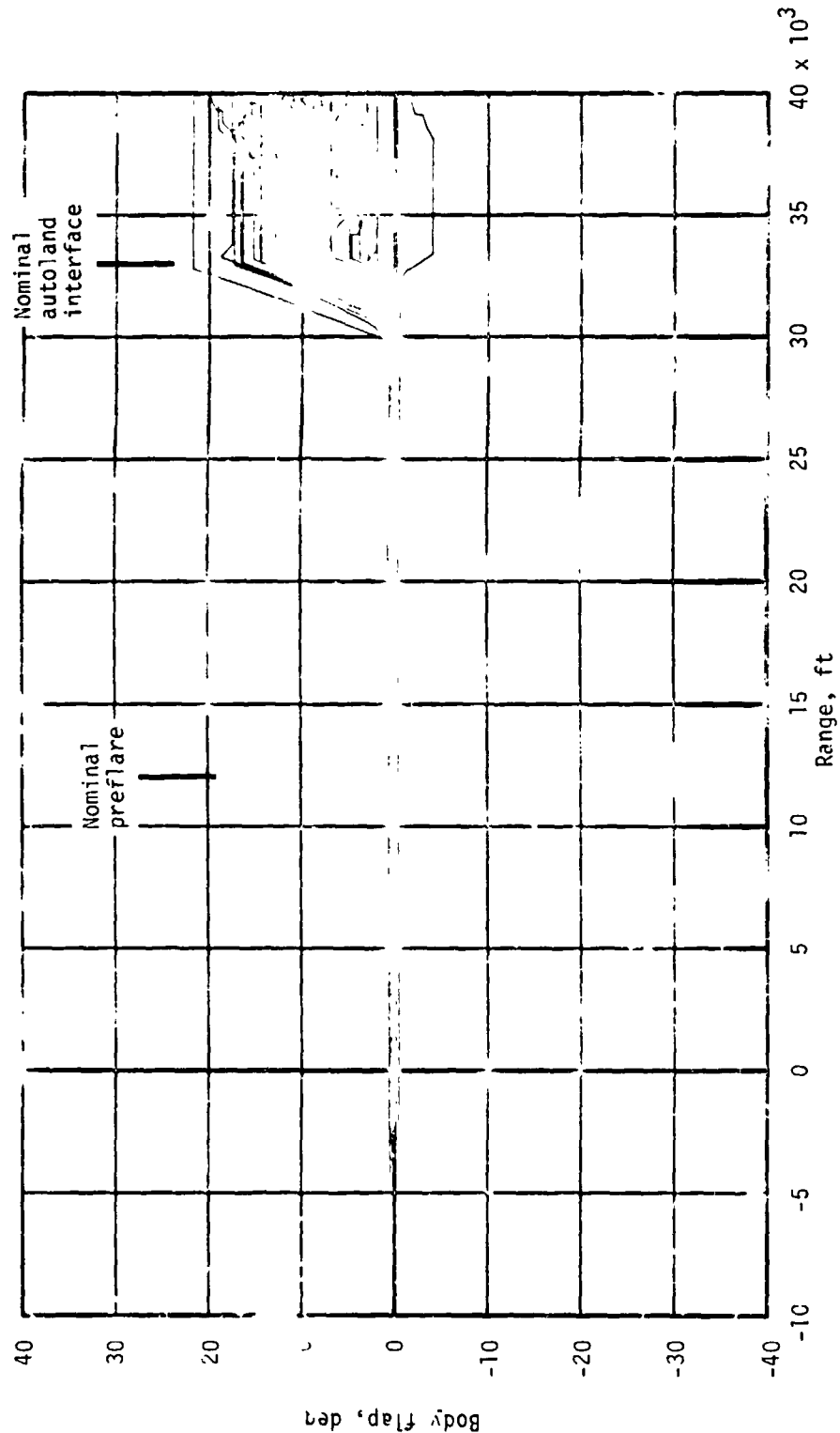
(r) Body-flap deflections.

Figure 7.- Continued.

88
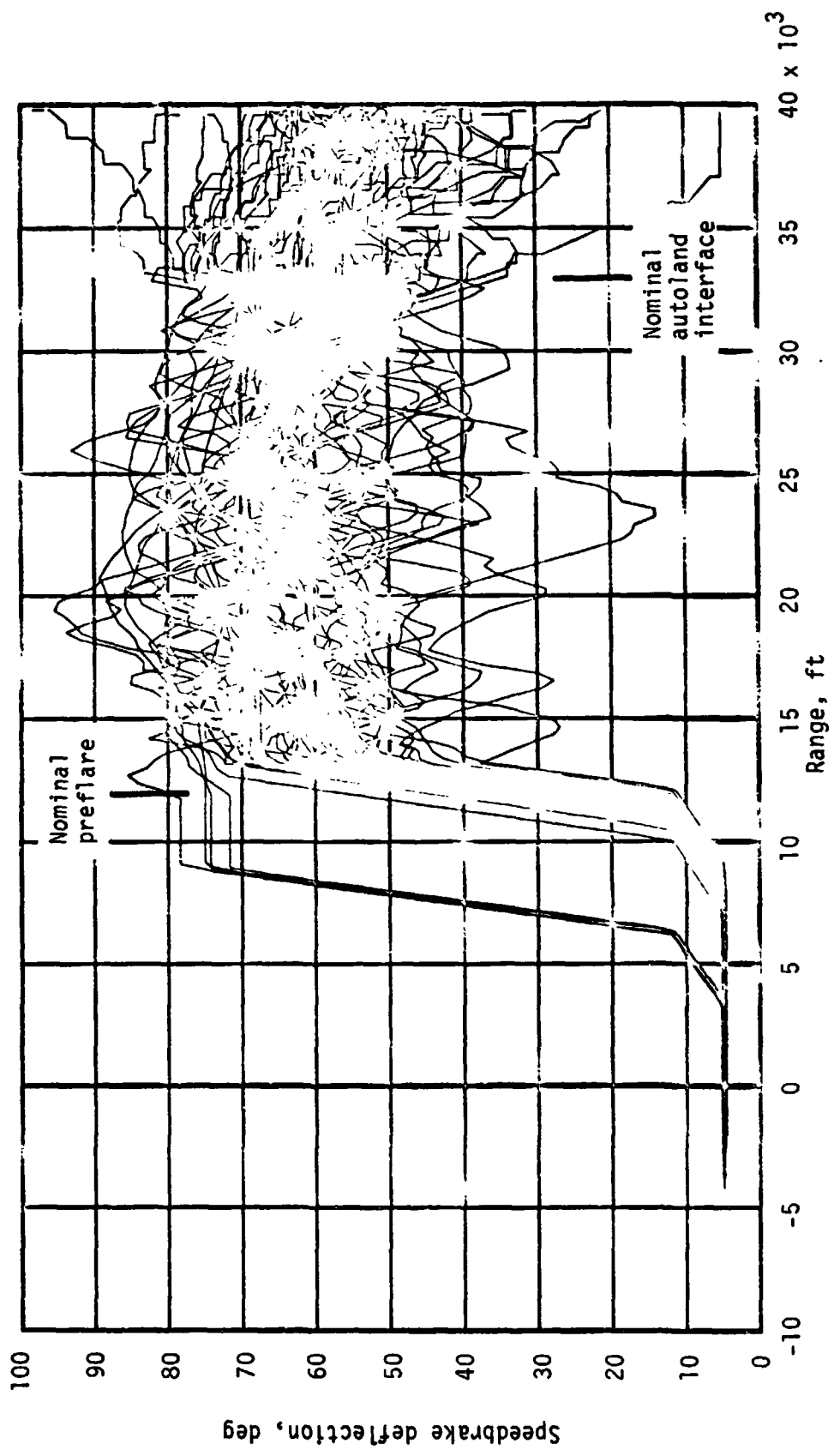
(s) Speedbrake deflections.
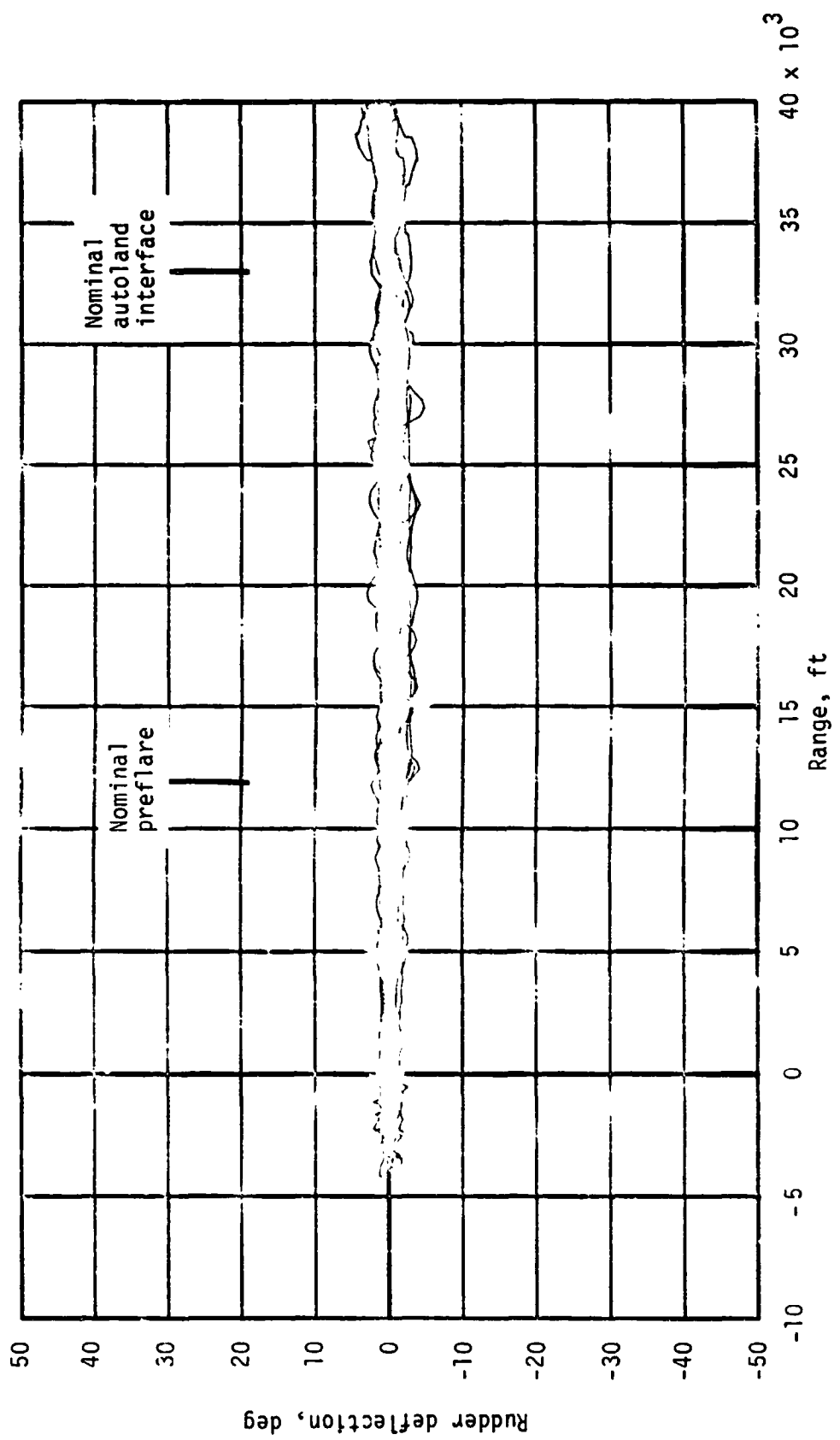
Figure 7.- Continued.

(t) Rudder deflections.

Figure 7.- Continued.
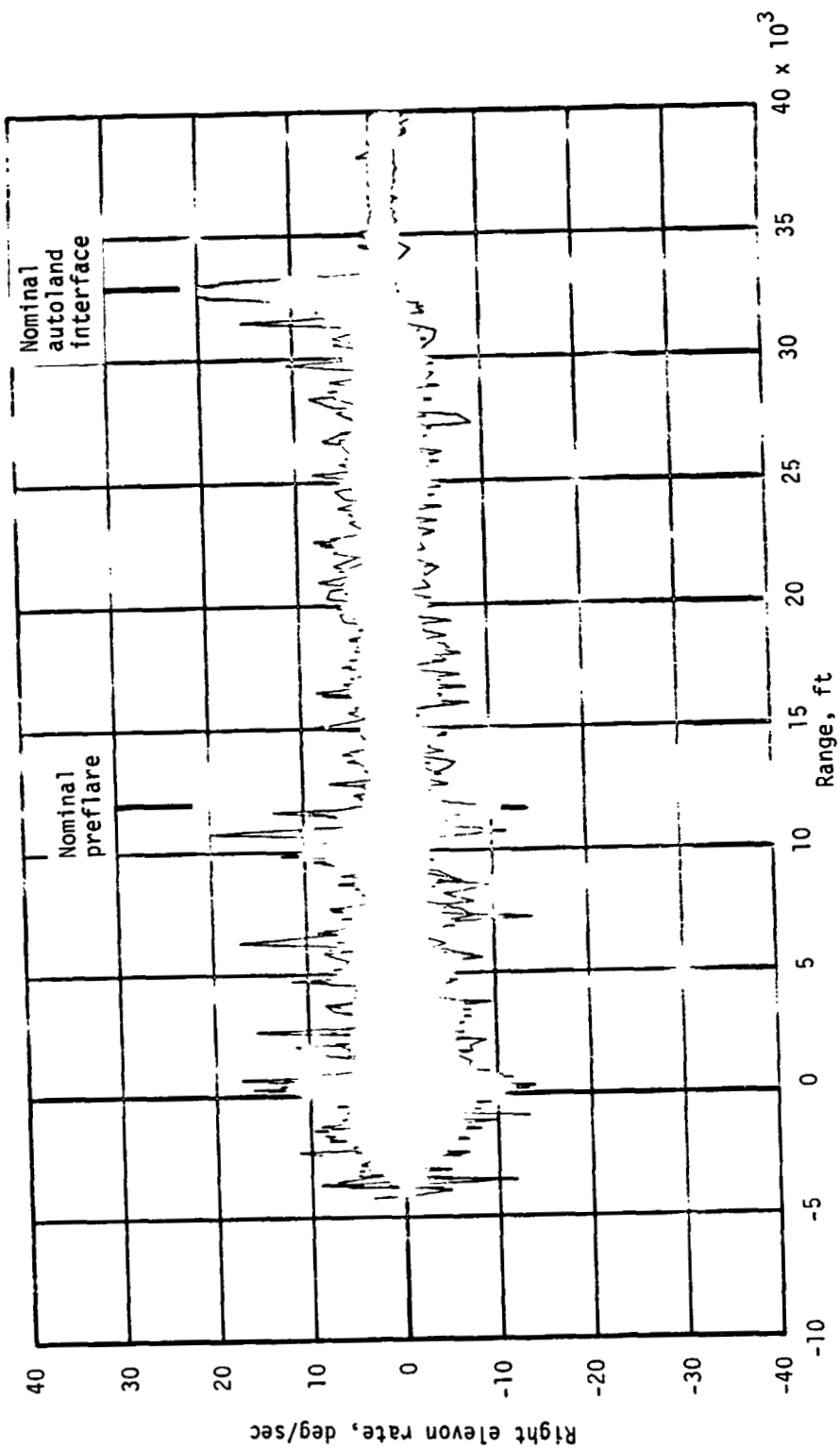
(u) Right elevon rate.

Figure 7.- Continued.
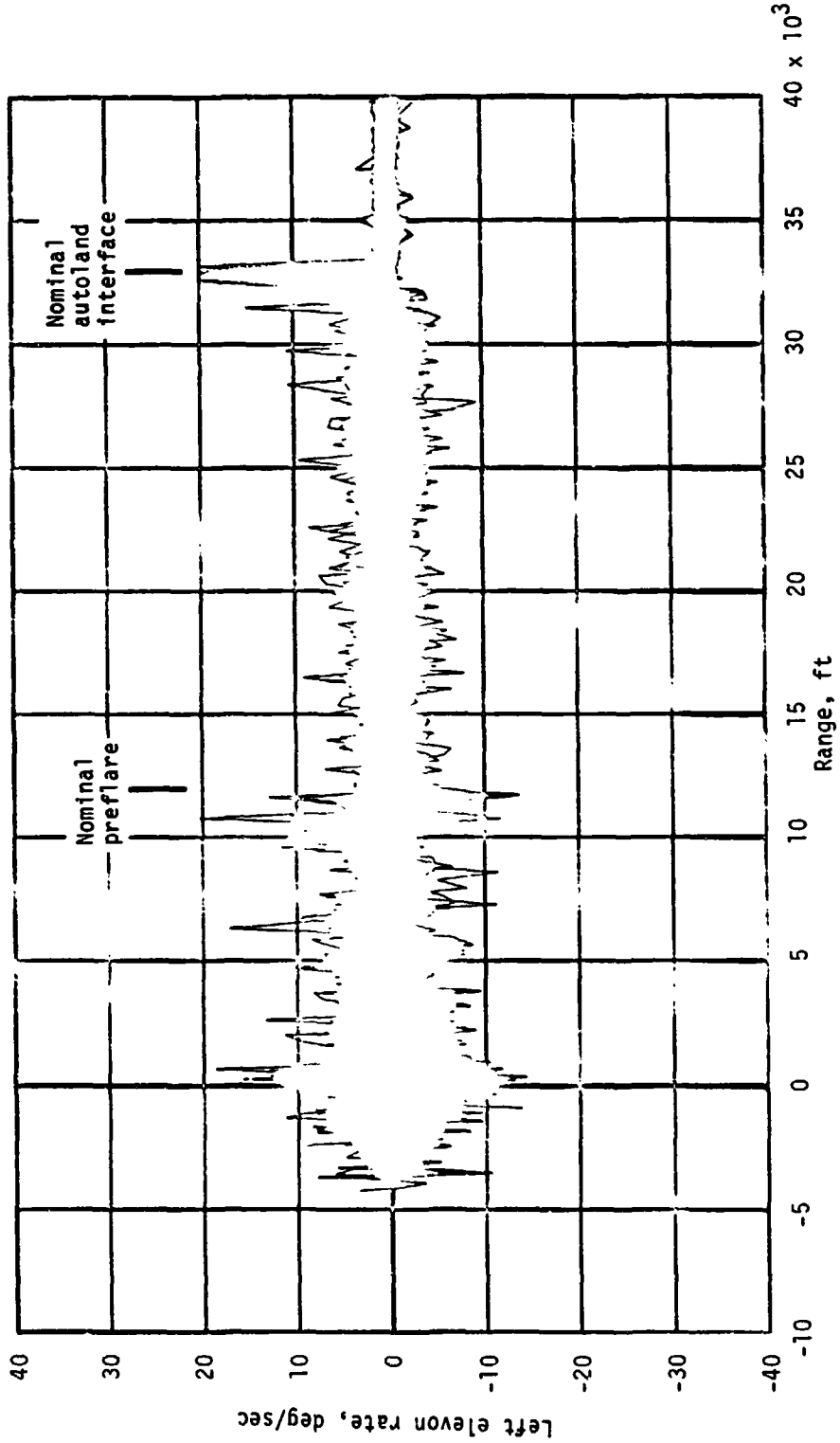
(v) Left elevon rate.

Figure 7.- Continued.
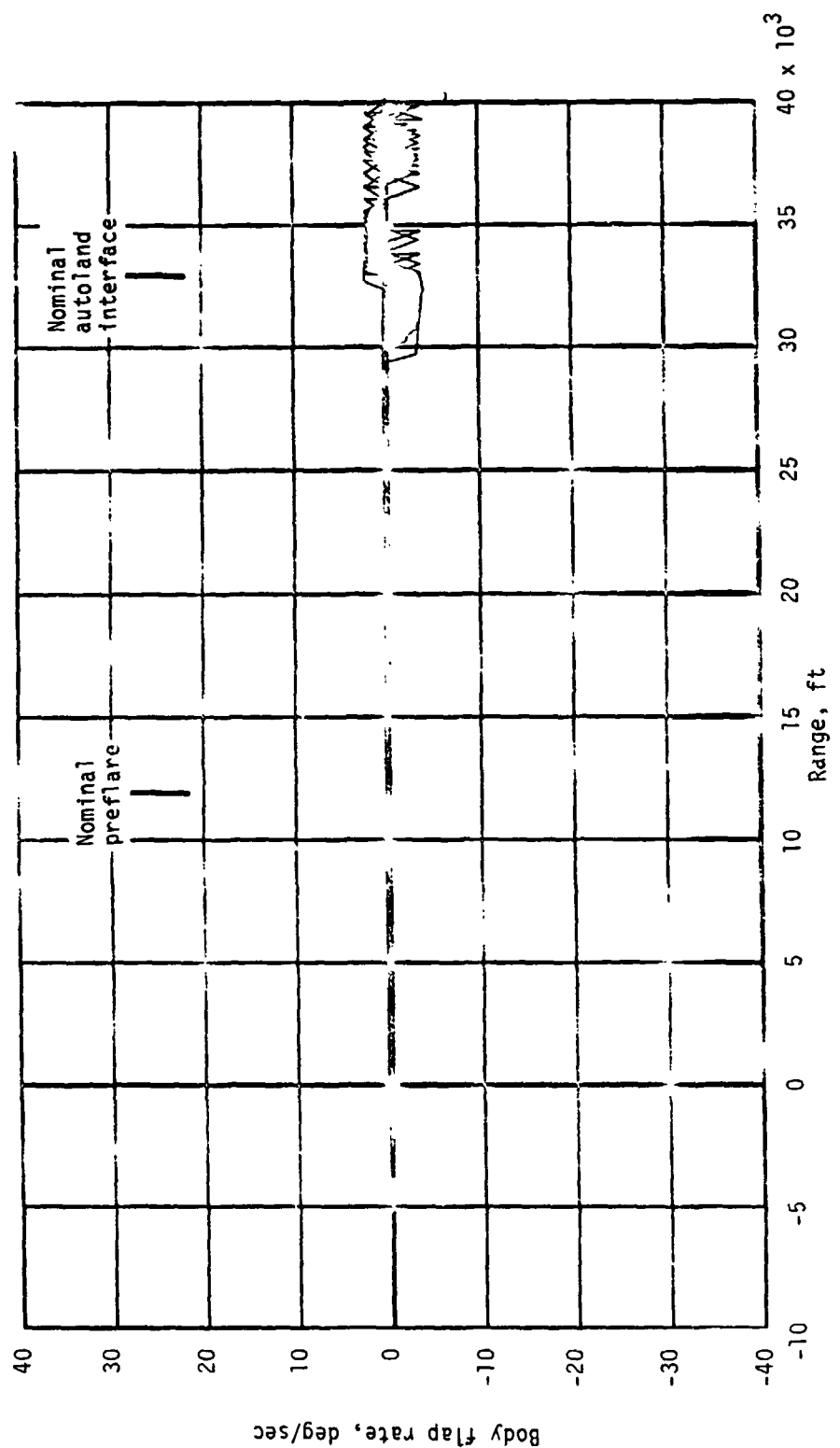
(w) Body-flap rate.

Figure 7.- Continued.
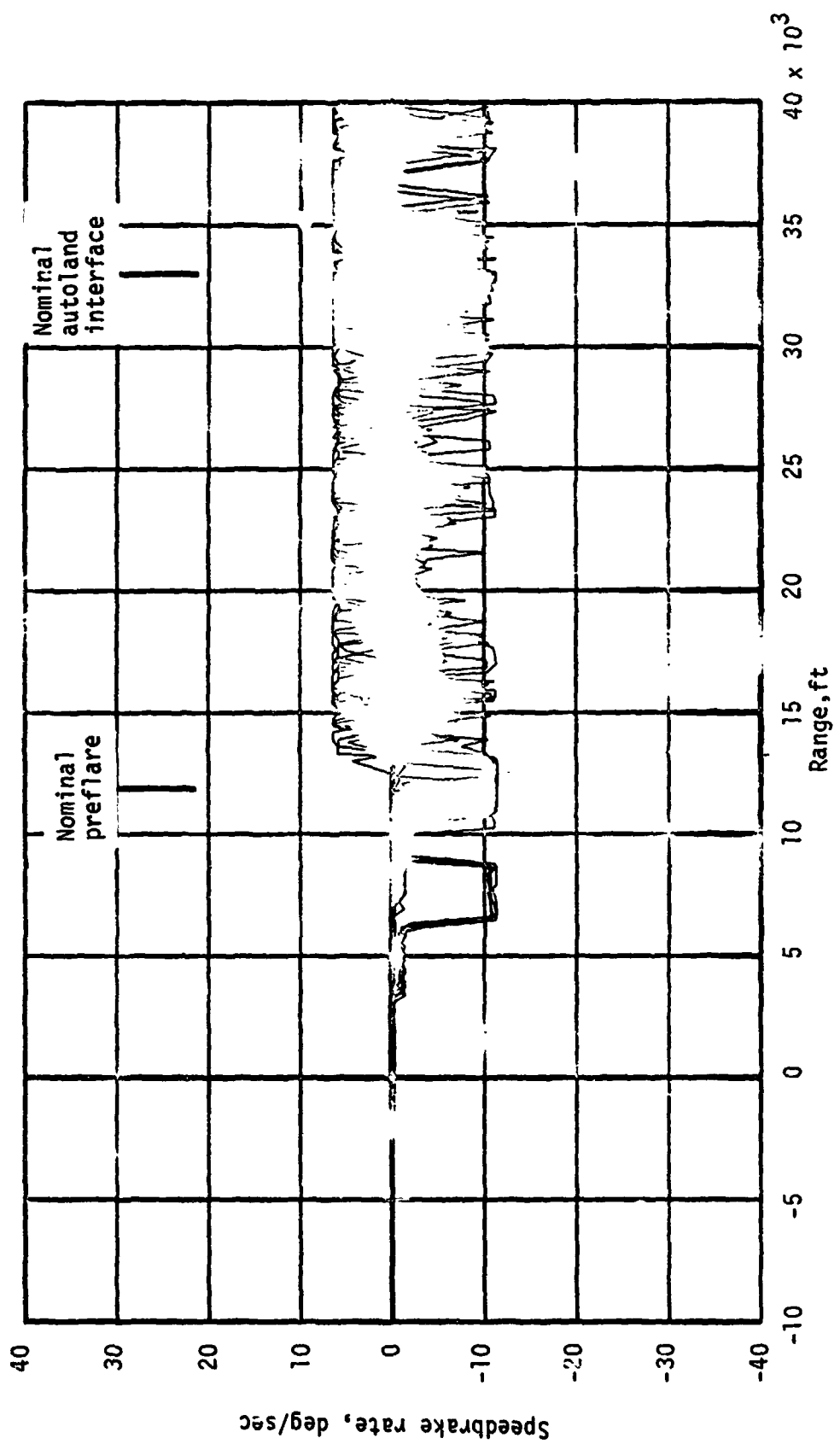
(x) Speedbrake rate.

Figure 7.- Continued.

94
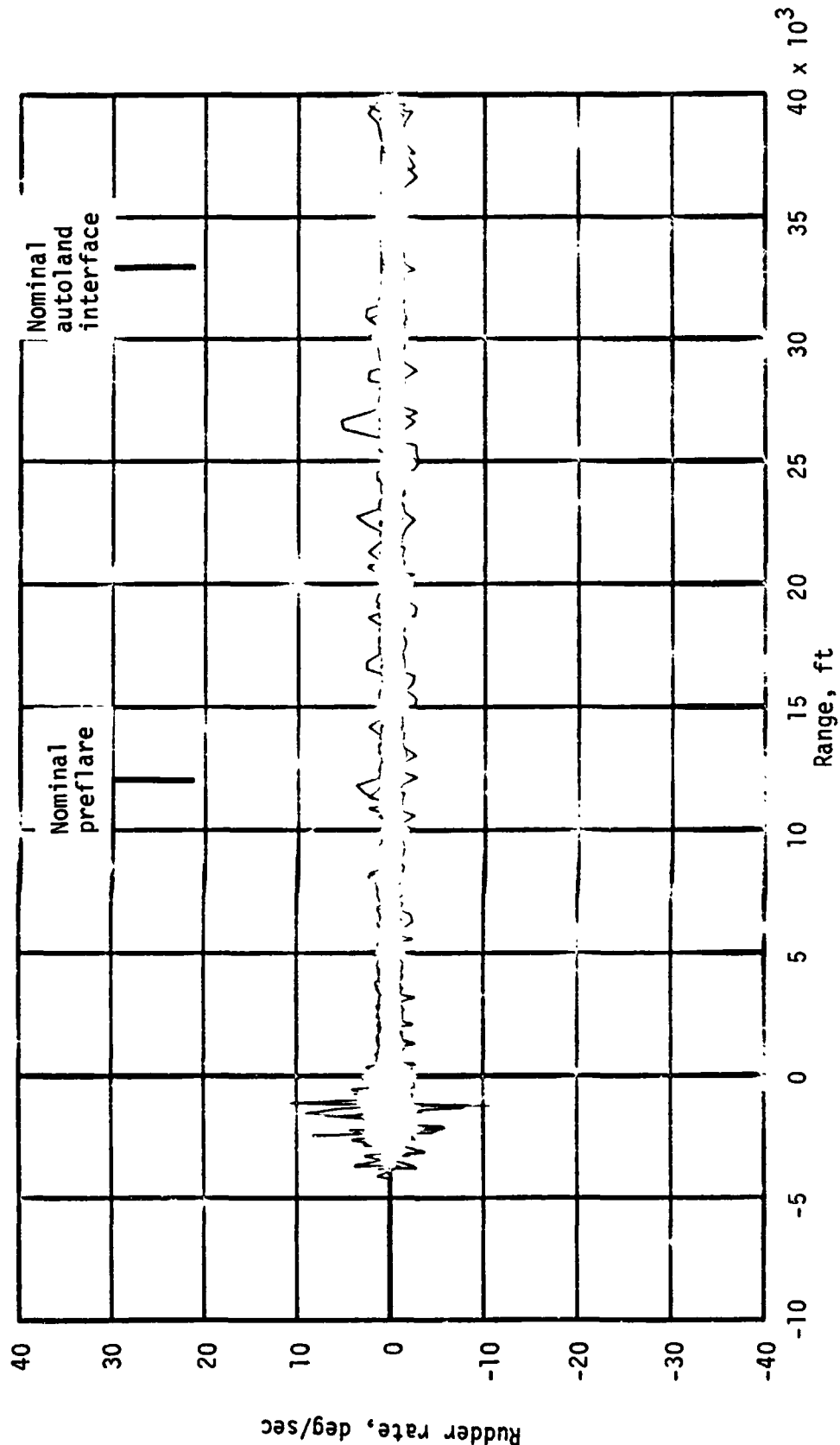
(y) Rudder rate.

Figure 7.- Continued.
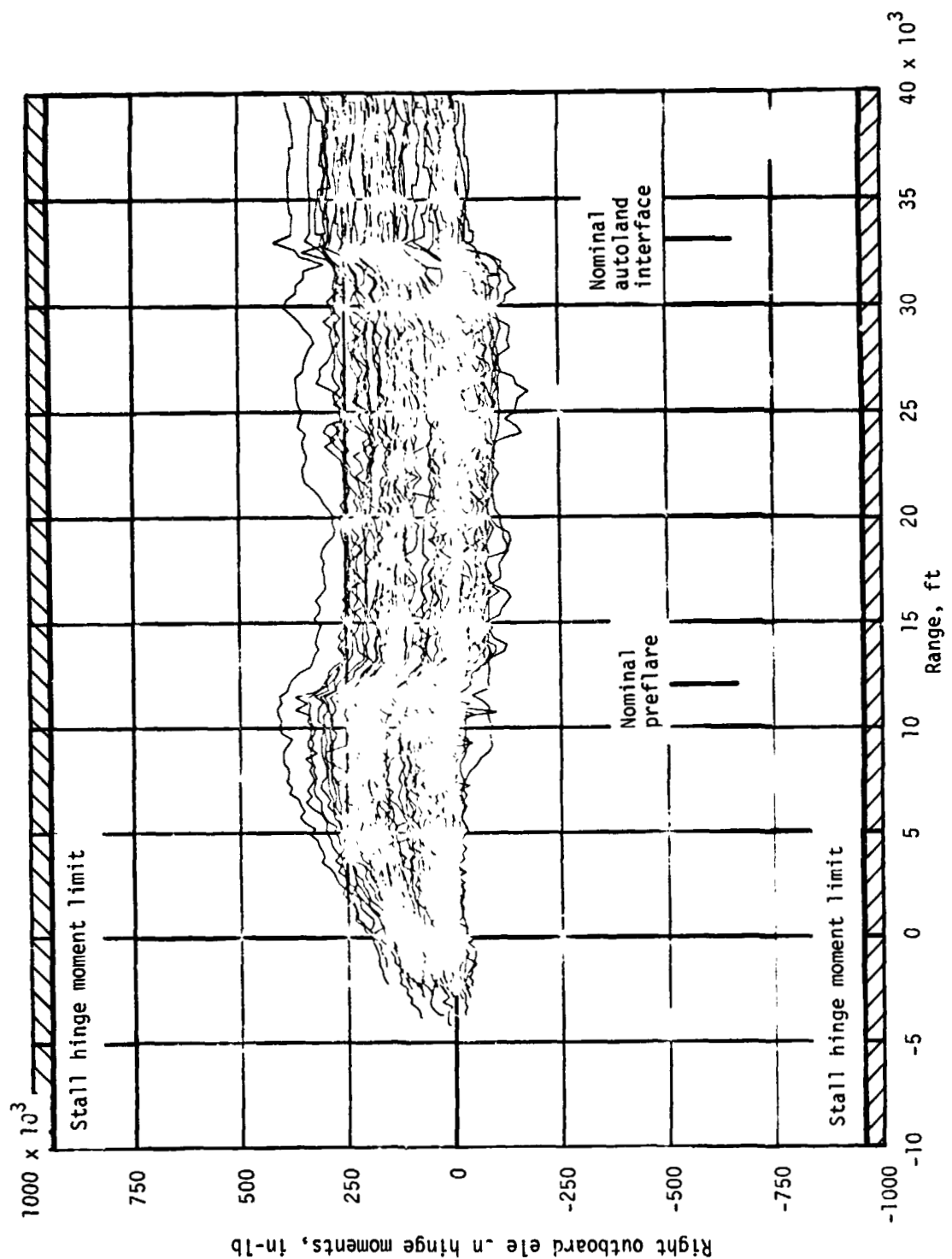
(z) Right inboard elevon hinge moments.

Figure 7.- Continued.

96
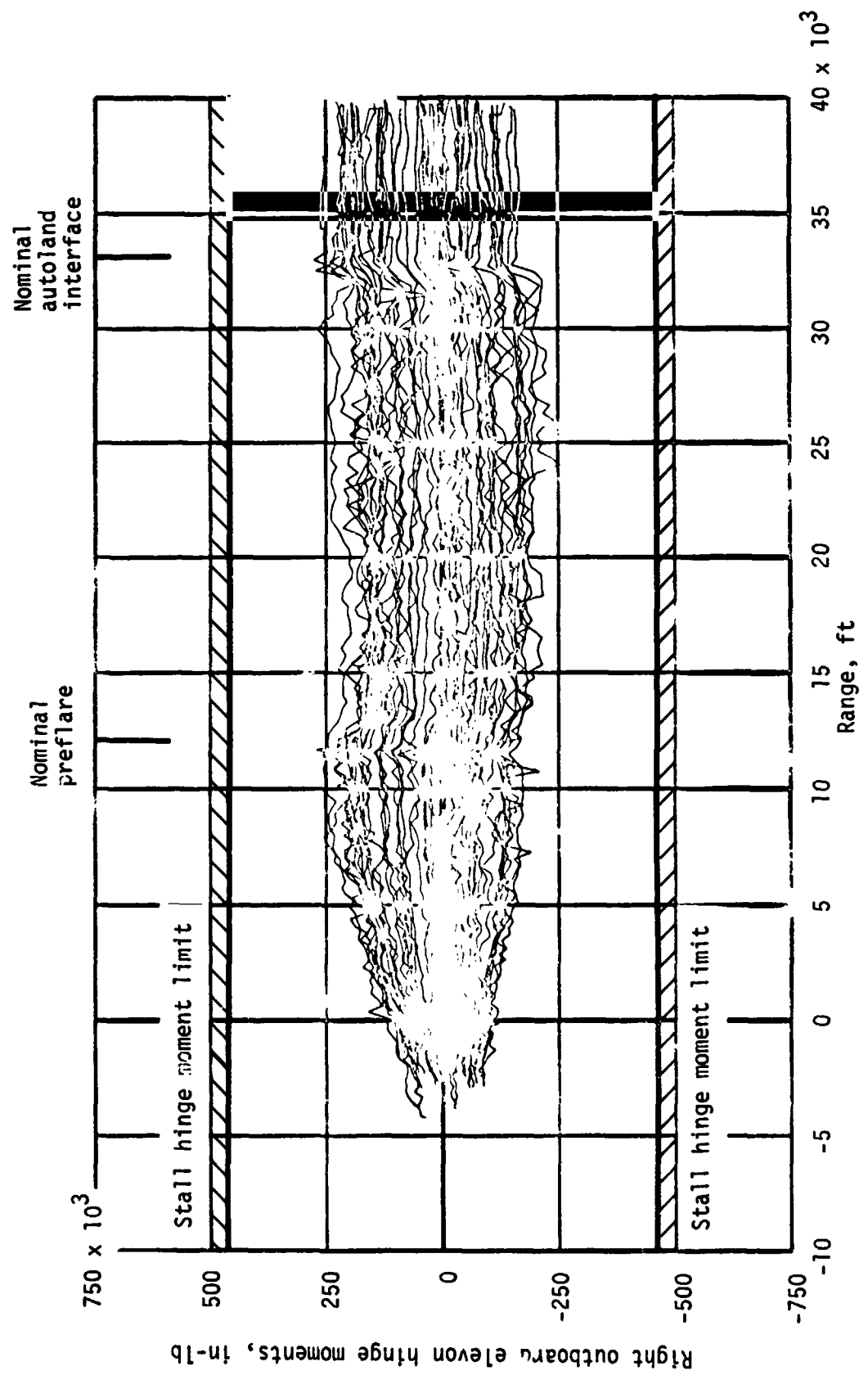
(aa) Right outboard elevon hinge moments.
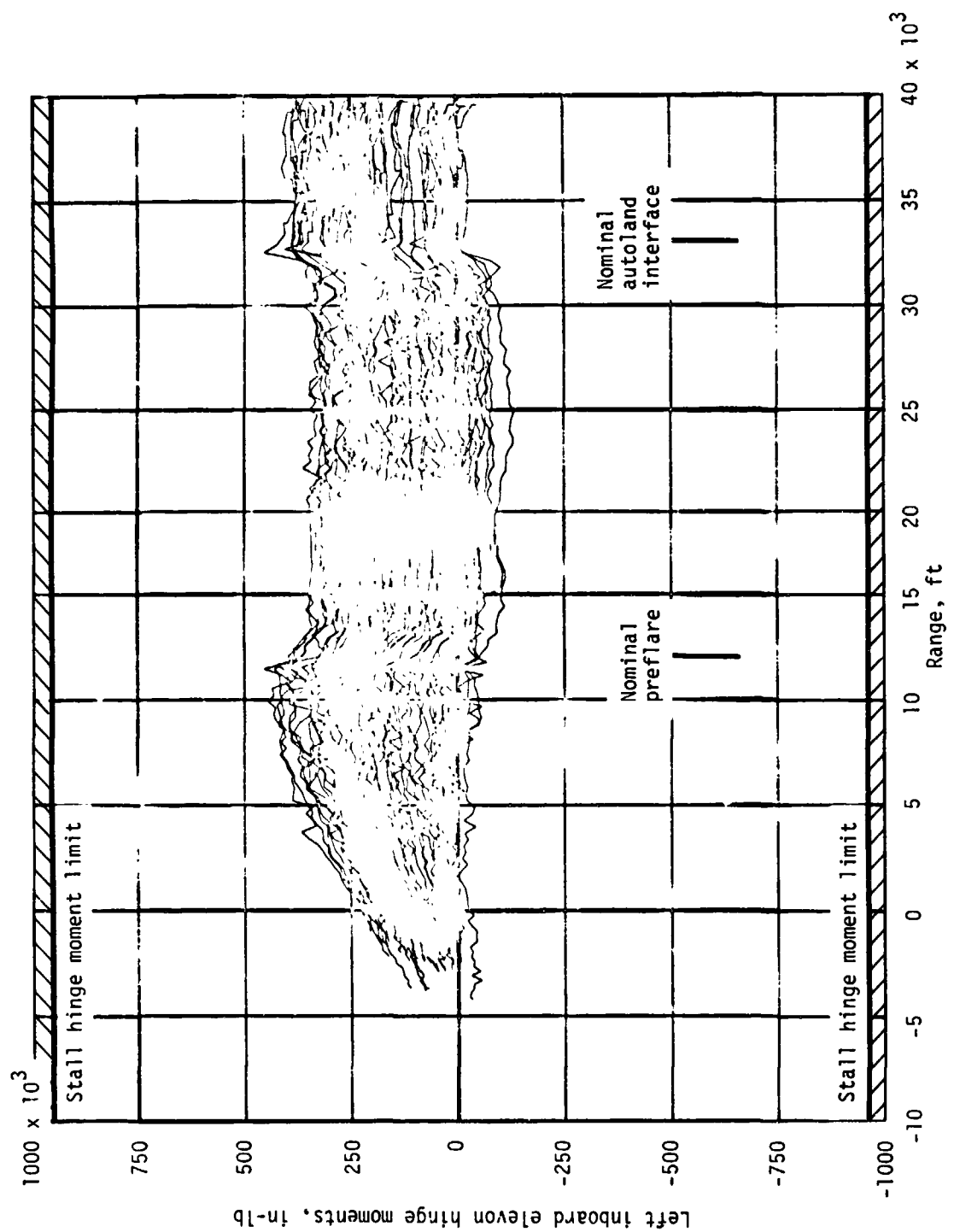
Figure 7.- Continued.

(bb) Left inboard elevon hinge moments.
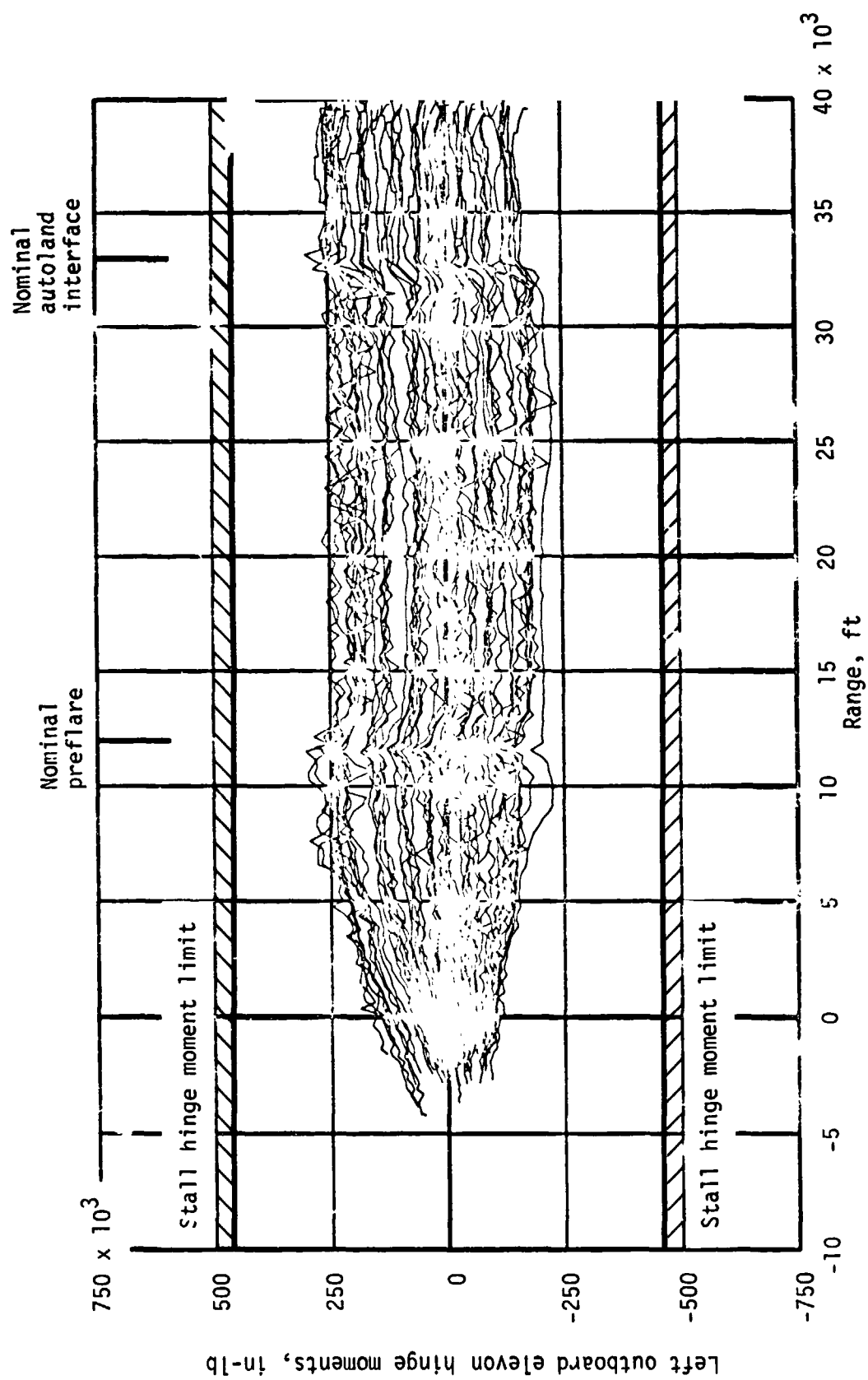
Figure 7.- Continued.

(cc) Left outboard elevon hinge moment.

Figure 7.- Continued.
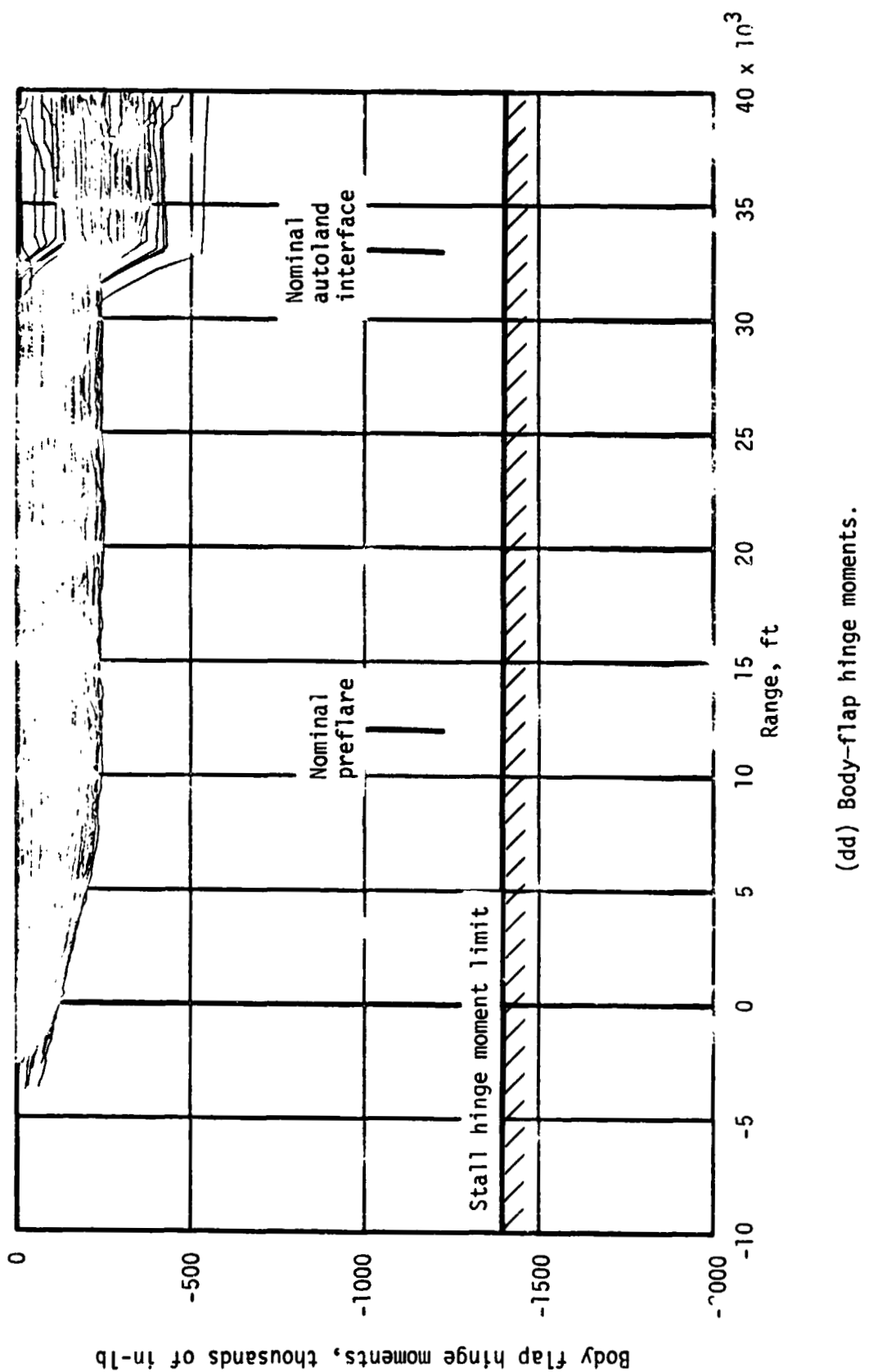
(dd) Body-flap hinge moments.
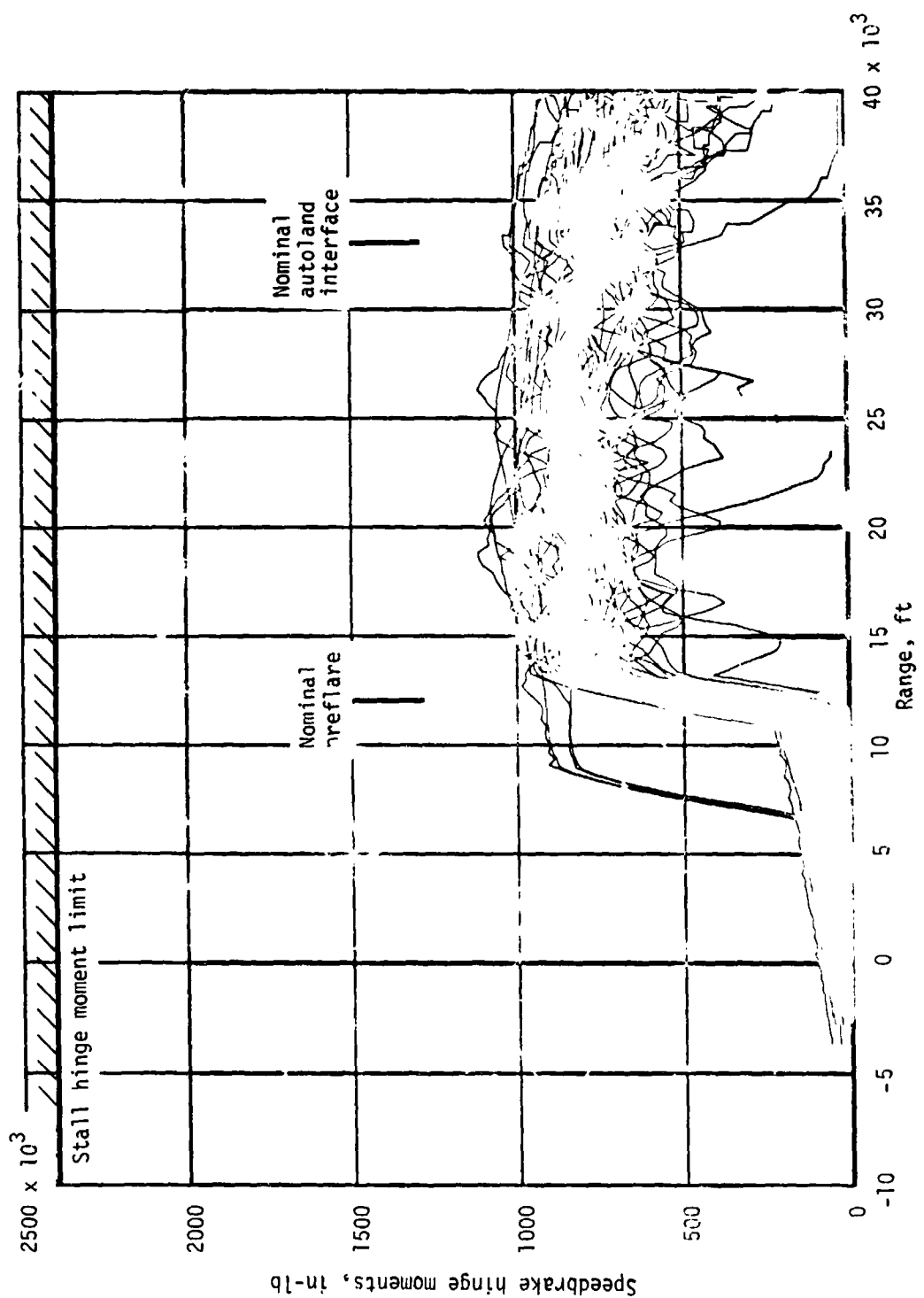
Figure 7.- Continued.

(ee) Speedbrake hinge moments.
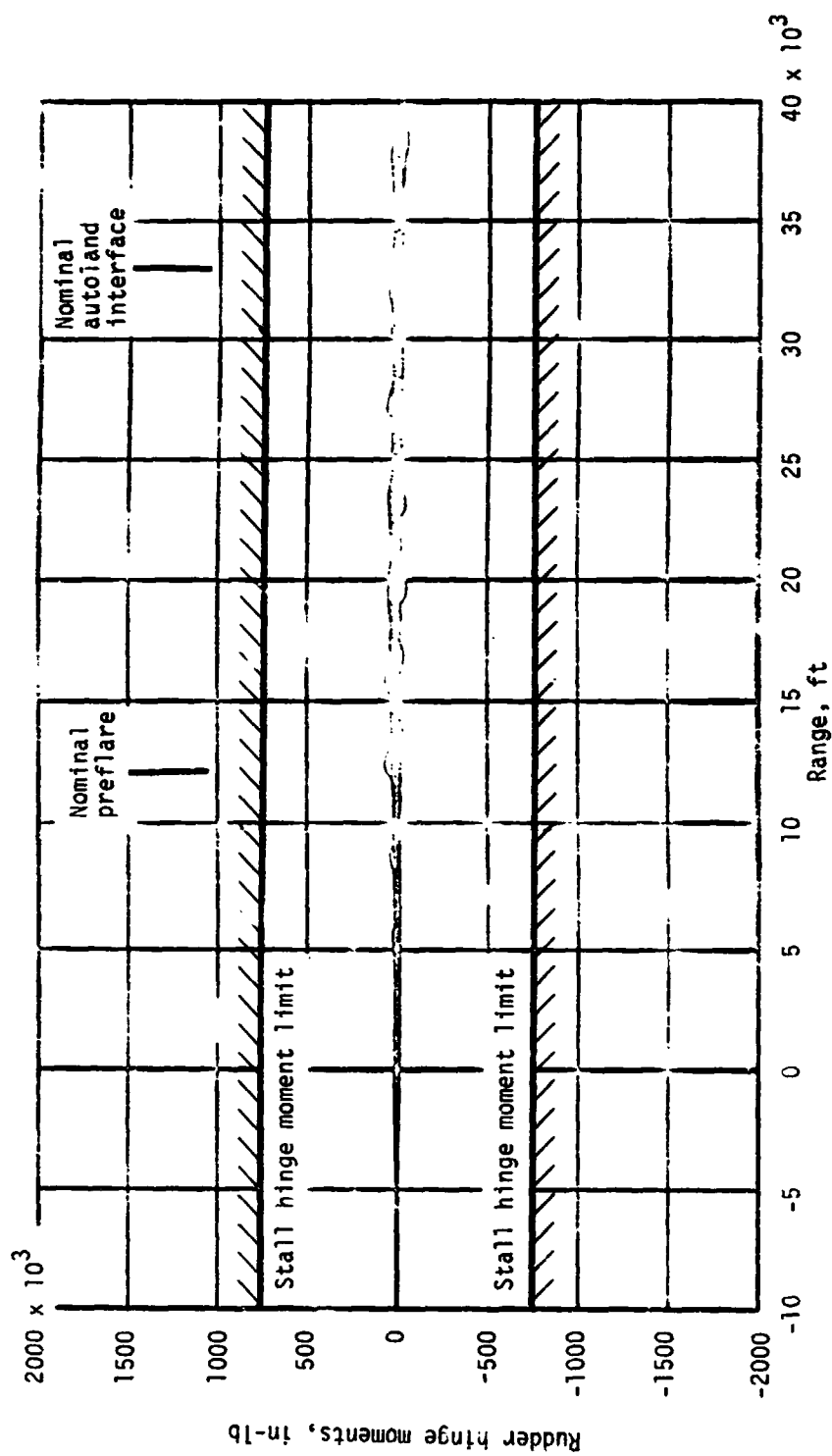
Figure 7.- Continued.

(ff) Rudder hinge moments.

Figure 7.- Concluded.
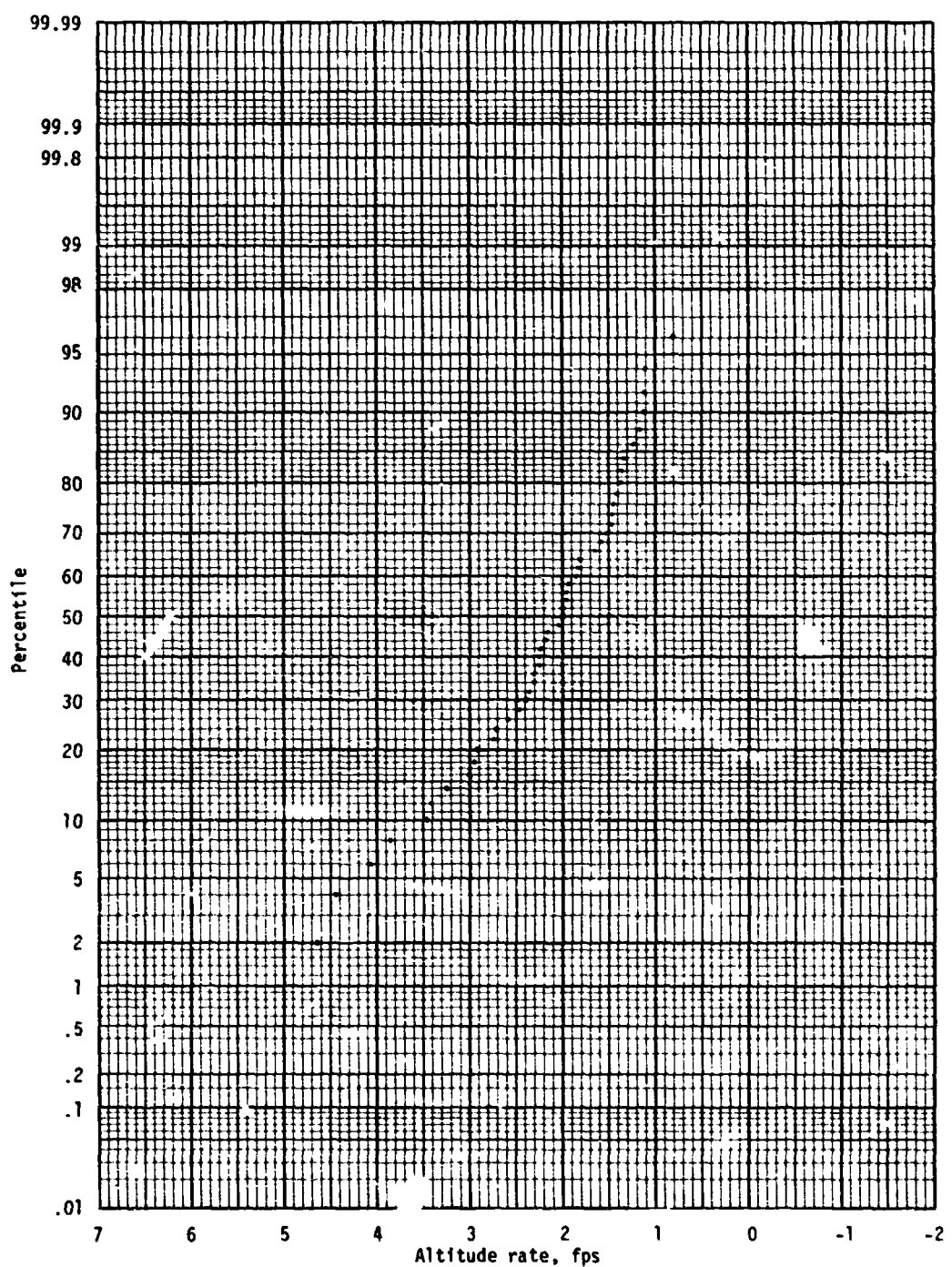
(a) Altitude te.

Figure 8.- Landing statistics.
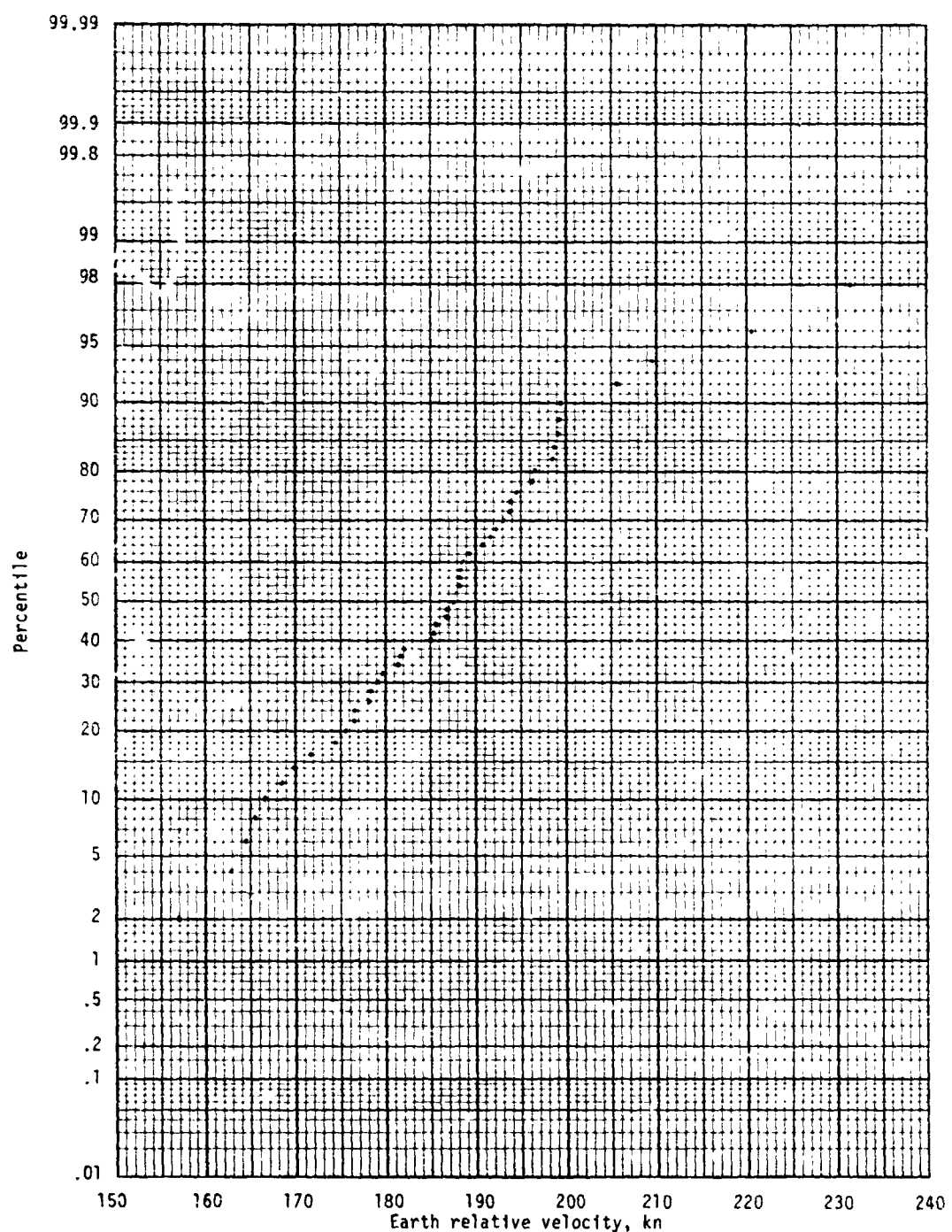
(b) Earth-relative velocity.

Figure 8.- Continued.
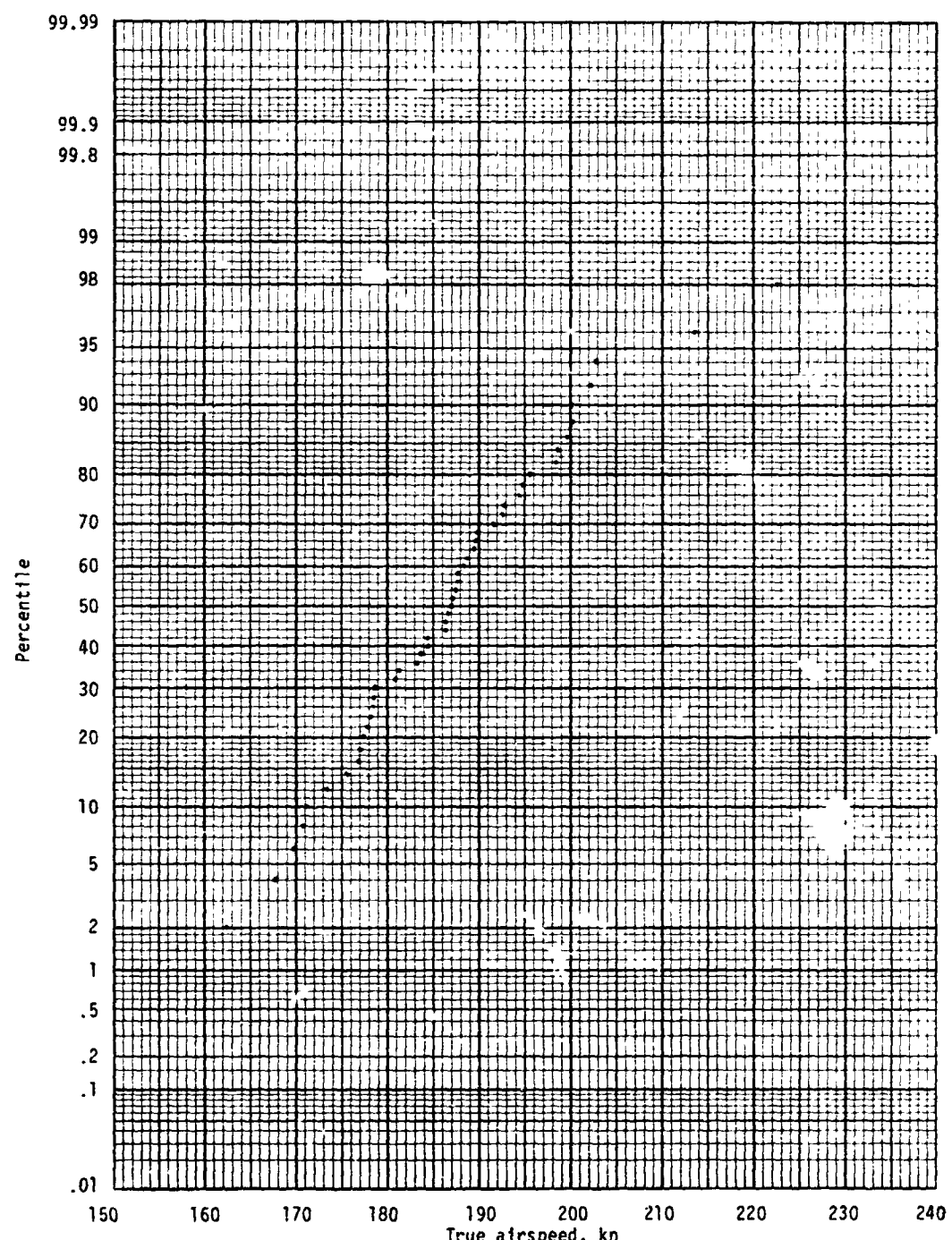
(c) True airspeed.

Figure 8.- Continued.

105
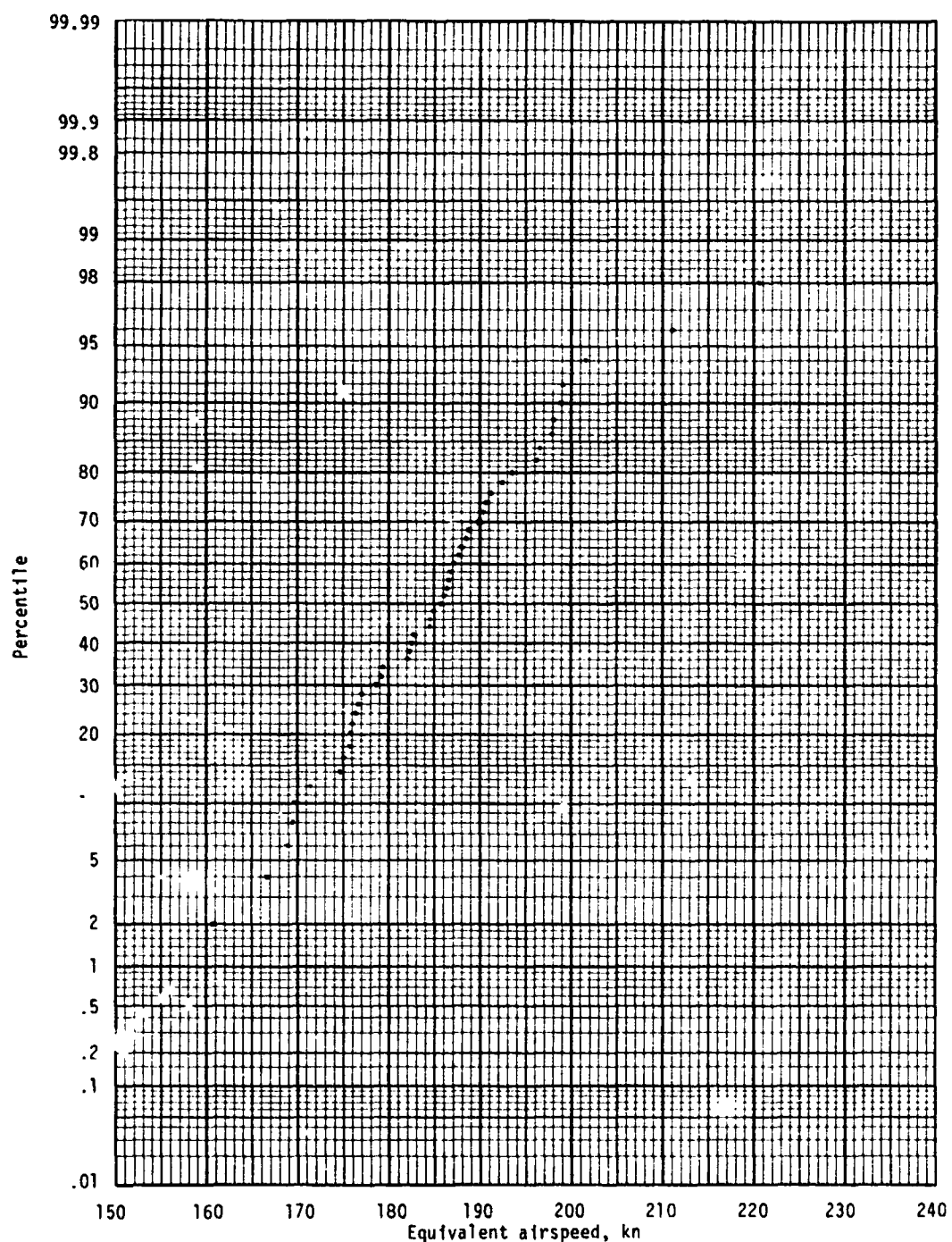
(d) Equivalent airspeed.

Figure 8.- Continued.
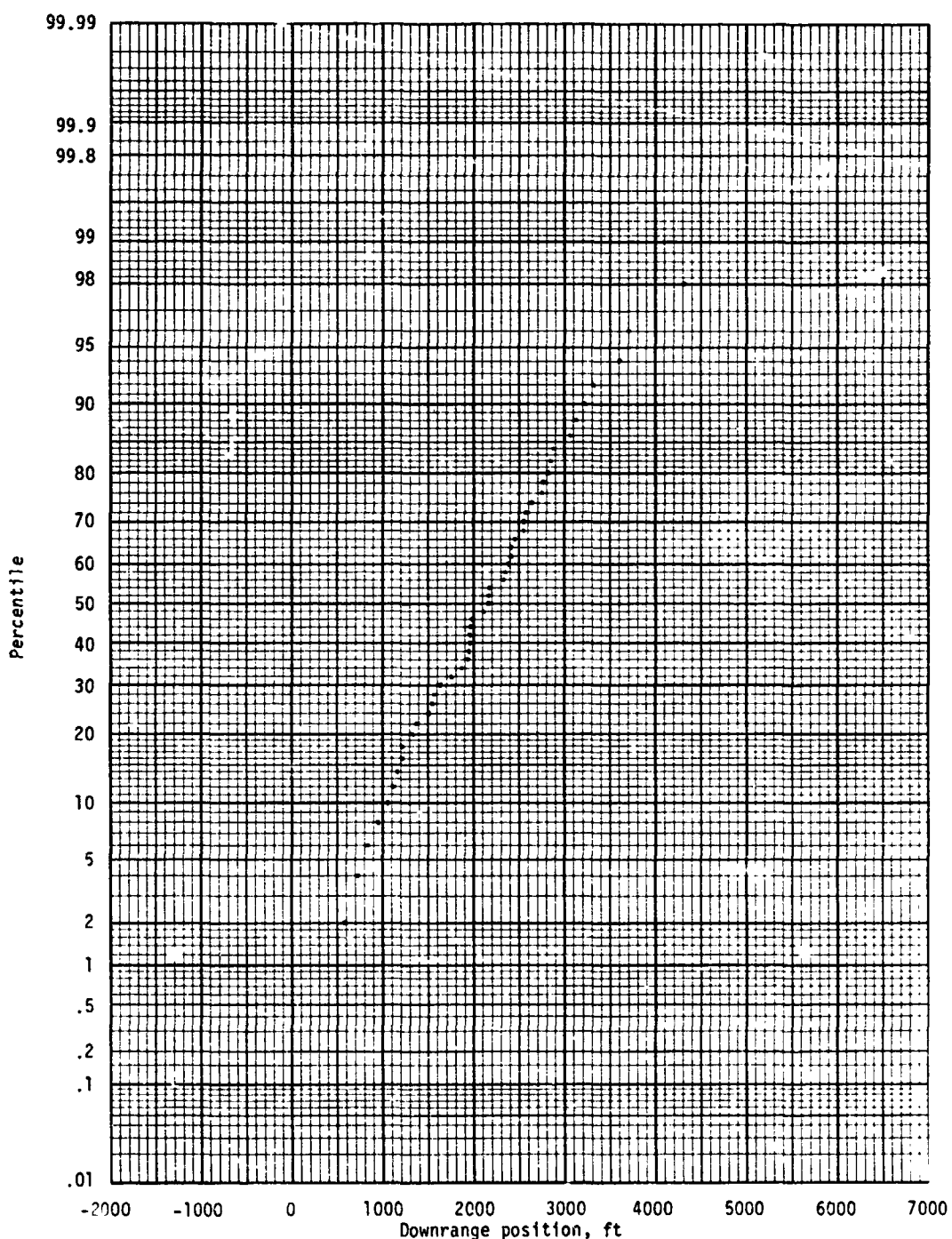
(e) Downrange position.

Figure 8.- Continued.
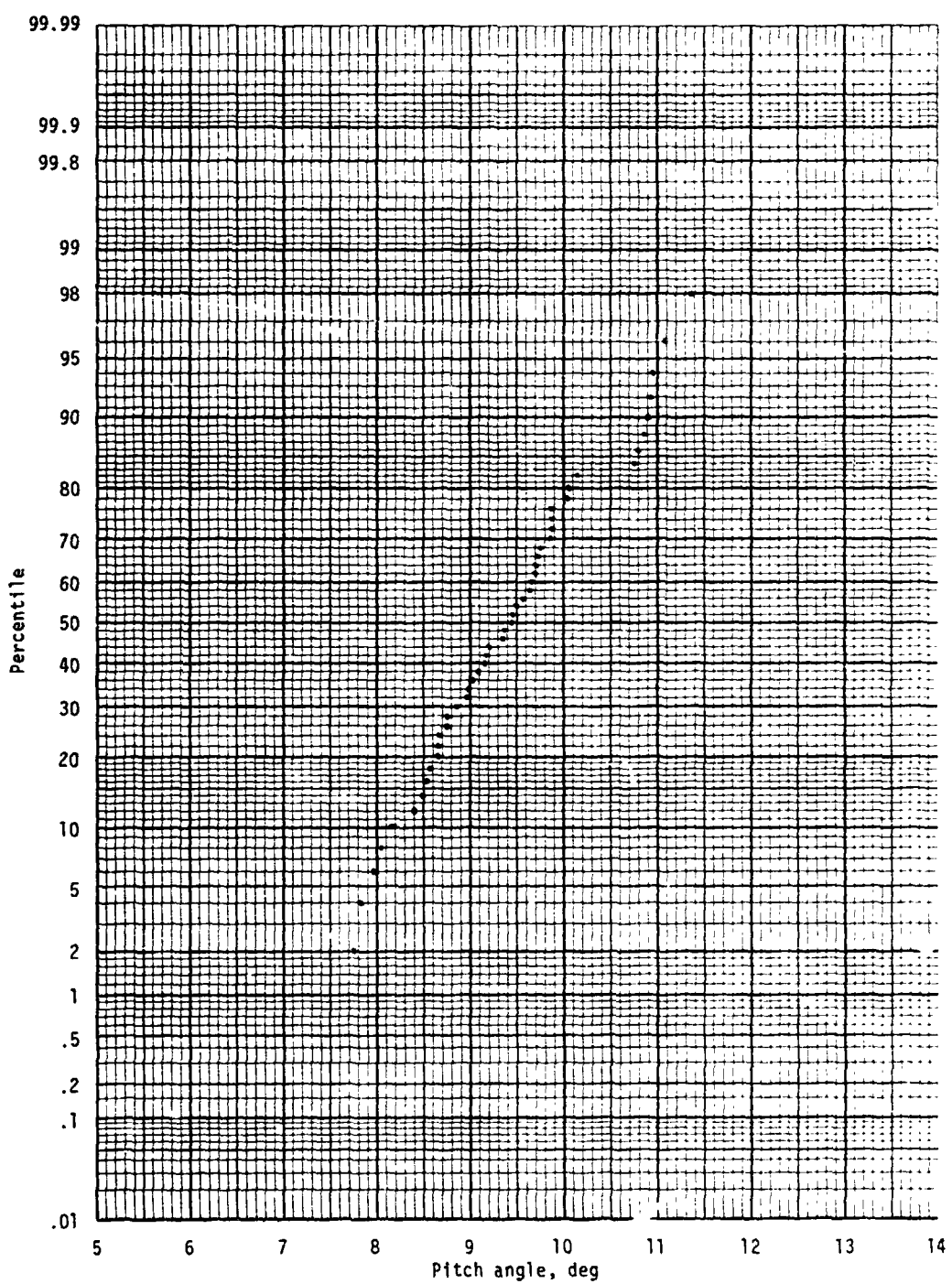
(f) Pitch angle.

Figure 8.- Continued.
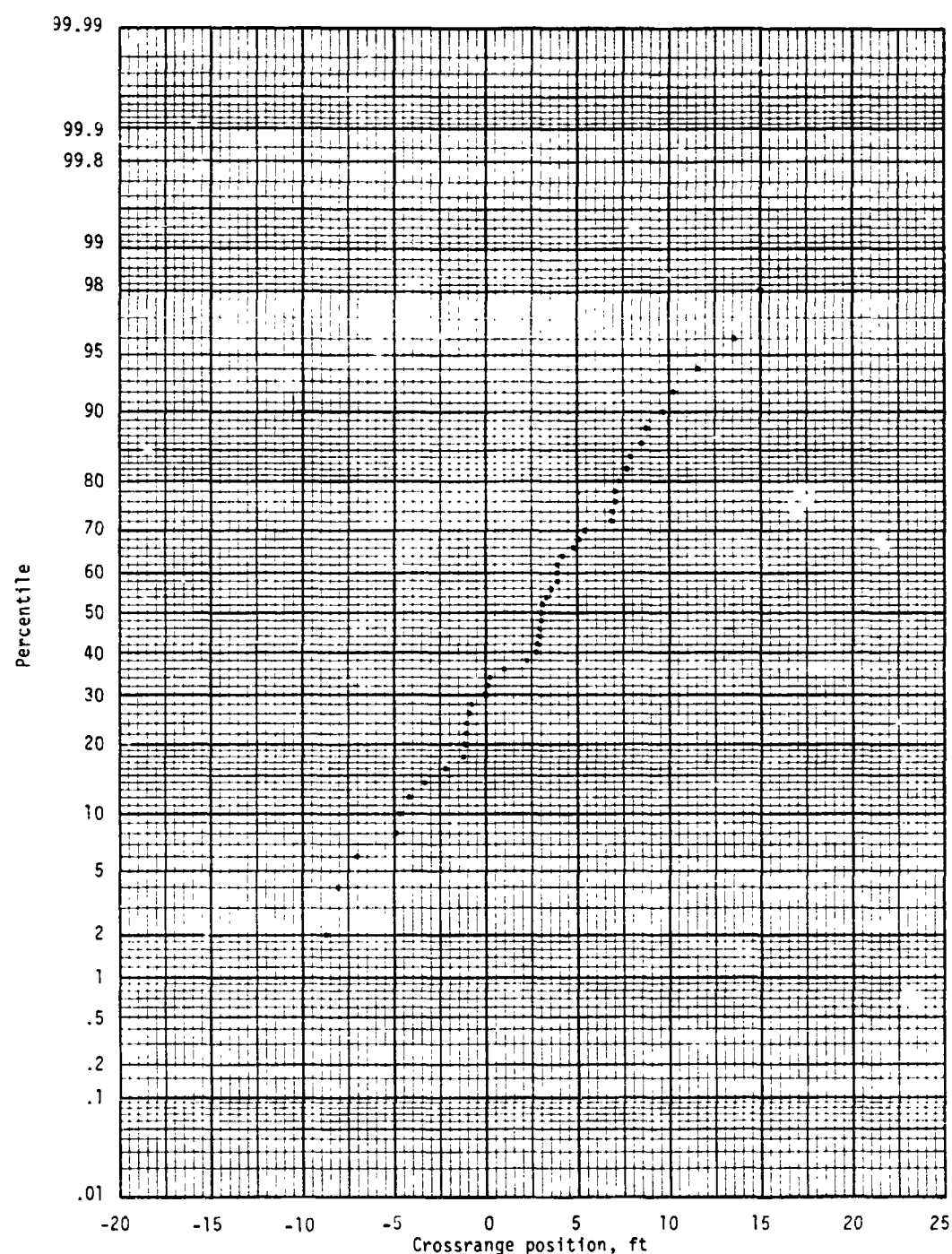
(g) Crossrange position.

Figure 8.- Continued.
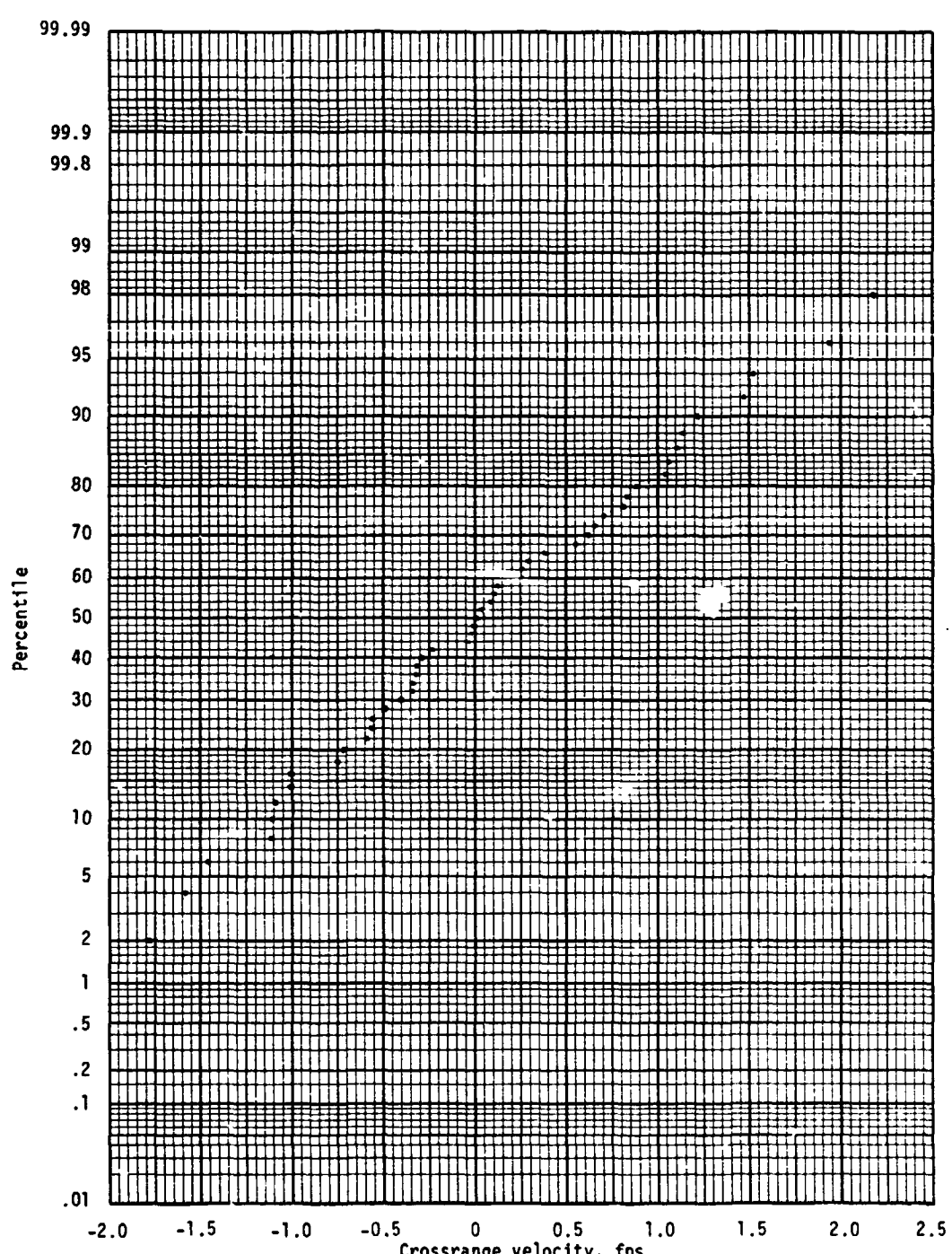
(h) Crossrange velocity.

Figure 8.- Concluded.
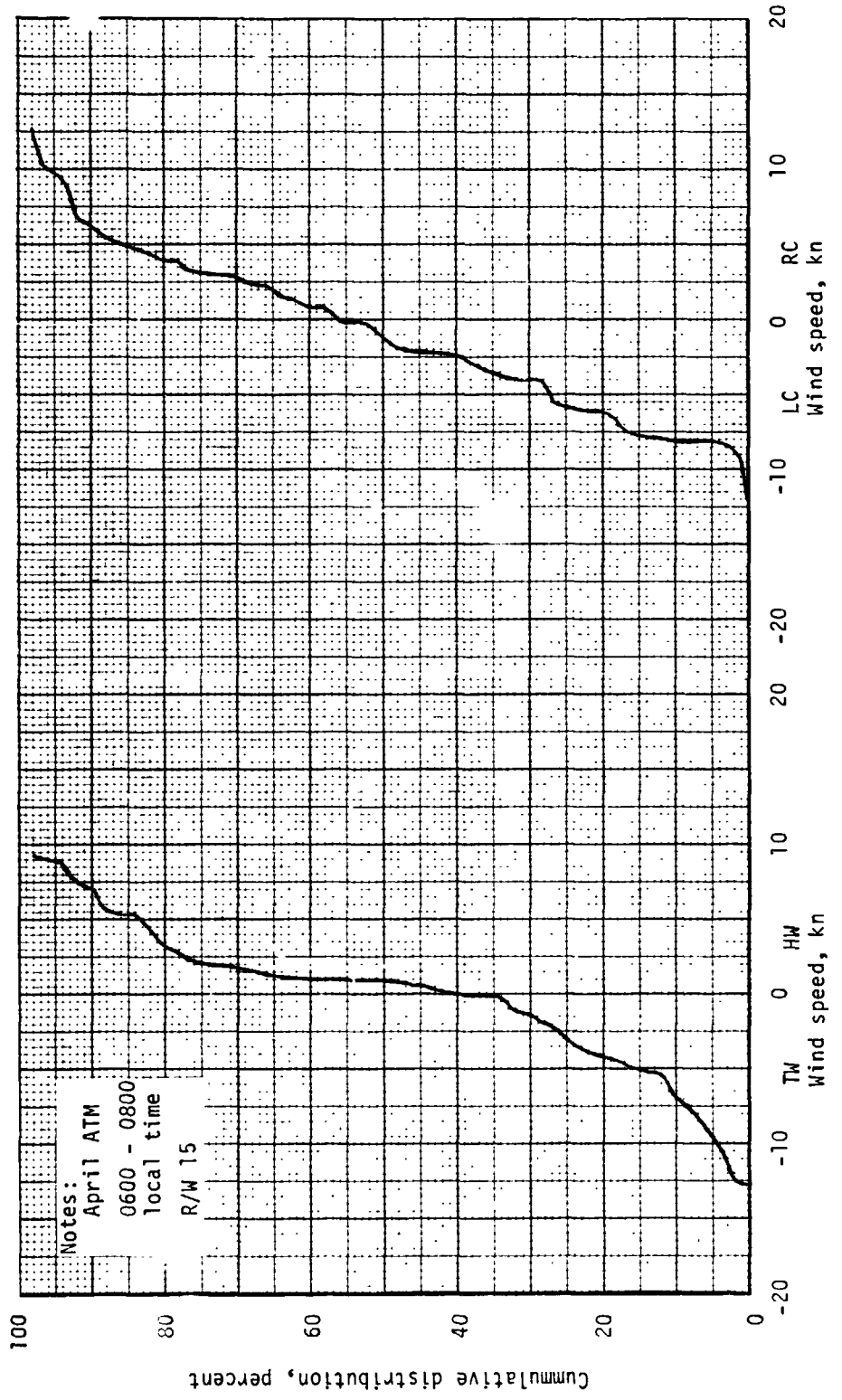
(a) Head and tail wind magnitude.

(b) Crosswind magnitude.

Figure 9.- KSC surface wind statistics.

NASA-JSC

111